THE ROLE OF LYSOPHOSPHATIDIC ACID AND AUTOTAXIN IN OBESITY-INDUCED CARDIAC INSULIN RESISTANCE

by

Carine Nzirorera

Submitted in partial fulfilment of the requirements
for the degree of Master of Science

at

Dalhousie University
Halifax, Nova Scotia
August 2017

TABLE OF CONTENTS

LIST OF FIGURES v

ABSTRACT vi

LIST OF ABBREVIATIONS USED vii

ACKNOWLEDGEMENTS x

CHAPTER 1: INTRODUCTION 1

1.1 Obesity as a Risk Factor for Diabetes and Cardiovascular Disease 1

1.2 Adipose Tissue Remodelling During Obesity Impairs Cardiac Insulin Sensitivity 3

1.2.1 Adipose Tissue Macrophage Infiltration During Obesity Promotes a Pro-inflammatory Environment That Leads to Systemic Insulin Resistance 3

1.2.2 Free Fatty Acid Release and Ectopic Lipid Accumulation in the Heart 5

1.3 Cardiac Insulin Signalling 7

1.3.1 Cardiac Insulin Signalling Mechanism 7

1.3.2 Cardiac Insulin Resistance 10

1.4 Adipokines 11

1.4.1 Adipokines Influence Systemic Insulin Sensitivity 11

1.4.2 Direct Effects of Adipokines on Cardiac Function. 12

1.4.3 Autotaxin-LPA Axis is Implicated in Obesity and Diabetes. 14

1.4.4 Autotaxin-LPA Axis Effects on Cardiovascular Function. 16

CHAPTER 2: EXPERIMENTAL METHODS 22

2.1 Animal Models 22

2.1.1 Diet-Induced Obesity and Whole Heart Tissue Collection 22

2.1.2 Genomic DNA Isolation and PCR Genotyping of Wildtype and Heterozygous Autotaxin Knockout Mice. 23

2.2 Cell Culture 24

2.2.1 H9C2 Cell Culture 24
2.2.2 Adult Mouse Cardiomyocyte Isolation and Culture 24
2.2.3 Neonatal Rat Cardiomyocytes Isolation and Culture 26
2.2.4 Preparation of Lysophosphatidic Acid Solution 27
2.2.5 Preparation of Palmitate Solution 28
2.2.6 Experimental Design for Cell Culture 28
2.2.6.1 Incubation of H9C2 Cells with LPA and Insulin Stimulation 28
2.2.6.2 Incubation of H9C2 cells with palmitate and LPA 29
2.2.6.3 Insulin stimulation of isolated adult cardiomyocytes 30
2.2.6.4 Incubation of neonatal rat cardiomyocytes with palmitate and LPA 30
2.2.7 Fluorescence Microscopy 30
2.2.8 Assessment of Cell Viability 31
2.3 Immunoblot Analysis 32
2.4 Sarcomere Shortening Analysis 33
2.5 Statistical Analysis 33
CHAPTER 3: RESULTS 34
3.1 Lysophosphatidic Acid Upregulates Insulin Signalling Targets in Insulin-Sensitive H9C2 Cells. 34
3.2 Incubation With Palmitate Leads to Insulin Resistance in H9C2 Cells. 38
3.3. LPA Promotes Insulin Resistance in the Presence of Palmitate in H9C2 Cells 42
3.4 LPA Does not Influence Palmitate-Induced Inflammatory Signalling and Apoptosis in H9C2 Cells. 45
3.5 LPA Increases Oxidative Stress in the Presence of Palmitate in H9C2 Cells. 49
3.6 LPA Exacerbates Insulin Resistance in The Presence of Palmitate in Neonatal Rat Cardiomyocytes. 51

3.7 Heterozygous Autotaxin Knockout Mice Fed High Fat-High Sucrose Diet, Show Reduced Weight Gain and are Protected From Myocardial Insulin Resistance. 53

3.8 Cardiomyocytes Isolated From Heterozygous Autotaxin Knockout Mice Fed High-Fat High-Sucrose Diet Show Improved Insulin Sensitivity. 57

3.9 Cardiomyocytes Isolated From Heterozygous Autotaxin Knockout Mice are Protected From High-Fat High-Sucrose Diet-Induced Contractile Dysfunction.....58

CHAPTER 4: DISCUSSION.....62

CHAPTER 5: CONCLUSION AND FUTURE DIRECTIONS 71

REFERENCES 73

LIST OF FIGURES

Figure 1. 1. Insulin signaling pathway and fatty acid interaction in cardiomyocytes.....19
Figure 1. 2. Autotaxin mediated LPA signalling 20
Figure 1. 3. Lysophosphatidic acid synthesis from various lipid species. 21
Figure 3. 1. Lysophosphatidic acid (18:1) increases phosphorylation of proteins downstream of PDK1 at baseline and following insulin stimulation. 37
Figure 3. 2. Experimental design for H9C2 cell incubation with palmitate and mechanism of palmitate-induced insulin resistance.....39
Figure 3. 3. Incubation of H9C2 cells with palmitate induces insulin resistance. 41
Figure 3. 4. Co-incubation of H9C2 cells with 0.8 mM palmitate and 20 μM LPA decreases levels of AKT pS473. 44
Figure 3. 5. Co-incubation of H9C2 cells with palmitate and LPA does not attenuate palmitate-induced inflammation and apoptosis. 48
Figure 3. 6. Co-incubation of H9C2 cells with low palmitate and LPA increases oxidative stress. 50
Figure 3. 7. Palmitate and LPA co-incubation decreases protein level of downstream insulin signalling targets in neonatal rat cardiomyocytes. 52
Figure 3. 8. Heterozygous autotaxin knockout mice fed high-fat high-sucrose diet show reduced weight gain and blood glucose drop after 10U/kg insulin injection is evident in all groups. 55
Figure 3. 9. Heterozygous autotaxin knockout mice fed high-fat high-sucrose diet show improved insulin sensitivity compared to wildtype mice. 56
Figure 3. 10. Cardiomyocytes isolated from heterozygous autotaxin knockout mice fed high-fat high-sucrose diet show improved insulin sensitivity compared to wildtype mice. 58
Figure 3. 11. Cardiomyocytes isolated from heterozygous autotaxin knockout mice fed high-fat high-sucrose diet show increased sarcomere length although within normal range. 60
Figure 3. 12. Cardiomyocytes isolated from heterozygous autotaxin knockout mice fed high-fat high-sucrose diet show improved cardiac function compared to wildtype mice. 61

ABSTRACT

The metabolic changes to adipose tissue during obesity can induce cardiac insulin resistance. During obesity and diabetes, cardiac metabolic flexibility is reduced, which may lead to impaired ATP production, elevated reactive oxygen species production, mitochondrial dysfunction and apoptosis. The adipokine, autotaxin (ATX), which generates bioactive lipids called lysophosphatidic acids (LPA), has been linked to obesity-induced insulin resistance in both mouse models and humans. This study is the first to examine the role of ATX/LPA in obesity-induced cardiac insulin resistance and cardiac dysfunction and the role of LPA in palmitate-induced lipotoxicity. Pre-incubation with LPA reduced the magnitude of insulin stimulation of AKT compared to baseline. In the presence of palmitate, LPA exacerbated cardiac insulin resistance in H9C2 cells and neonatal rat cardiomyocytes. Lastly, a reduction in ATX/LPA levels protected against obesity-induced cardiac insulin resistance and cardiac dysfunction. Collectively, these results suggest that increasing levels of ATX/LPA aide in the progression of cardiomyopathy during obesity and insulin resistance/diabetes.

LIST OF ABBREVIATIONS USED

4EBP-1	4E binding protein-1
AKT	Protein kinase B/PKB
AMCM	Adult Mouse cardiomyocyte
AMPK	AMP-activated protein kinase
Angpt14	Angiopoietin-like 14
As160	Akt substrate of 160 kDa
ATP	Adenosine triphosphate
ATX	Autotaxin
BCA	Bicinchoninic acid
BSA	Bovine Serum Albumin
cAMP	Cyclic AMP
CC2	Cryptocyanin 2
CCR2	C-C chemokine receptor type 2
CD11c	Integrin, alpha X
CD36	Cluster of differentiation 36
HG	High glucose
DAG	Diglyceride/Diacylglycerol
DMEM	Dulbecco's modified Eagle's medium
DOX	Doxorubicin
ECM	Extracellular matrix
EDTA	Ethylenediaminetetraacetic acid
eIF4E	Eukaryotic translation initiation factor 4E
eNOS	Endothelial nitric oxide synthase 3
ERK	Extracellular signalling regulated kinase
FAT	Fatty acid translocase
FBS	Fetal bovine serum
FFA	Free fatty acids
FoxO	Forkhead box O
g	Relative centrifugal force
Gab1	Grb2-associated binder-1
GLUT1	Glucose transporter 1
GLUT4	Glucose transporter 4
GRB10	Growth factor receptor bound protein 10
GS	Glycogen synthase
GSK3	Glycogen synthase kinase 3
h	Hour
H9C2	*Rattus norvegicus* myoblastic cells
HCAEC	Human coronary artery endothelial cells
Het	Heterozygous
HFHS	High-fat high-sucrose

HSL	Hormone-sensitive lipase
IFN-γ	Interferon gamma
IKK	IκB kinase
IKKß	Inhibitor of nuclear factor kappa-B kinase
IL-6	Interleukin 6
iNOS	Inducible nitric oxide synthase
IRS	Insulin receptor substrate
IR	Insulin receptor
JNK	c-Jun N-terminal kinase
kcal	Kilocalorie
KO	Knockout
LC Acyl-CoA	Long chain acyl-coenzyme A
LCFA	Long chain fatty acid
LKB1	Liver kinase B1
LPA	Lysophosphatidic acid
LPAR	Lysophosphatidic acid receptor
LPP3	Lipid phosphate phosphatase
MAPK	Ras-mitogen-activated protein kinase
MCP-1	Monocyte chemoattractant protein-1
MEK	Mitogen-activated protein kinase kinase
MIF	Macrophage migration inhibitory factor
MitoSOX	Red mitochondrial superoxide indicator
MMP2	Matrix metallopeptidase 2
MMP9	Matrix metallopeptidase 9
mTORC1	Mechanistic target of rapamycin complex 1
mTORC2	Mechanistic target of rapamycin complex 2
NEFA	Non-esterified fatty acids
NRCM	Neonatal rat cardiomyocytes
p70S6K1	p70 ribosomal protein S6 Kinase 1
PAI-1	Plasminogen activator inhibitor-1
PBS	Phosphate-buffered saline
PCR	Polymerase Chain Reaction
PDK1	Phosphoinositide-dependent protein kinase 1
PI3K	Phosphatidylinositol kinase 3
PIP_3	Phosphatidylinositol (3,4,5)-triphosphate
PKA	Protein kinase A
PKC	Protein Kinase C
PTP1B	Protein tyrosine phosphatases 1B
RHEB	Ras-homolog enriched in brain
RhoA	Ras homolog gene family, member A
ROCK	Rho-associated protein kinase
rpm	Rotation per minute

s	Seconds
S6	Ribosomal Protein S6
SDS-PAGE	Sodium dodecyl sulfate polyacrylamide gel electrophoresis
SEM	Standard error of the mean
Shc	Src-homology-2-containing
SIRPs	Signalling-regulatory proteins
SOCS	Suppressor of cytokines signalling
SOS	Son of sevenless
TAG	Triglyceride/Triacylglycerol
Th1	T helper cell
TLR4	Toll-like receptor 4
TNF-α	Tumor necrosis factor alpha
TSC1/2	Tuberous sclerosis complex 1 and 2
VEGF	Vascular endothelial growth factor
WT	Wildtype

ACKNOWLEDGEMENTS

I would like to take this opportunity to acknowledge the many people who supported and encouraged me through my Master's program. I would acknowledge the funding agency that made my project possible: NSERC, DMNB and NHSRF.

I would like to thank Dr. Petra Kienesberger, for her support and guidance. It has been a great privilege to be mentored by her. Her enthusiasm and love for research is infectious, and has opened my eyes to the importance of research in advancing our knowledge in healthcare. I would like to thank Kenneth D'Souza, Purvi Trivedi, Andrew Cowie, Liliam Rios and Logan Slade for answering all my many questions, the hours spent on dissection days and the long days of cardiomyocyte extractions. I would like to thank the members of Dr. Pulinilkunnil, Dr. Brunt and Dr. Reiman lab for being an inspiring and knowledgeable scientific community, a peer review panel when needed, and cheerful group of friends to share laughs with. I would also like to thank the supporting staff whose help has been immeasurable: Animal care technician Shelley Nauss, who helped us care of all our mice cohorts, lab technicians Rattina Dasse, Dr. Giban Ray and Dr. Lester Perez for microscopy and cell culture help.

Lastly, I would like to thank my family for their support throughout my program, and their patience when scheduling and rescheduling birthdays, dinners, and celebrations around my lab hours. I could not have completed this program without your wise counsel and encouragement.

CHAPTER 1: INTRODUCTION

1.1 Obesity as a Risk Factor for Diabetes and Cardiovascular Disease

According to a 2014 report from Statistics Canada the prevalence of overweight and obese individuals has reached 54% among adult Canadians and is increasing annually with the highest rates seen in the Atlantic Provinces. Worldwide, between 1980 and 2013, the prevalence of overweight or obese children increased by 47.1% and adults by 27.5%, leading to a total of 2.1 billion individuals who are overweight or struggling with obesity [1]. Obesity is the accumulation of excessive adipose tissue that can be detrimental to systemic health and lead to insulin resistance. In lean and metabolically healthy individuals, insulin increases triglyceride (TAG) storage in adipose tissue by promoting adipocyte differentiation, increased glucose and fatty acid uptake, inhibiting lipolysis and promoting lipogenesis in mature adipocytes [2]. In obese and metabolically unhealthy individuals, hypertrophied adipocytes have a reduced response to insulin, leading to increased free fatty acid release (or lipolysis), increased macrophage recruitment in the adipose tissue, and reduced adipose tissue glucose and fatty acid uptake, which can result in systemic insulin resistance. These functional alternations are driven by the rapid expansion of the adipose tissue and resulting inadequate vascularization of the adipose tissue [3]. During this condition, areas of hypoxia and necrosis occur, promoting the recruitment of macrophages which increases inflammation in the area and, in turn, more macrophage recruitment occurs. This resulting vicious cycle leads to chronic inflammation. Adipocytes in the inflamed and hypertrophied adipose tissue release non-esterified fatty acids or free fatty acids (NEFA), and secrete pro-inflammatory adipokines. As a response to the increased level of circulating NEFA, other tissues not adapted for

lipid storage like the liver, muscle, and heart begin to accumulate FA and their metabolites, giving rise to tissue lipotoxicity. This can lead to impaired cellular function due to apoptosis, oxidative stress and endoplasmic reticulum stress, and initiate insulin resistance in these tissues. Additionally, the increased release of pro-inflammatory adipokines from macrophage-infiltrated adipose tissue promotes chronic systemic inflammation which induces systemic insulin resistance [4]. Adipokines are endocrine factors released by adipose tissue that function as chemokines, cytokines and hormones involved in energy homeostasis and inflammation. These endocrine factors are not always exclusively released by adipose tissue; currently, over 600 have been identified [5].

The metabolic changes to the adipose tissue during obesity not only induce systemic insulin resistance, but can also affect cardiac insulin sensitivity and can lead to myocardial dysfunction. Proper cardiac metabolism and function requires high rates of ATP production from glucose and fat oxidation. The healthy heart is metabolically flexible and can meet its high energy demands by rapidly adjusting to fluctuations in available circulating substrates [6, 7]. Systemic insulin resistance impairs the metabolic flexibility of the heart by chronically reducing the use of glucose and shifting the heart to a greater use of FA for energy [8, 9]. As a result, diabetic cardiac tissue has elevated reactive oxygen species production, mitochondrial dysfunction and apoptosis. These changes can cause alterations in structure and function of the myocardium leading to cardiomyopathy and eventual heart failure. To date, the molecular mechanisms and cardiomyocyte signalling pathways that underlie obesity/diabetes-associated cardiac insulin resistance remain incompletely understood. It has recently been proposed that adipokines may influence cardiac insulin function in obesity and diabetes.

1.2 Adipose Tissue Remodelling During Obesity Impairs Cardiac Insulin Sensitivity

1.2.1 Adipose Tissue Macrophage Infiltration During Obesity Promotes a Pro-inflammatory Environment That Leads to Systemic Insulin Resistance

Adipose tissue remodelling is an ongoing process that rapidly responds to alterations to nutrient deprivation and excess. In the obese state, this process becomes accelerated and pathological. Healthy adipose tissue expansion/remodeling occurs through recruitment of adipocyte precursor cells that differentiate into small adipocytes, the recruitment of other stromal cell types, subsequent vascularization, minimized recruitment of extracellular matrix and minimal inflammation [10].

On the contrary, pathological adipose tissue expansion seen in obese and metabolically unhealthy individuals occurs through rapid growth of existing adipocytes, increased macrophage infiltration, restricted vessel development and massive fibrosis [10]. Poor vascularization to the expanded tissue, results in localized hypoxia. This has also been verified clinically showing adipose tissue of obese individuals is poorly oxygenated [3, 20]. Studies using animal models and isolated murine adipocytes have shown that hypoxia upregulates the release of pro-inflammatory adipokines such as macrophage migration inhibitory factor (MIF), the matrix metalloproteinases MMP2 and MMP9, Interleukin 6 (IL-6), Angptl4, plasminogen activator inhibitor (PAI)-1, vascular endothelial growth factor (VEGF), and leptin [21-23]. These increased pro-inflammatory adipokines create an environment that promotes macrophage mobilization into the adipose tissue. In obese adipose tissue, monocyte accumulation is also regulated by chemokines, small pro-inflammatory molecules that promote macrophage mobilization from bone marrow to tissue. These chemokines are derived from

macrophages and/or hypertrophic adipocytes in the adipose tissue and active MCP-1/CC2 pathways [24-26].

In the lean state, the resident macrophages are largely in the M2 status [11, 12]. These M2 macrophages release factors that promote tissue repair, angiogenesis for the increasing adipose tissue mass, removal of dead and dying adipocytes, recruitment and differentiation of adipocyte progenitors and preservation of normal adipocyte function [13]. During obesity, macrophages are polarized into an M1 form. M1 macrophages are positively correlated with insulin resistance and express pro-inflammatory factors such as F4/80, CD11c, TNF-α, IL-6, iNOS and CCR2 [12, 14] when induced by lipopolysaccharide and T helper cell (Th1) cytokine IFN-γ. In fact, conditional ablation of CD11c positive macrophages in adipose tissue of high fat diet (HFD)-fed obese mice results in reduced pro-inflammatory adipose tissue macrophage accumulation and rapid whole body normalization of insulin sensitivity [15].

Adipocyte death, hypoxia, enhanced chemokine secretion and dysregulation of fatty acid fluxes are four independently acting mechanisms, through which macrophages are recruited and infiltrate the adipose tissue [10]. In advanced obesity, macrophages aggregate, forming crown-like structures surrounding necrotic adipocytes [16-18]. Additionally, massive adipocyte death can cause rapid accumulation of adipose tissue macrophages, which was shown using a transgenic model of inducible lipoatrophy by targeted caspase 8 activation [19].

FFA fluxes, either high rates of lipolysis or an influx of saturated FFA into adipocytes, can cause temporary inflammation within the tissue [27]. This primes the adipose tissue for increased macrophage infiltration which accelerates adipose tissue

inflammation, impairing adipose tissue insulin sensitivity and leading to systemic insulin resistance. NEFA serve as ligands for TLR4 complex activating TNF-α release by the accumulated macrophages which in turn stimulates adipocyte lipolysis releasing saturated NEFA [27, 28]. This paracrine loop between macrophages and adipocytes results in accelerated adipose tissue inflammation.

1.2.2 Free Fatty Acid Release and Ectopic Lipid Accumulation in the Heart

Enlarged adipocytes as observed during obesity generally have higher rates of lipolysis and as such release higher levels of NEFA into the circulatory system. Lipolysis normally increases after fasting, as a method for stored fatty acids in the adipose tissue to be sent to organs for substrate utilization during conditions of poor substrate availability [29]. Once released from adipose tissue, NEFA bound to albumin are transported to the liver and packaged into very-low density lipoproteins. Hepatic production of TAG-rich lipoproteins is heavily dependent on circulating FA. These lipoproteins are released into the circulation and transport fatty acids to other organs, which requires TAG breakdown by lipoprotein lipase. During obesity, regulation of adipose tissue lipolysis is altered and rates of FFA release are increased despite already high levels of available substrates [30]. This translates to an impaired ability of adipose tissue to store of FAs and ectopic accumulation of FAs in other organs like liver, muscle and heart.

The heart increases fatty acid uptake in response to the increased fatty acid availability during obesity. Subsequently, the heart is susceptible to TAG and lipid metabolite accumulation in the myocardium. It is believed that TAGs are non-toxic lipid forms and that saturated FA and their metabolites, such as long chain acyl-coenzyme A (LC acyl-CoA), ceramides and diacylglycerol (DAG), can impair insulin signalling by

promoting the activation of protein kinases. These include multiple isoforms of protein kinase C (PKC), mitogen activated protein kinase (MAPK), c-Jun N-terminal kinase (JNK), and the inhibitor of nuclear factor κB kinase β (IKK β) [31-33]. In mice fed HFD for 10 weeks, decreased cardiac glucose oxidation was associated with increased DAGs [34], suggesting that this lipid metabolite may play a role in HFD-induced cardiac insulin resistance.

Lipolysis is stimulated by catecholamines and glucagon which bind to beta-adrenergic receptors and glucagon receptors, respectively, activating Gs-protein that sends a stimulatory signal to adenylyl cyclase (AC) to generate cyclic AMP (cAMP) [35]. cAMP binds to protein kinase A (PKA), increasing the activity of the enzyme by exposing PKA's catalytically active subunits [36]. PKA polyphosphorylates hormone-sensitive lipase (HSL) on multiple sites (Ser-563, Ser-659 and Ser660), which causes activation and subsequent translocation of HSL from the cytosol to the lipid droplet [37, 38]. PKA also phosphorylates perilipin on the lipid droplet, causing movement of perilipin away from the lipid droplet [39], opening the lipid droplet for lipolytic attack [40], and causing perilipin-mediated activation of HSL activity at the surface of the lipid droplet [41]. The resulting effect is increased adipose tissue lipolysis.

Insulin functions as an antilipolytic hormone, as it binds to its receptor causing autophosporylation and subsequent phosphatidylinositol kinase-3 (PI3K) activation. Protein kinase B (AKT) is subsequently phosphorylated and activates phosphodiesterase 3B, which degrades cAMP in adipocytes. This prevents cAMP binding to PKA resulting in decreased lipolysis. Additionally, insulin stimulates the phosphorylation of the regulatory subunit of protein phosphatase-1 which dephosphorylates and deactivates HSL

leading to decreased lipolysis [42]. Conversely, insulin resistance may increase basal lipolysis seen in obesity. For instance, decreased insulin-mediated suppression of adipocyte lipolysis has been reported in obese rats and women with visceral obesity. Additionally, chronic and acute peripheral administration of leptin in rats increased TAG hydrolysis by 9 to 16-fold [43, 44]. Increased levels of leptin may also enhance lipolysis by inhibiting insulin and its antilipolytic effects by attenuating the inhibition of beta-adrenergic receptor-mediated lipolysis and PKA activation caused by insulin [45].

1.3 Cardiac Insulin Signalling

1.3.1 Cardiac Insulin Signalling Mechanism

To understand cardiac insulin resistance, one must first clarify molecular mechanisms of insulin signalling in the heart. In the lean and metabolically healthy state, the heart uses FA as the main substrate for ATP production, fatty acid β-oxidation accounts for 60-70% of the energy needed for cardiac contractile function [9]. However, in conditions of increased circulating glucose and insulin levels (such as after a meal) the heart is able to shift to primarily glucose metabolism. Insulin signalling in the heart is initiated by insulin secretion into the circulatory system from pancreatic β-cells. Circulating insulin then binds to the tyrosine kinase domains on the α subunits of the cell surface insulin receptors inducing auto-phosphorylation of the β subunits [46]. This trans-phosphorylation reaction activates adjacent substrates such as insulin receptor substrates (IRS1 – IRS4), Src-homology-2-containing (Shc) adaptor proteins, signalling-regulatory proteins (SIRPs), and Grb2-associated binder-1 (Gab1) [47]. Tyrosine phosphorylation of IRS1/2 activates two signalling pathways (Figure 1.1) 1) the phosphatidylinositol 3 kinase (PI3K) –AKT/protein Kinase B (PKB) pathway, and 2) the Ras-mitogen-activated protein

kinase (MAPK) pathway, which regulates transcription, protein synthesis, cell growth and differentiation [48].

After PI3K activation, its product phosphatidylinositol (3,4,5)-trisphosphate (PIP_3) activates the kinase phosphoinositide-dependent protein kinase 1 (PDK1) which phosphorylates protein kinase AKT at Thr308 [49]. Protein kinase AKT is also phosphorylated at Ser473 by mechanistic target of rapamycin complex 2 (mTORC2), increasing AKT activity 50-fold [50, 51] (Figure 1.1). There are three isoforms of AKT (AKT 1, 2 and 3), of which AKT2 is central to insulin signalling [52]. One substrate of AKT2, AKT substrate of 160 kDa (AS160), dissociates from vesicles containing glucose transporter 4 (GLUT4) upon phosphorylation. This initiates translocation of GLUT4 from intracellular vesicles to the plasma membrane resulting in myocardial glucose uptake. Cardiomyocytes mostly utilize GLUT1 and GLUT4 glucose transporters for glucose uptake. During fetal and early postnatal life GLUT1 is the predominant glucose transporter and resides in the sarcolemma under basal conditions. In adult cardiomyocytes, GLUT4 becomes the dominating isoform. It resides in intracellular membrane compartments and translocates to the cell surface once stimulated by insulin (catecholamines, ischemia, or increased workload can also trigger GLUT4 translocation) [53-55]. Aside from increased expression in adult cardiomyocytes, GLUT4 (Km: 4-7 mM) also has higher affinity for glucose than GLUT1 (Km: 20-26 mM), therefore, at physiological glucose concentrations (4 – 7 mM) GLUT4 is the major regulator of cardiomyocyte glucose uptake [56]. In pathological conditions such as post-ischemic reperfusion, post-infarcted heart failure, and pressure overload hypertrophy, GLUT4 expression is repressed and GLUT1 expression is concurrently increased [57-59]. Murine

myocardium knockout of *glut4* leads to a 3-fold overexpression of GLUT1 compared to wildtype myocardium [60].

In parallel with mediating glucose uptake, insulin-activated AKT2 also triggers glycogen synthesis by suppressing glycogen synthase kinase 3 (GSK3) which activates glycogen synthase (GS) [61] (Figure 1.1). In addition to promoting glucose storage as glycogen, insulin induces long chain fatty acid (LCFA) uptake in cardiomyocytes by inducing translocation of LCFA transporters FAT/CD36 [62]. Phosphorylation of AKT also inhibits tuberous sclerosis complex 1 and 2 (TSC1/2) which releases the inhibition of Ras homolog enriched in brain (RHEB) to activate mTORC1 complex. This enhances protein synthesis through activation of eukaryotic translation initiation factor 4E binding protein-1 (4E-BP) and p70 ribosomal protein S6 kinase 1 (p70S6K1). Additionally, AKT inhibits forkhead box O (FoxO) activity by translocating into the nucleus (Figure 1.1), phosphorylating FoxO and inducing 14-3-3 protein association [63]. The 14-3-3 FoxO complex translocates to the cytoplasm inhibiting FoxO transcriptional activity. FoxO proteins mediate transcription of genes involved in oxidative stress, autophagy, aging and apoptosis [64].

Aside from tyrosine phosphorylation, IRS can also be phosphorylated at serine residues, inhibiting insulin signalling. During normal insulin signalling conditions these inhibitory serine residues are phosphorylated by extracellular signalling regulated kinase (ERK), and p70S6K1 [65] through a regulatory negative feedback loop. Insulin-activated ERK attenuates AKT activation by phosphorylating IRS1 at Ser-612 [66]. Additionally, mTORC1 complex activation induces p70S6k1 phosphorylation of IRS-1 at multiple serine residues [67].

1.3.2 Cardiac Insulin Resistance

During obesity, circulating levels of saturated FAs and inflammatory factors such as TNF-α increase. TNF-α and saturated NEFA activate JNK and nuclear factor kB kinase β (IKKβ) leading to Ser-307 phosphorylation of IRS and inhibition of insulin signalling [68]. Increased FA and fatty acid metabolites during obesity can activate PKCs (α β1 δ λ ε θ and ζ) and inhibit insulin signalling by promoting serine phosphorylation of IRS1 [69]. In addition, there are inhibitory molecules of insulin signalling such as the protein tyrosine phosphatases 1B (PTP1B), the suppressor of cytokines signalling (SOCS) and the growth factor receptor bound protein 10 (Grb10) that induce insulin receptor de-phosphorylation, physical blocking of substrates phosphorylation and degradation of the insulin receptor and/or IRS.

In addition to inhibition of insulin signalling, increased circulating levels of long chain fatty acids during obesity cause a shift in cardiac substrate utilization to predominantly FA oxidation [70]. FA oxidation inhibits glucose uptake and catabolism. Glucose oxidation is prevented at pyruvate dehydrogenase by acetyl-coA production [71]. As FA levels continue to increase, the liver converts FAs into ketone bodies that are released into the blood to be used in other organs. In poorly controlled diabetes, ketone bodies become the major substrate for ATP production in the heart and inhibit both glucose and FA oxidation [72]. Animal models of severe insulin resistance such as ob/ob and db/db mice and long-term exposure to high-fat diets have impaired activation of intracellular signalling kinases, such as AKT [73-75]. This reduction in insulin signalling in the heart contributes to left ventricular dysfunction through increased mitochondrial dysfunction, decreased angiogenesis, and increased fibrosis [76-79]. Alterations to insulin

signalling pathways during cardiac insulin resistance also increase the risk of developing cardiac hypertrophy, maladaptive left ventricular remodelling and eventual heart failure [80].

1.4 Adipokines

1.4.1 Adipokines Influence Systemic Insulin Sensitivity

In addition to being a major site for storage of excess energy in the form of TAGs, adipose tissue also has an endocrine function. Adipose tissue secretes multiple endocrine factors involved in energy homeostasis and inflammation such as chemokines, cytokines and hormones termed "adipokines" [5, 81]. Initially, it was thought that only white adipose tissue released adipokines, but recently brown adipose tissue was found to also have both autocrine and paracrine function [81]. Adipokines are also produced by a variety of other tissues and only a few are exclusively secreted by adipose tissue [81]. Adipokines play a role in energy homeostasis, thermogenesis, reproduction and immunity. Additionally, alterations to levels of adipokines, such as leptin, adiponectin and resistin, influence insulin signalling and contribute to obesity-associated type 2 diabetes. The role of three major adipokines in regulating insulin sensitivity is discussed below:

Leptin is mainly expressed by differentiated adipocytes in white adipose tissue [82] and both low and high levels of leptin are associated with obesity and diabetes development. Hyperleptinaemia induces an increased pro-inflammatory response: leptin controls TNF-α production, macrophage activation and triggers MCP-1 expression through mechanisms not fully understood [83]. Additionally, TNF-α and interleukin-6 stimulate adipocyte leptin production. Leptin plasma concentration [84] and mRNA

levels [85] are positively related to fat mass. Although high levels of leptin are associated with obesity severity and contribute to inflammation seen in obesity, the principal role of leptin is to suppress food intake, increase energy expenditure and improve insulin sensitivity through activation of AMP protein kinase [86].

Resistin expression increases during obesity. Administration of recombinant resistin to normal animals produces insulin resistance [87]. Additionally, resistin-gene knockout mice showed a decrease in fasting glucose, improved glucose tolerance and enhanced insulin sensitivity [88].

The adipokine adiponectin is under expressed in obese patients with insulin resistance or type 2 diabetes [89]. Through receptor AdipoR1 and R2 adiponectin promotes insulin sensitivity by PPARα and AMPK activation [90-92].

1.4.2 Direct Effects of Adipokines on Cardiac Function.

During obesity, adipose tissue expansion and increased accumulation of macrophages in the adipose tissue lead to increasing secretion of pro-inflammatory adipokines [93, 94] such as monocyte chemotactic protein (MCP)-1, tumor necrosis factor (TNF)-α, interleukin (IL)-1, IL-6 and IL-8 [95-97]. TNF-α and IL-6 stimulate both the c-Jun amino terminal kinase (JNK) and the IκB kinase-β (IKK-β)/nuclear factor-κB (NF-κB) pathways, resulting in upregulation of potential mediators of inflammation that can lead to cardiac insulin resistance [98]. In addition to modulating cardiac insulin sensitivity, adipokines also influence cardiovascular function and can broadly be grouped into cardio-protective adipokines (anti-inflammatory) and cardio-adverse adipokines (pro-inflammatory).

Many studies have shown plasma leptin levels are positively correlated to cardiovascular diseases. In humans, leptin levels increase after myocardial infarction [99] and in heart failure patients independent of body mass [100]. Leptin directly alters function of the heart. Leptin suppresses cardiac contractile function in ventricular myocytes, through endothelin-1 receptor and NADPH oxidase-mediated pathway [101]. Leptin can increase blood pressure and heart rate, which can increase myocardial workload and promote hypertrophy [102]. Leptin deficiency in mice leads to increased mortality when subjected to viral myocarditis [103] , greater cardiac hypertrophy [104] and greater remodelling in response to chronic ischemic injury [105, 106].

Adiponectin is cardio-protective and many studies have shown its protective actions on cardiovascular cell types such as smooth muscle cells, cardiac myocytes, and vascular endothelial cells [107]. Low serum adiponectin levels have been associated with hypertension, coronary artery disease, left ventricular hypertrophy and increased risk of myocardial infraction. Adiponectin decrease is associated with impaired AMP-activated protein kinase (AMPK) signalling. AMPK mediates energy balance in the heart [108]; when AMP:ATP ratio increases, AMPK is activated, stimulating ATP production by increasing glucose and FA uptake and oxidation [109-111]. AMPK directly upregulates fatty acid oxidation by inhibiting acetyl-CoA carboxylase, thereby blunting malonyl-CoA synthesis, the inhibitor of carnitine palmitoyltransferase 1. Additionally, adiponectin signalling stimulates NO production through AMPK-dependent activation of eNOS which has beneficial effects on endothelial cell function.

Studies using adiponectin-deficient mice have demonstrated that adiponectin plays a protective role in the cardiovascular system. Adiponectin protects against cerebral

ischemia-reperfusion [112], promotes revascularization of ischemic limbs [113], and protects against salt-induced hypertension through eNOS activity [114]. Some studies have shown that overexpression of adiponectin inhibits atherosclerotic lesion formation, while adiponectin deficiency leads to augmented atherosclerosis.

1.4.3 Autotaxin-LPA Axis is Implicated in Obesity and Diabetes.

Autotaxin (ATX) is a newly identified adipokine that has recently been implicated in obesity-associated comorbidities. Serum ATX levels increase with obesity-induced insulin resistance in mouse models [115]. In addition, our group has found that serum ATX levels correlate with measures of obesity and insulin resistance in obese humans [116, 117]. ATX is a unique adipokine as it is a major generator and regulator of lysophosphatidic acid (LPA). LPA is a glycerol phospholipid with one polar phosphate group and one fatty acid chain [118]. Currently, five isoforms of ATX have been isolated (ATX_α, ATX_β, ATX_γ, ATX_δ and ATX_ε) and all are catalytically active [119]. ATX_β is the most abundant isoform, found in the brain, peripheral tissues and nervous system [119]. ATX functions as a constitutively active lysophospholipase D, generating LPA from lysophosphatidylcholine (LPC) in plasma and extracellular media as the primary pathway for LPA generation [119, 120] (Figure 1.2). The catalytic domain of ATX possesses a threonine 209 residue that is essential for its phospholipase D activity. Through its somatomedin-B like 1 (SMB1) and somatomedin-B like 2 (SMB2) domains, ATX binds to activated integrins which aids to localize LPA production to the plasma membrane [121] (Figure 1.2). Additionally, ATXα has a unique polybasic insertion loop (located in the catalytic domain) that allows binding to heparan sulfate proteoglycans [121] (Figure

1.2). ATX can bind the plasma membrane via SMB1, SMB2, and the polybasic insertion loop, facilitating LPA binding to its membrane receptors.

Alternatively, extracellular LPA can also be generated from phosphatidic acid. Phosphatidic acid is generated from phospholipids or DAG and then deacylated by phospholipase A1 or phospholipase A2 to form LPA [122] (Figure 1.3). Circulating lipoproteins and albumin are a large source of lysophosphatidylcholine (Figure 1.2). There are also degradative pathways that reduce LPA levels. One pathway involves lipid phosphate phosphatase 1 and 3. As transmembrane exophosphatases, LPP1 and 3 degrade LPA by removal of its phosphate group [123]. LPP1 mutant mice have increased plasma LPA levels and metabolize intravenously injected LPA 4-fold less than wildtype mice [124]. LPP3 deficiency in mice is embryonically lethal due to abnormal blood vessel formation [125]. Similar defects to vascular development are seen in ATX-deficient mice, suggesting strict regulation of LPA levels during embryonic development is essential for vasculature development [126].

The influence of ATX on insulin sensitivity and ultimately glucose homeostasis implicates LPA as a possible modulator of tissue insulin signalling. Originally LPA was considered just an intermediate in *de novo* lipid synthesis, and a component of the plasma membrane. LPA is now known as a potent extracellular signalling messenger that acts through G protein-coupled receptors. Currently, six receptors have been identified ($LPAR_{1-6}$) in mammals [127], which mediate cell proliferation, apoptosis, cell migration, cytokine and chemokine secretion, platelet aggregation and smooth muscle contraction [118]. Previous studies show that the ATX-LPA signalling axis both promotes and hinders insulin signalling and glucose uptake. *In vitro*, LPA increased glucose uptake of

L6 myotubes and 3T3 L1 adipocytes [128], while ex vivo cultures of mouse islet cells showed decreased insulin secretion in mice intraperitoneally injected with 18:1 LPA (50 mg/kg ~ 78 μmol/kg) [115]. Additionally, mesangial cells had increased hexokinase activity, when incubated with LPA in both a concentration- and time-dependent manner [129]. Hexokinases phosphorylate glucose, trapping it in the cell and promoting continuous transport of glucose into the cell. Intravenous injection of 18:1 15 μmol/kg LPA in mice decreased blood glucose comparable to the insulin (0.6 U) injected group [128]. The opposite was seen when chow- and HFD-fed mice were intraperitoneally injected with of 50 mg/kg 18:1 LPA, with both responding with an increase in blood glucose post-injection [115]. Additionally, specific knockout of ATX in mice adipocytes was shown to improve glucose tolerance [130]. These studies suggest that LPA concentration and/or injection site can dictate how LPA influences glucose homeostasis.

1.4.4 Autotaxin-LPA Axis Effects on Cardiovascular Function.

Autotaxin-LPA axis has been implicated in affecting cardiovascular function, especially the progression of atherosclerosis. Few studies have investigated the effects of LPA on myocardial function and fewer yet have studied the effect of autotaxin. LPA receptors 1 and 3 mediate LPA-induced hypertrophy in NRCMs. LPA-induced hypertrophy in cardiac myocytes involves AKT and NF-Kappa B signalling pathways. Additionally, it has been suggested that LPA receptors 1 and 3 mediate left ventricular remodelling in rats subjected to myocardial infarction [131]. LPA modulates myocardial contraction of human atrial and ventricular myocytes by reducing isoprenaline-induced contractions, and was suggested to exert an antiadrenergic effect by inhibiting adenylyl cyclase activity through LPA receptors 1 and 3 [132]. In rats, intravenous injection of

LPA increased left ventricular systolic and diastolic pressure which was abolished by pre-treatment with L703606, a neurokinin type 1 receptor antagonist, and verapamil, a Ca^{2+} channel antagonist [133]. In perfused isolated rat hearts, 20-50 uM LPA elevated left ventricular diastolic pressure [133]. LPA has also been suggested to influence cardiac fatty acid uptake. Specifically, LPA increased lipoprotein lipase activity in cardiomyocytes potentially increasing lipid utilization and deposition [134]. Decreased contractile function of hearts in diabetic animals was related to increased expression of RhoA and ROCK [135], which are effectors of LPA signalling. Moreover, it has been shown that inhibition of the RhoA/ROCK pathway improves contractile function of diabetic rat hearts [135]. Recently, pre-treatment with LPA was found to protect against ischemic reperfusion in immature hearts [136]. LPA pretreatment enhanced cardiac function, reduced myocardial infarct size, increased pro-survival signalling molecules expression and decreased myocardial apoptosis [136]. Despite growing evidence showing that autotaxin and LPA can influence cardiac function, and that circulating levels of autotaxin-LPA increase during obesity and diabetes, the role of the autotaxin-LPA axis in cardiomyocyte insulin signalling and obesity-induced cardiac insulin resistance remain unclear. Therefore, we hypothesized that increased levels of autotaxin-LPA as seen in obesity and diabetes contribute to the development of cardiac insulin resistance. To investigate this, 1) cardiomyocytes were cultured in normal and lipotoxic conditions and incubated with or without LPA and stimulated with insulin to determine how LPA influences insulin sensitivity in these conditions. 2) To determine if mice with lower circulating plasma levels of autotaxin-LPA show improved cardiac insulin sensitivity during obesity, heterozygous ATX-knockout mice were fed a high-fat high-sucrose

(HFHS) diet and cardiac insulin sensitivity was evaluated. 3) Lastly, to determine if lowering plasma levels of autotaxin-LPA improves obesity-induced cardiac dysfunction, sarcomere shortening of cardiomyocytes isolated from heterozygous ATX knockout mice was analyzed.

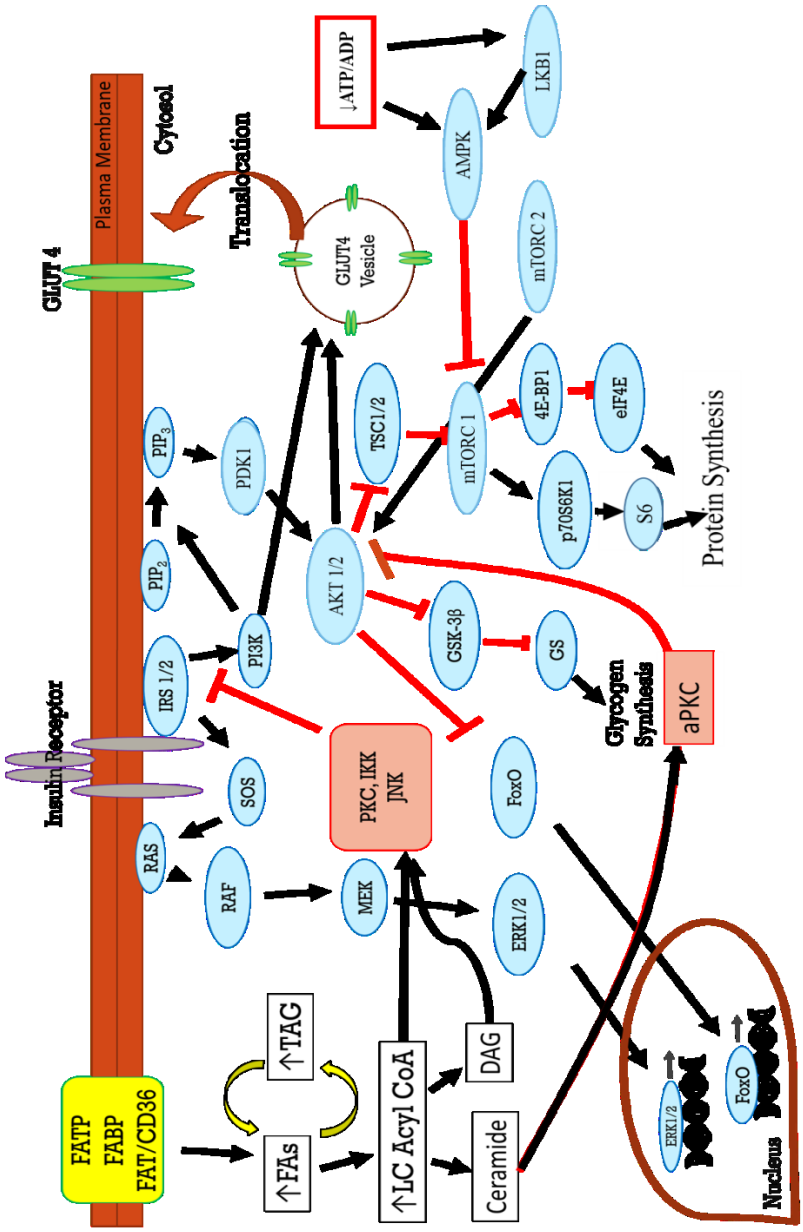

Figure 1. 1. Insulin signaling pathway and fatty acid interaction in cardiomyocytes.

Insulin activates auto-phosphorylation of its receptor which initiates signal transduction of both the AKT and ERK1/2 pathway. AKT is phosphorylated and activated by both PDK1 and RICTOR from mTOR complex 2. AKT inhibits the mTOR complex 1 inhibitor tuberous sclerosis complex 1 and 2 (TSC1/2) activating protein synthesis. Through inhibitory phosphorylation of GSK3, AKT activates glycogen synthesis. AKT also inhibits FoxO proteins translocation to the nucleus and prevents transcription of genes involved in oxidative stress, autophagy, aging and apoptosis. Under lipotoxic conditions, cellular levels of long chain fatty acids can increase leading to increased levels of DAG and ceramides which inhibit insulin signalling through IRS serine phosphorylation and inhibition of AKT activation.

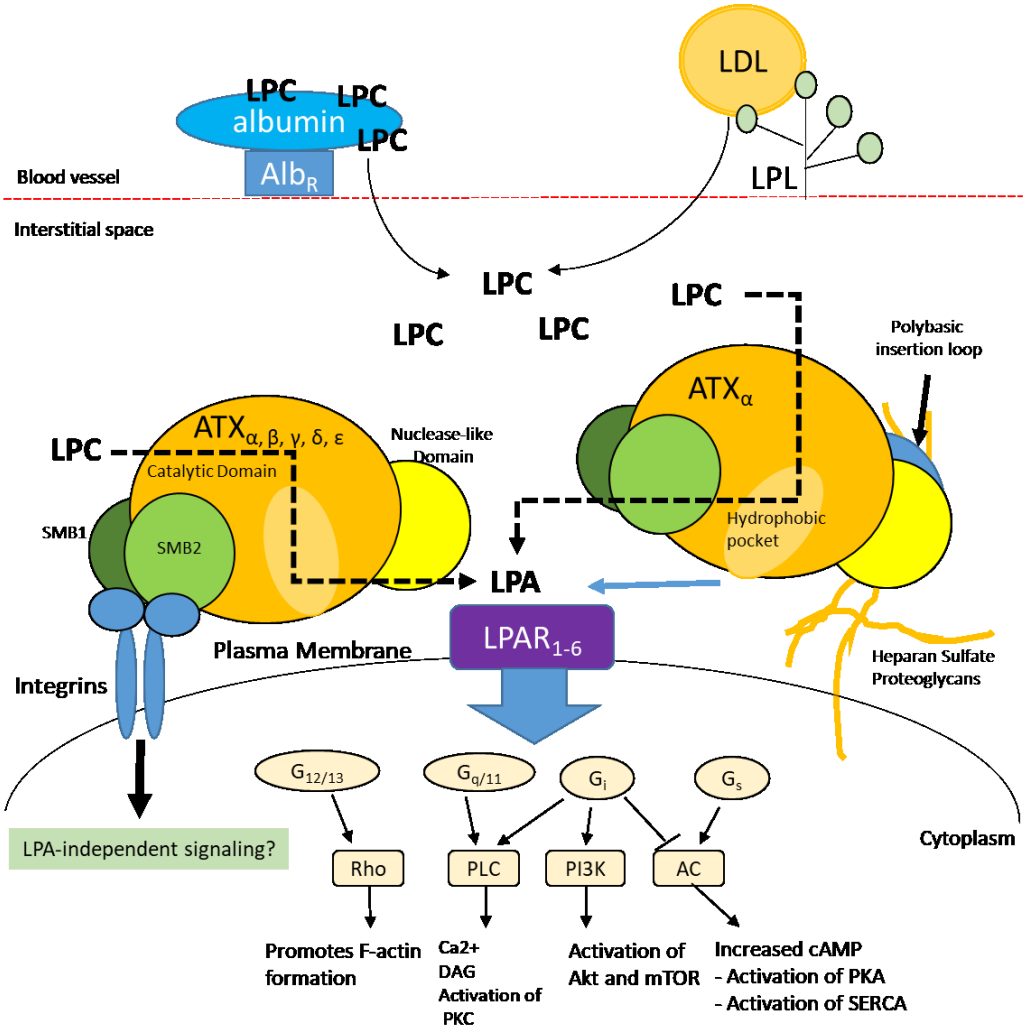

Figure 1. 2. Autotaxin mediated LPA signalling

All autotaxin isoforms (α, β, γ, δ, and ε) have four major domains. Somatomedin-B like 1 (SMB1) and somatomedin-B like 2 (SMB2) domains allow ATX to bind to activated integrins. Residue threonine 209 in the catalytic domain is essential for the lysophospholipase D activity of ATX. ATX also has a C-terminal nuclease-like domain which, together with the SMB1 and SMB2 domains, stabilizes the proper location of the catalytic threonine residue. Unique to the ATX isoform, ATXα, is a polybasic insertion loop that allows for binding to heparan sulfate proteoglycans. ATX can bind the plasma membrane via SMB1, SMB2, and the polybasic insertion loop, resulting in localized LPA production. ATX binding to integrins may induce LPA-independent signalling, but further research is required.

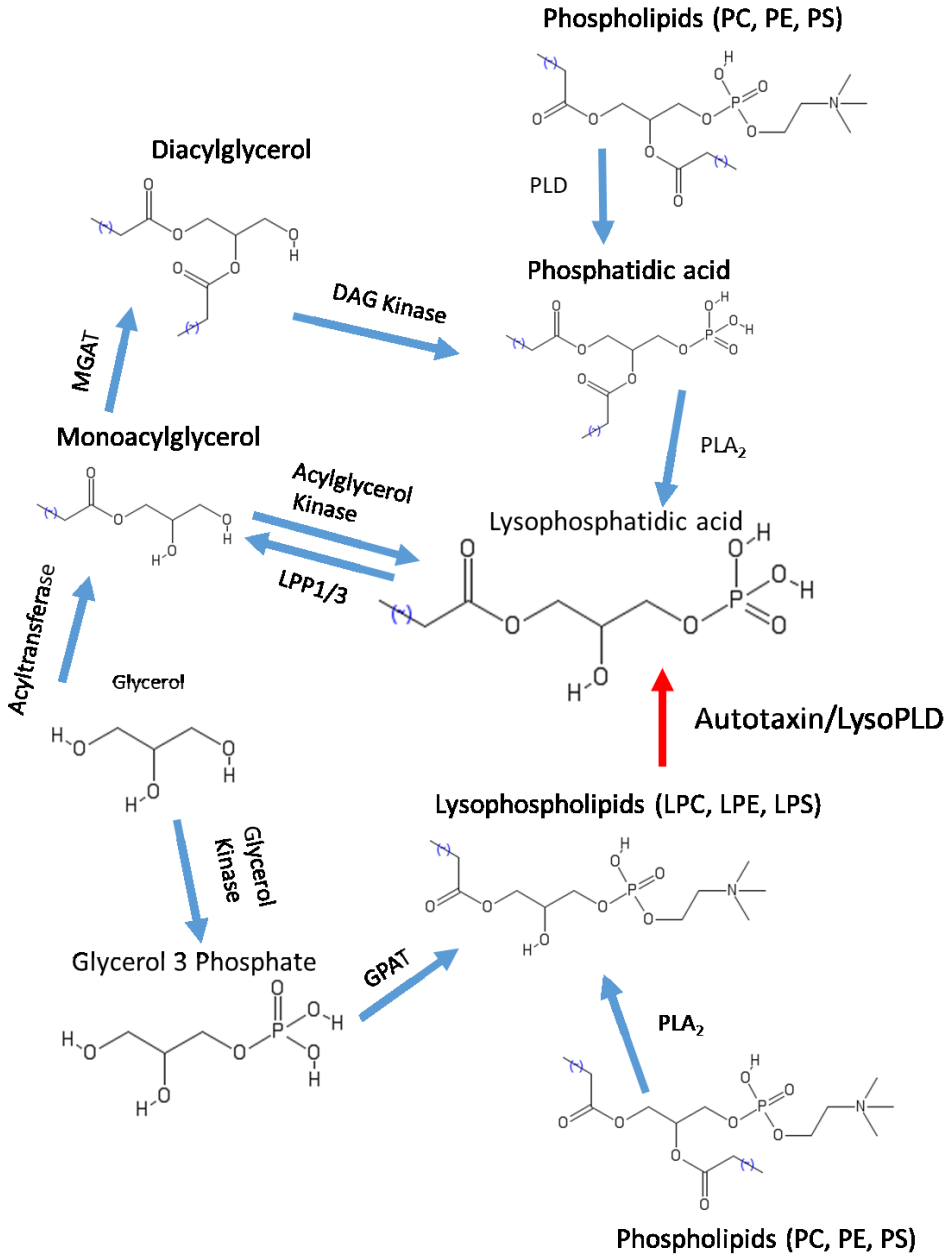

Figure 1. 3. Lysophosphatidic acid synthesis from various lipid species.

DAG: Diacylglycerol, GPAT: Glycerol-3-phosphate acyltransferase, LPC: Lysophosphatidylcholine, LPE: Lysophosphatidylethanolamine, LPP1/3: Lipid phosphate phosphatase 1 or 3 LPS: Lysophosphatidylserine, MGAT: Monoacylglycerol acyltransferase, PLA_2 Phospholipase A_2, PLD: Phospholipase D, PC: phosphatidylcholine, PE: phosphatidylethanolamine, PS: phosphatidylserine.

CHAPTER 2: EXPERIMENTAL METHODS

2.1 Animal Models

Breeding pairs of C57BL/6 wildtype (WT; *Enpp2*$^{+/+}$) and C57BL/6 heterozygous autotaxin knockout mice (Het ATX-KO; *Enpp2*$^{+/-}$) were given by the laboratory of Dr. Vassilis Aidinis and were used to breed cohorts of Het ATX-KO mice and control littermate wildtype mice. Mice were housed on a 12 h light and 12 h dark cycle with ad libitum access to chow diet (5001; Lab diet, St Louis, MO, USA) containing protein (30 kcal%), fat (13.5 kcal%) and carbohydrates (58 kcal%) (3.83% sucrose) until 9-10 weeks of age before they were used in the diet-induced obesity study. All protocols (Protocol number: 16-053) involving rodents were approved by Dalhousie University, Institutional Animal Care and Use Committee.

2.1.1 Diet-Induced Obesity and Whole Heart Tissue Collection

Nine- to ten-week old male Het ATX-KO and wildtype mice were randomly assigned to groups fed either chow or HFHS diet (12451; Research Diets, New Brunswick, NJ, USA) with protein (20 kcal%), fat (45 kcal%) and carbohydrates (35 kcal%) (17% sucrose) for 20 weeks. Body weight was recorded weekly and body weight gain was quantified as fold change by dividing weekly average weight by average starting weight for each diet group. After 20 weeks, mice were subjected to a 3 h food withdrawal and injected with either saline or insulin (10 U/kg). Ten min thereafter, mice were euthanized by decapitation using a guillotine. Heart ventricles were collected and frozen between two spatulas chilled in liquid nitrogen and stored at -80˚C until further processing. Frozen hearts were powdered using mortar and pestle chilled in liquid nitrogen and homogenized in ice-cold lysis buffer containing Tris-HCl pH 7.4 (20 mM), EDTA (5 mM), $Na_4P_2O_7$ (10 mM,

567540; Calbiochem, EMD Chemicals, Gibbstown, NJ, USA), NaF (100 mM), Nonidet P-40 (1%), Na_3VO_4 (2 mM), protease inhibitor cocktail (10 µl/ml, P8340; Sigma, St Louis, MO, USA) and phosphatase inhibitor cocktail (10 µl/ml, 524628; Calbiochem). Homogenates were centrifuged at 10,000 g for 10 min at 4℃ and the supernatant containing membrane, cytosolic and nuclear proteins was transferred to another microcentrifuge tube. Protein concentration was determined using the bicinchoninic acid (BCA) protein assay kit (23255; Pierce, Thermo Fisher Scientific, Waltham, MA, USA). Lysates were stored at -80℃ for subsequent biochemical analysis.

2.1.2 Genomic DNA Isolation and PCR Genotyping of Wildtype and Heterozygous Autotaxin Knockout Mice.

DNA was isolated from mouse ear punches using the Extracta DNA Prep for PCR –tissue kit (Quanta Biosciences 95091). Mouse ear punches were submerged in 50 µL of extraction reagent and incubated at 95˚C (for 30 mins). After incubation, samples (now containing PCR ready genomic DNA) were cooled to room temperature and of stabilization buffer (50 µL) was added. In the PCR reaction mix (AccuStart II GelTrack PCR Supermix (6.25 µL; Quanta Biosciences 95136), primer A1 (2 µL; 10 pmol), primer B2 (1 µL; 5 pmol), primer C1 (1 µL; 5 pmol), and nuclease-free water (1.25 µL)) extracted DNA (2 µL) was added. Primer sequences used were: A1: CGC ATT TGA CAG GAA TTC TT; B2: TAC ACA ACA CAG CCG TCT CA, and C1: ATC AAA ATA CTG GGG CTG CC; Primer set A1/C1 yields a 223 bp PCR product for the wild type (WT) alleles. Primer set A1/B2 yields a 422 bp PCR product of 422 bp for the knockout allele. PCR products were visualized using the Qiaxcel Advanced automated capillary electrophoresis.

2.2 Cell Culture

2.2.1 H9C2 Cell Culture

H9C2 rat embryonic cardiomyoblasts (CRL-1446; ATCC) were cultured at a cell density of 5 x10^5 per 35 mm plate and maintained in Dulbecco's modified Eagle's high-glucose medium (SH30243.01; DMEM-HG; Hyclone Laboratories) supplemented with 10% fetal bovine serum (1400-500; FBS, Seradigm) for 48 h until 90% confluency. H9C2 cardiomyoblasts were then differentiated for 48 h in DMEM 1X media (11966025; Thermo Fisher Scientific, MA, USA) supplemented with FBS (0.5%) and glucose (5 mM). After 48 h of differentiation, cells were used in experiments detailed in section 2.2.6. Cells were then harvested in phosphate-buffered saline (PBS, 0780; Amresco), followed by centrifugation to pellet the cells (10,000 g, 10 min, 4˚C). Cell pellets were sonicated in lysis buffer, followed by centrifugation (10,000 g, 10 min, 4˚C). The supernatant was transferred to another microcentrifuge tube and protein concentration was determined using the BCA protein assay kit. Lysates were stored at -80˚ C for subsequent immunoblot analysis.

2.2.2 Adult Mouse Cardiomyocyte Isolation and Culture

Adult mouse cardiomyocytes were isolated from hearts of 29-30 week-old wildtype and Het ATX-KO mice fed chow or HFHS diet. Hearts were excised and immersed in ice-cold perfusion buffer (pH 7.4) containing NaCl (113 mM), KCl (4.7 mM), KH_2PO_4 (0.6 mM), Na_2HPO_4 (0.6 mM), $MgSO_4$ •$7H_2O$ (1.2 mM), $NaHCO_3$ (12 mM), HEPES (10 mM), Taurine (30 mM), 2,3 Butandione monoxime (BDM, 10 mM) and Glucose (5.5 mM). Hearts were then retrogradely perfused through the aorta on a Langendorff perfusion rig. Initially, hearts were equilibrated by perfusing them with

oxygenated perfusion buffer (37ºC) for 6 minutes. Thereafter, hearts were perfused with recirculating collagenase digestion (1.6 mg/ml, Worthington Lot: 45D15719) buffer for 20-25 min. After collagenase digestion, hearts were removed from the Langendorff rig, placed in a 60 mm cell culture dish, and minced into small pieces. Used collagenase buffer was collected from the rig and used to make a suspension of the minced heart. This suspension was passed through a 100 µm filter to further dissociate tissue, and transferred to a 50 ml centrifuge tube. The suspension was filled up to 30 ml, and 10 ml of stopping buffer (perfusion buffer, FBS (2.4 mg/ml) and $CaCl_2$ (12.5 µM)) was added to stop digestion. The cell suspension was spun to pellet the cells (1,000 g for 45 s) and the supernatant was decanted. Cells were then made calcium-tolerant by resuspending the cell pellet in stopping buffer with increasing $CaCl_2$ concentration (C1:100 µM, C2:400 µM and C3:900 µM). Cells were incubated in each solution for 10 min in a 37 ˚C water bath. After each incubation, viable cells settle to the bottom of the centrifuge tube and the supernatant was removed using a Pasteur pipette, followed by the addition of the next calcium solution with higher concentration. Following incubation with C3, the supernatant was removed and 1 ml of plating medium was added to resuspend and count cells. Cells were seeded at 25,000-50,000 cells on laminin-coated 25 mm x 25 mm slides or 35 mm plates, and were incubated in plating medium for 2 h before cells were used for experiments detailed in 2.2.6.4 and 2.4. Cells were then harvested in phosphate-buffered saline (PBS; 0780, Amresco), followed by centrifugation to pellet the cells (10,000 g for 10 min at 4˚C). Cell pellets were sonicated in lysis buffer, followed by centrifugation (10,000 g for 10 min at 4˚C). The supernatant was transferred to another microfuge tube

and protein concentrations were determined using the BCA protein assay kit. Lysates were stored at -80˚C for subsequent immunoblot analysis.

2.2.3 Neonatal Rat Cardiomyocytes Isolation and Culture

Neonatal rat cardiomyocytes were isolated from 1- to 2-day old Sprague-Dawley rat pups. Hearts were excised and atria were removed to collect the ventricles. Blood was removed from the ventricles by slicing ventricles lengthwise and rinsing in fresh phosphate-buffered saline (PBS). Ventricles were then minced into small pieces and thoroughly washed with ice cold PBS. An average of 20 minced ventricles were transferred to a T25 flask and the volume was topped to 17 ml with PBS. Collagenase- type 2 (2% W/V), DNase (0.5% W/V) and trypsin (2% W/V) (Worthington Biochemical Corporation) were added and the mixture was stirred (80 rpm and 37˚C for 20 mins) to dissociate tissues. Dissociated tissue was added to DF20 Medium (20 mL) composed of DMEM/F12 (D6421; Sigma), FBS (25%, Sigma F1051), penicillin-streptomycin (1%, 30-002-CI, Corning, NY, USA) and gentamycin (50 µg/ml, 30-005-CR; Corning) in a 50 ml centrifuge tube and spun at room temperature for 1 min and 800 rpm. Supernatant containing debris, red blood cells and fibroblasts was discarded and 17 ml of PBS were added to the centrifuge tube to resuspend the pellet. The resulting mixture was transferred to another T25 flask for a second incubation with proteolytic enzymes. This was repeated for a total of 3 incubation steps. To maximize cell yield, the supernatant collected in the second centrifugation step was spun at 1800 rpm for 7 min and only the pellet was retained. Twenty ml of DF20 medium and dissociated cell suspension from the third incubation was added to the centrifuge tube containing the centrifuged pellet. This final suspension was spun at 1800 rpm for 7 min at room temperature. The supernatant was

discarded and cell pellet was then resuspended using 12 ml plating medium composed of DMEM/F12 HAM (D6421; Sigma), FBS (10%, Sigma F1051), horse serum (15%, Life Technologies, 16050-122), penicillin-streptomycin (1%, 30-002-CI, Corning, NY, USA) and gentamycin (50 µg/ml, 30-005-CR; Corning), and transferred to a T75 flask for 2 h differential plating to eliminate non-cardiomyocytes. Supernatant from differential plating containing cardiomyocytes was collected and suspended in growth medium containing DMEM/F12 HAM , FBS (10%), cytosine-β-D-arabinofuranoside (10 µM, C1768; ARAC, Sigma), Insulin Transferrin-Selenium (25800-CR, ITS, Corning), 1% penicillin-streptomycin (1%, 30-002-CI, Corning, NY, USA) and gentamycin (50 µg/ml, 30-005-CR; Corning) and plated using Primeria Falcon plastic plates. The following day, cells were washed in PBS and cultured in serum-free medium containing DMEM 1X (11966025; Thermo Fisher Scientific), ARAC (10 µM), gentamycin (50 µg/ml), penicillin-streptomycin (1%) and glucose (10 mM) for 24 h. Thereafter, cells were treated as described in section 2.2.6.5. Cells were then harvested in PBS, followed by centrifugation to pellet cells (10,000 g for 10 min at 4˚C). Cell pellets were sonicated in lysis buffer, followed by centrifugation (10,000 g for 10 min at 4˚C). The supernatant was transferred to another microfuge tube and protein concentration was determined using the BCA protein assay kit (23255; Pierce, Thermo Fisher Scientific). Lysates were stored at -80˚C for subsequent immunoblot analysis.

2.2.4 Preparation of Lysophosphatidic Acid Solution

Oleoyl-LPA (18:1 Avanti polar lipids 857130C) was complexed to fatty acid-free BSA in ice cold PBS. Fatty acid-free BSA was first dissolved in PBS to make a 0.1% (w/v) BSA solution, by spinning BSA powder layered over PBS (2000g for 5 min at 4ºC).

Meanwhile in a glass tube, 50 µl of LPA stock solution in chloroform (10 mg/ml) was evaporated using nitrogen gas. To make a working stock of LPA (272 µM), 4 ml of 0.1% BSA in PBS solution was added to the glass tube to resuspend the chloroform-free LPA. The working stock of LPA and remaining solution of 0.1% BSA in PBS was sterile filtered and used to incubate cells.

2.2.5 Preparation of Palmitate Solution

BSA-complexed fatty acid (FA) solution was prepared in DMEM 1X (11966025; Thermo Fisher Scientific, MA, USA) medium. A stock solution of sodium palmitate (120 mM, P9767; Sigma) was prepared in DMEM 1X medium and warmed to 100˚C to dissolve. The stock solution was used to make desired concentrations of palmitate by mixing with a pre-warmed (50 ℃) fatty acid-free BSA solution (2%) prepared in DMEM 1X (11966025; Thermo Fisher Scientific, MA, USA) medium. The resulting palmitate and BSA solution was then allowed to complex (37 ℃ for 30 min). Thereafter, the medium was sterile-filtered (0.20 µm) and immediately used to incubate cells.

2.2.6 Experimental Design for Cell Culture

2.2.6.1 Incubation of H9C2 Cells with LPA and Insulin Stimulation

Differentiated H9C2 cells were serum-starved for 24 h in DMEM 1x (11966025; Thermo Fisher Scientific, MA, USA) medium with glucose (5 mM). After serum starvation medium was changed to 0.1% vehicle control medium (DMEM 1X, glucose (5 mM) and BSA (0.1%)) containing LPA (10 µM or 20 µM) and cells were incubated for 16 h. Thereafter, cells were incubated for 15 min with DMEM 1X and glucose (5 mM) with or without insulin (400 nM) to determine the effect of LPA signalling on insulin signalling. Through trial and error, 400 nM insulin was determined to be the lowest

concentration able to stimulate insulin response in our H9C2 cells (200 nM insulin was used on other cell-types which required lower concentrations to elicit a response). Cells were rinsed with PBS before every media change. After incubation with/without insulin, cells were rinsed with ice cold PBS and then harvested in 1 ml of ice cold PBS.

2.2.6.2 Incubation of H9C2 cells with palmitate and LPA

Differentiated H9C2 cells were serum-starved for 24 h in DMEM 1X (11966025; Thermo Fisher Scientific, MA, USA) medium with glucose (5 mM). After serum starvation medium was changed to 0.2 mM PA medium (palmitate (0.2 mM), BSA (2%), glucose (5 mM) in DMEM 1X) and 2% vehicle control medium BSA (2%), glucose (5 mM) in DMEM 1X), and incubated for 24 h, or changed to 0.8 mM PA medium (palmitate (0.8 mM), glucose (5 mM) in DMEM 1X) and 2% vehicle control medium and incubated for 16 h. For co-incubation of cells with LPA and palmitate, differentiated H9C2 cells were serum-starved (24 h) and medium was changed to 2% vehicle control medium, 20 μM LPA medium, 0.8 mM PA medium or 20 μM LPA and 0.8 mM PA medium (BSA (2%), LPA (20 μM), palmitate (0.8 mM), and glucose (5 mM) in DMEM 1X) and incubated for 16 h. For co-incubation of cells with lower palmitate concentration (0.2 mM), media was changed to 2% vehicle control, 20 μM LPA medium, 0.2 mM PA medium or 20 μM LPA and 0.2 mM PA medium and incubated for 24 h. To examine insulin signalling, cells were then incubated with DMEM 1X and glucose (5 mM) medium with or without insulin (400 nM) for 15 min. Cells were rinsed with PBS before every media change. After the 15 min incubation cells were rinsed with ice cold PBS, then harvested in ice cold PBS (1 ml).

2.2.6.3 Insulin stimulation of isolated adult cardiomyocytes

Cardiomyocytes isolated from wildtype and Het ATX-KO mice fed chow or HFHS were allowed to attach to laminin-coated plates (50,000 cells/35 mm plate) for 2 h and then serum-starved for 2 h in serum-free plating medium. After serum starvation, cells were incubated for 15 mins with either DMEM 1X and glucose (5 mM) with and without insulin (200 nM) to determine insulin signalling. Cells were rinsed with PBS before every media change. After the last incubation, cells were rinsed with ice cold PBS, then harvested in 1 ml of ice cold PBS.

2.2.6.4 Incubation of neonatal rat cardiomyocytes with palmitate and LPA

After serum starvation, media was changed to DMEM 1X (11966025; Thermo Fisher Scientific, MA, USA), BSA (2%), ARAC (10 µmol), gentamycin (50 µg/ml), penicillin-streptomycin (1%), glucose (10 mM) supplemented with either LPA (20 µM), PA (0.8 mM), or a combination of, or PA (0.8 mM) and LPA (20 µM) and incubated for 16 h. To assess insulin signalling, cells were incubated for 15 mins with either DMEM 1X and glucose (5 mM) with or without insulin (200 nM). Cells were rinsed with PBS before every media change. After the last incubation, cells were rinsed with ice-cold PBS and then harvested in 1 ml of ice cold PBS.

2.2.7 Fluorescence Microscopy

To determine the effects of co-incubation of LPA and palmitate on oxidative stress, differentiated H9C2 cells were incubated in vehicle control medium or 0.8 mM PA, 20 µM LPA or 0.8 mM PA and 20 µM LPA media for 16 h. Because this concentration of palmitate increases inflammation and apoptosis, the effect of co-incubation of LPA with lower concentration of palmitate was also tested. H9C2 cells

were incubated with vehicle control medium, 0.2 mM PA medium, 20 μM LPA medium or 0.2 mM PA with 20 μM LPA medium for 24 h. Thereafter, media were changed to DMEM 1X medium with glucose (5 mM) and MitoSOX (3 μM; Stock 5 mM MitoSOX in DMSO, Thermo Fisher scientific, M36008 Ex/Em 510/580 nm), and incubated for 15 min followed by counter staining of nuclei with Hoechst 33342 (Thermo Fisher scientific) for 7 min. Live cell images at 20X magnification were obtained using an EVOS microscope and Zeiss near confocal microscope, and fluorescence intensity was measured using Cell Profiler software (Carpenter Lab, Broad Institute of Harvard and MIT).

2.2.8 Assessment of Cell Viability

To evaluate cell viability and proliferation of H9C2 cells following incubation with palmitate and/or LPA, cells were seeded in a 96 well plate (10,000 cells/well) and incubated in the presence or absence of LPA and palmitate as indicated in section 2.2.6.2 and cell viability was assessed using PrestoBlue™ Cell Viability Reagent (Life Technologies A13262,), which is reduced by metabolically active cells transforming the solution from blue to a pink and increasing absorbance compared to metabolically inactive cells. After incubation with palmitate and/or LPA, media were carefully removed using a multichannel pipette to not disrupt the cell monolayer. Cells were rinsed with PBS and incubated with 1X PrestoBlue™ Cell Viability Reagent (1:10 dilution in media containing glucose (5 mM) in DMEM 1X)(2 h at 37 °C and 5% CO_2). Absorbance was measured at 570 nm using the Synergy H4 Hybrid Microplate reader and absorbance of medium alone was used as reference normalization.

2.3 Immunoblot Analysis

Heart lysates were subjected to sodium dodecyl sulfate-polyacrylamide gel electrophoresis (SDS – PAGE), proteins were transferred onto a nitrocellulose membrane and blotted proteins were visualized using reversible Coomassie stain (24580; MemCode Reversible protein Stain, Pierce, Thermo Fisher Scientific). Reversible stain was erased and membrane was blocked in 5% skim milk in Tris-buffered saline with Tween 20 (TBS-T; Tris (20 mM), NaCl (150 mM), Tween 20 (0.1%)) for 1 h. Targets were probed overnight (4ºC) using the primary antibodies (1:1000, milk (1%) in TBST): anti-Cleaved Caspase 3 (9664; Cell Signaling), anti-pJNK T183/Y185(4688; Cell Signaling), anti-JNK (sc-571; Santa Cruz), anti-pP70S6K Thr389 (9234; Cell Signaling), anti-p70S6K (9202; Cell Signaling), anti-pS6 Ser240/244 (2215; Cell Signaling), anti-S6 (2217; Cell Signaling), anti-Pan Actin (sc-1616; Santa Cruz), anti-pAKT Ser473 (sc-7985; Santa Cruz), anti-pAKT Thr308 (9275; Cell Signaling), anti-AKT (5-591; Millipore), anti-IR 1162/1163 (44804G; Life Technologies), anti-IR beta (sc-713; Santa Cruz), anti-pGSK3α/β Ser21/9 (9331; Cell Signaling), anti-GSK3 (9315; Cell Signaling), anti-SDHA (ab14715; Abcam), anti-IRS1 Y612 (44-816; Novex), anti-RAN (610341; BD Biosciences). Incubation with horseradish peroxidase-conjugated anti-rabbit (sc-2054; Santa Cruz), anti-mouse (sc-2055; Santa Cruz), or anti-goat (sc-2020-dup11501; Santa Cruz) secondary antibody (1:2000 in 5% skim milk in TBS-T) was performed (room temperature for 1 h). Immunoblots were developed using the Western Lightning Plus-ECL enhance chemiluminescence substrate (Perkin Elmer, Waltham, MA). Densitometry analysis was performed using Image lab software (Bio-Rad) and band intensity was corrected to protein stain then loading control or total protein.

2.4 Sarcomere Shortening Analysis

From each group of wildtype and Het ATX-KO mice fed HFHS or chow diet, hearts were excised and cardiomyocytes were isolated as described in section 2.2.4 and seeded at 25,000 cells/coverslip in plating medium on 25 mm by 25 mm coverslips. After 2 h to allow cardiomyocytes to attach to laminin coated coverslips, cardiomyocytes were used to determine contractility of wildtype versus Het ATX-KO cardiomyocytes after 20 weeks of chow or HFHS diet. Cardiomyocytes in EBSS medium (14155063; Thermo Fisher Scientific) containing calcium (1.25 mM), were electrically stimulated (10 V at 1 Hz for 1-1.5 mins; Ionoptix electrical stimulator). Sarcomere length was determined using the PTI RatioMaster (HORIBA) monochromator-based wide-field microscope system. The sarcomere shortening module of the PTI RatioMaster was set to collect 30 measurements of sarcomere length per contraction. From each contraction, baseline length, percent sarcomere shortening, rate of contraction and rate of relaxation was measured. Each cardiomyocyte analyzed for sarcomere length was considered an n of 1 and 10 contractions were averaged to determine baseline length, the percentage sarcomere shortening, rate of contraction and rate of relaxation for each cardiomyocyte.

2.5 Statistical Analysis

Results are expressed as mean ± S.E.M. Comparison between multiple groups was performed using a One-way or Two-way analysis of variance (ANOVA) followed by Tukey multiple comparison test or Sidak multiple comparison test. Unpaired t-tests were also performed where indicated using GraphPad Prism software. P-value of less than 0.05 were considered statistically significant.

CHAPTER 3: RESULTS

3.1 Lysophosphatidic Acid Upregulates Insulin Signalling Targets in Insulin-Sensitive H9C2 Cells.

Insulin signalling activates PI3K, which leads to PDK1 activation and upregulation of both AKT and P70S6K pathways [137]. Signalling through LPA receptors activates PI3K and therefore may influence insulin signalling (Figure 3.1 B) [138]. Through activation of PI3K, LPA can upregulate AKT and P70S6K pathways [139, 140] and therefore may be an enhancer of insulin signalling. On the other hand, chronic upregulation of P70S6K can trigger a negative feedback loop, which results in the inhibition of insulin receptor substrate, and decrease of insulin signalling [67, 141, 142]. To examine the effects of LPA on cardiac insulin signalling, I employed an *in vitro* model of differentiated H9C2 cardiomyofibroblast cells incubated in the absence or presence of oleoyl-LPA (18:1), which is an abundant LPA species in plasma and commonly used in laboratory experiments [140]. H9C2 cells are derived from embryonic rat heart, can be differentiated to myotubes, and exhibit signalling properties that are similar to cardiac muscle cells [143]. In this study, differentiated H9C2 cells were incubated with LPA (10

μM and 20 μM) bound to delipidated BSA (0.1%), mimicking physiological and pathophysiological serum concentrations, respectively [127, 140, 144], for 16 h. Control cells were incubated with BSA (0.1%). Thereafter, cells were further incubated with or without insulin (400 nM, for 15 mins) and phosphorylation of major insulin signalling targets, specifically AKT, P70S6K and S6, in cell lysates was examined by immunoblotting analysis (Figure 3.1 C).

At baseline, LPA (10 μM and 20 μM) significantly increased levels of AKT phosphorylated at S473 4.7-fold and 6.5-fold, respectively, compared to vehicle control (Figure 3.1 D). Incubation with insulin led to the significant upregulation of AKT pS473 levels in all groups. Pre-incubation with LPA (20 μM) significantly increased levels of insulin stimulated AKT pS473 compared to insulin-stimulated vehicle control (Figure 3.1 D), while insulin-stimulated AKT pS473 levels were unchanged upon pre-incubation with LPA (10 μM) (Figure 3.1 D). Despite the upregulation of insulin-stimulated AKT pS473 by LPA (20 μM), the fold stimulation of AKT pS473 levels comparing insulin-stimulated vs. control groups was lower upon LPA pre-incubation. In the vehicle group, insulin stimulation resulted in a 6-fold upregulation of AKT pS473 while only a 1.7 and 1.5-fold upregulation was observed in the LPA (10 μM and 20 μM) groups, respectively (Figure 3.1 D). Taken together, these data suggest that LPA increases AKT pS473 levels in H9C2 cells, but reduces the effectiveness of insulin to stimulate AKT pS473.

Similar to the upregulation of AKT pS473, LPA (10 μM and 20 μM) increased levels of P70S6K phosphorylated at T389 2.0-fold compared to vehicle control (Figure 3.1 E). Incubation with insulin resulted in the upregulation of P70S6K pT389 in all groups. However, the fold stimulation compared to no-insulin control was less upon pre-

incubation with LPA (2.6-fold in vehicle group, 1.7-fold in 10 μM LPA group, 1.8-fold in 20 μM LPA group), suggesting that LPA reduces the insulin-stimulated increase in P70S6K pT389 in H9C2 cells.

In comparison to AKT pS473 and P70S6K pT389, LPA-induced changes in phosphorylated levels of S6 were less pronounced. At baseline, LPA (20 μM) significantly increased levels of S6 phosphorylated at S240/244 by 1.5-fold compared to vehicle control (Figure 3.1 F) while LPA (10 μM) had no effect. Levels of insulin-stimulated S6 p S240/244 were similar between groups with a 1.6-fold, 1.3-fold, and 1.3-fold increase from baseline in vehicle, LPA (10 μM LPA and 20 μM) groups, respectively. These results suggest that, similar to the trend seen in AKT phosphorylated at S473 and P70S6K phosphorylated at T389, pre-incubation with LPA increased baseline levels of S6 phosphorylation at S240/244, resulting in lower insulin-stimulated increase in S6 pS240/244 levels. Taken together, these trends may indicate that increasing concentration of circulating LPA as seen in obesity and insulin resistance, may reduce insulin-stimulated upregulation of key targets in the insulin signalling pathway.

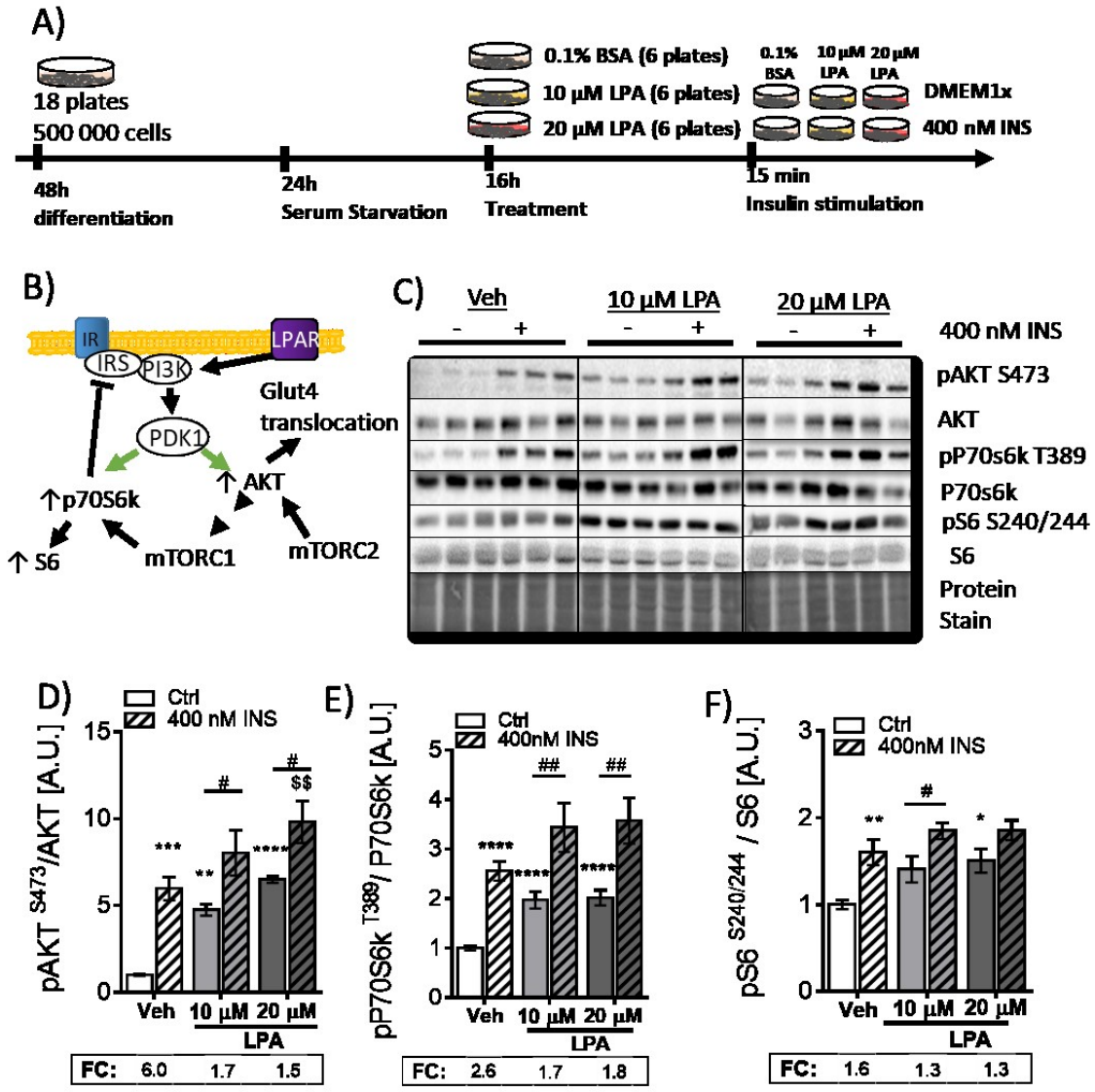

Figure 3. 1. Lysophosphatidic acid (18:1) increases phosphorylation of proteins downstream of PDK1 at baseline and following insulin stimulation.

A) Experimental design and timeline for the incubation of H9C2 cells with BSA (0.1%), LPA (10µM), or LPA (20µM) for 16h and subsequent stimulation with 400nM insulin for 15 minutes. B) Schematic showing how LPA and insulin receptor signalling pathways intercept at PI3K. C) Immunoblot and D) densitometric analysis of AKT phosphorylation at S473 E) densitometric analysis of P70S6K phosphorylation at T389 F) densitometric analysis of S6 phosphorylation at S240/244 normalized to protein stain and respective total protein. Means are noted above bars and fold change to no-insulin control is noted above dotted lines. Graph represents mean ± S.E.M., comparison to vehicle control indicated by *, comparison to vehicle insulin indicated by $, degree of significance is indicated by number of symbols: 1 symbol - $P < 0.05$, 2 symbols - $P<0.01$, 3 symbols - $P<0.001$, 4 symbols - $P<0.0001$; Two-way ANOVA, followed by Sidak's multiple comparison test; n = 9 (three independent experiments with three replicates); Ctrl: no-insulin control, INS: insulin, A.U.: arbitrary units, FC: fold change.

3.2 Incubation With Palmitate Leads to Insulin Resistance in H9C2 Cells.

To determine whether LPA alters insulin signalling in H9C2 cells subjected to conditions mimicking obesity/diabetes, i.e. high concentrations of circulating FA, I sought to establish a lipotoxicity-induced H9C2 insulin resistance model. Lipotoxicity may induce insulin resistance by several mechanisms. Increasing circulating levels of FAs are taken up into cardiac cells by FA transporters, lipoprotein lipase and through passive diffusion, leading to the accumulation of FAs in the cytoplasm that are converted into LC acyl-CoAs [145], which can be oxidized or incorporated into other lipids, e.g. diacylglycerols (DAGs) and ceramides (Figure 3.2 B), which also have lipotoxic properties and can induce apoptotic cell death and interfere with insulin signalling [146]. Specifically, DAGs and LC acyl-CoAs may activate JNK, IKK, and PKC signalling cascades that lead to serine phosphorylation and inhibition of IRS. Additionally, ceramides can inhibit AKT by promoting serine 473 dephosphorylation (Figure 3.2 B) [147, 148].

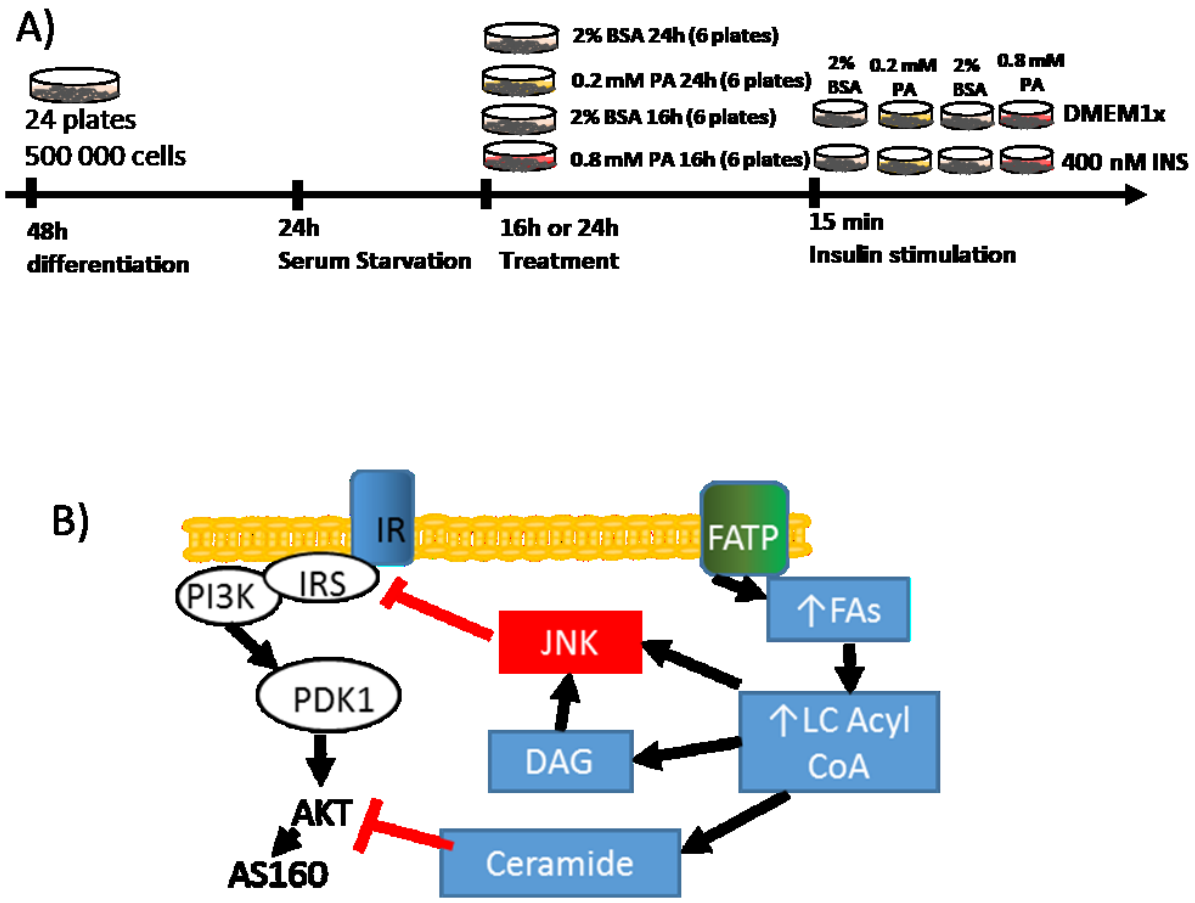

Figure 3. 2. Experimental design for H9C2 cell incubation with palmitate and mechanism of palmitate-induced insulin resistance.
A) Experimental design and timeline of palmitate treatment of H9C2 cells. B) Schematic of how palmitate-induced cellular effects interact with insulin receptor signalling to induce insulin resistance.

To establish a lipotoxicity-induced H9C2 insulin resistance model, I incubated H9C2 cells with either PA (0.2 mM for 24 h) or PA (0.8 mM for 16 h), followed by stimulation with insulin (Figure 3.2 A). Palmitate induces lipotoxic events in cardiac muscle cells [149-151], however, only recently has palmitate been used in H9C2 cells to establish an in vitro myocardial insulin-resistance model [152]. To determine whether incubation with palmitate induces lipotoxicity-induced apoptosis in H9C2 cells, I examined protein levels of cleaved caspase 3 in cell lysates (Figure 3.3 A, B). While

incubation with PA (0.8 mM for 16 h) markedly increased cleaved caspase 3 protein levels compared to control (incubated with delipidated BSA (2%)), incubation with PA (0.2 mM for 24 h) had a much more nuanced effect, leading to only a trend towards increased cleaved caspase 3 protein levels (Figure 3.3 A, B). These data suggest that palmitate stimulates apoptosis in H9C2 cells in a dose-dependent manner. Examination of insulin-stimulated phosphorylation of IRS1 at Y612, AKT at S473 and AS160 at T642 in cell lysates showed that both concentrations of palmitate blunted the insulin-stimulated increase in protein levels of phosphorylated IRS1, AKT, and AS160 (Figure 3.3 A, C-E). These data suggest that low and high concentrations of palmitate induce insulin resistance in H9C2 cells.

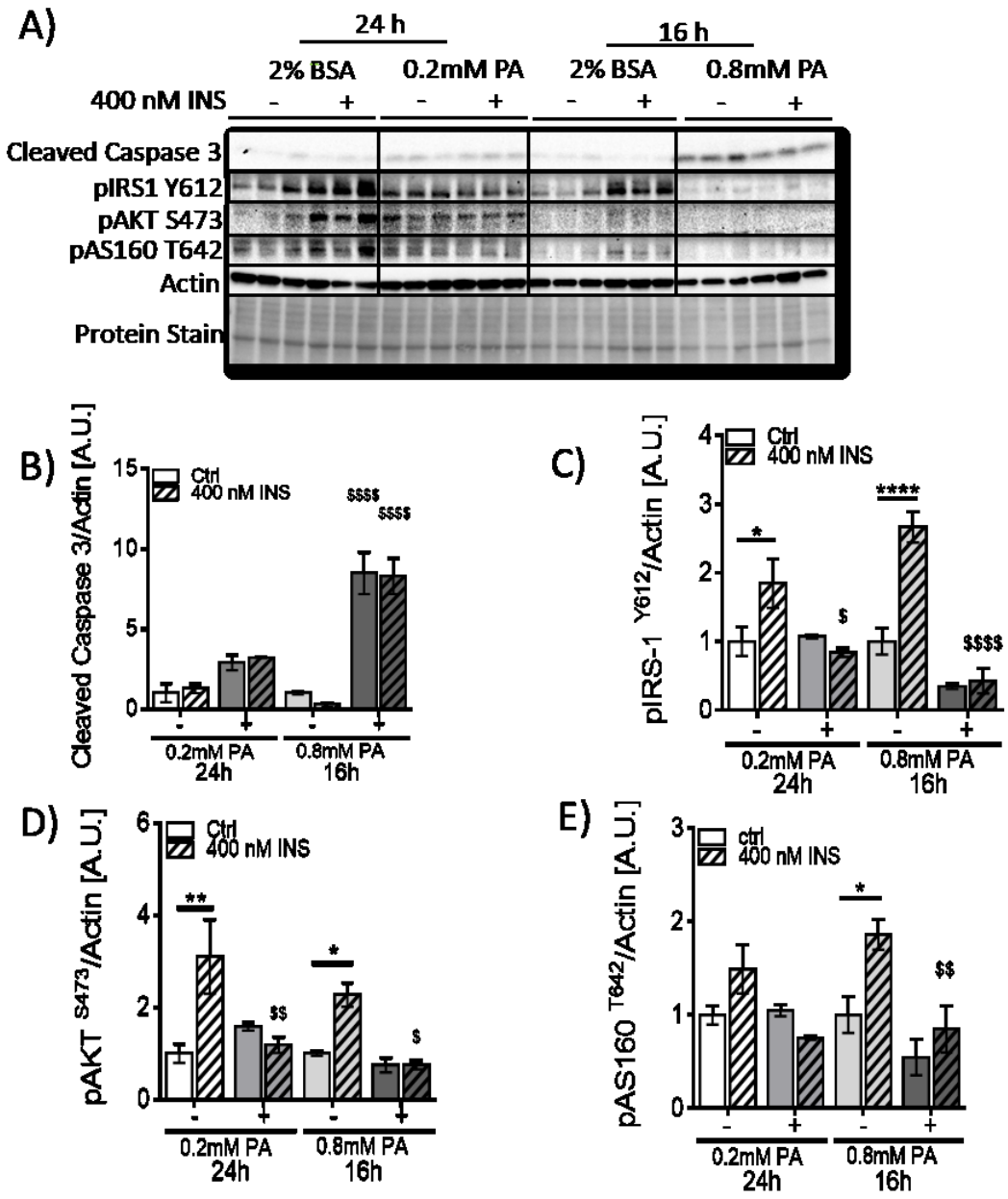

Figure 3. 3. Incubation of H9C2 cells with palmitate induces insulin resistance.
A) Immunoblot and B) densitometric analysis of cleaved caspase 3, C) densitometric analysis of IRS-1 phosphorylation at Y612, D) densitometric analysis of AKT phosphorylation at S473 and E) densitometric analysis of AS160 phosphorylation at T642 normalized to protein stain and actin. Graphs represent mean ± S.E.M., comparison between control and insulin incubated indicated by *; comparison to insulin incubated vehicle is indicated by $, degree of significance is indicated by number of symbols: 1 symbol - $P < 0.05$, 2 symbols - $P<0.01$, 3 symbols - $P<0.001$, 4 symbols - $P<0.0001$; Two-way ANOVA, followed by Sidak's multiple comparison test; n = 3 (1 independent experiment with three replicates). Ctrl: no-insulin control, INS: insulin. A.U.: arbitrary units

3.3. LPA Promotes Insulin Resistance in the Presence of Palmitate in H9C2 Cells

To examine whether LPA can precipitate lipotoxicity-induced insulin resistance, I co-incubated H9C2 cells with LPA and palmitate and performed immunoblot analysis of the cell lysates. Insulin stimulation resulted in a significant upregulation of AKT phosphorylation at S473 in cells pre-incubated with vehicle control medium, medium containing LPA (20 μM) and medium containing PA (0.8 mM), resulting in a 4.3, 2.1 and 2.4-fold increase, respectively. Interestingly, insulin-stimulated upregulation of AKT pS473 phosphorylation was blunted in cells incubated with a combination of LPA (20 μM) and PA (0.8 mM) ($p = 0.09$, Figure 3.4 C). Additionally, insulin-stimulated cells pre-incubated with both LPA and PA had significantly lower AKT phosphorylation compared to cells pre-incubated with 2% vehicle medium and medium containing PA (0.8 mM). These results suggest that co-incubation of H9C2 cells with LPA and palmitate reduced insulin sensitivity compared to other treatment groups stimulated with insulin. Due to variability in protein levels of total AKT protein, notably in the PA (0.8 mM) group (Figure 3.4 D), protein levels of AKT phosphorylated at S473 were also expressed relative to the loading control, SDHA (Figure 3.4 E). When corrected to loading control SDHA, levels of phosphorylated AKT at S473 at baseline significantly increased (2.2-fold) after incubation with LPA (20 μM) compared to vehicle control (Figure 3.4 E), consistent to results in Figure 3.1 D. Moreover, pre-incubation with PA (0.8 mM) resulted in significantly lower AKT pS473 levels following insulin stimulation (2.8-fold increase) compared to vehicle control cells stimulated with insulin (4.0-fold increase) (Figure 3.4 E). Additionally, co-incubation with PA (0.8 mM) and LPA (20 μM) significantly decreased insulin stimulated upregulation of AKT phosphorylated at S473 (1.7-fold

increase) compared to cells pre-incubated with BSA (2%) (4.0-fold increase), LPA (20 μM) (3.2-fold increase and PA (0.8 mM) (2.8-fold increase). Taken together, these data suggest that pre-incubation of H9C2 cells with LPA and palmitate leads to marked insulin resistance at the level of AKT.

Protein levels of phosphorylated P70S6K pT389/P70S6K were significantly increased in insulin-treated groups pre-incubated with palmitate (3.2-fold increase) and palmitate co-incubated with LPA (2.9-fold increase) in comparison to insulin stimulated cells pre-incubated with BSA (2%) or cells pre-incubated with LPA (20 μM) alone (Figure 3.4 F). P70S6K pT389 phosphorylation was also expressed over loading control because palmitate incubation was found to significantly reduce total P70S6K level (Figure 3.4 G). Comparison of non-insulin stimulated groups show total P70S6K level was significantly decreased in cells pre-incubated with PA (0.8 mM), compared to cells incubated with BSA (2%) or LPA (20 μM) (Figure 3.4 G). P70S6K pT389 protein level expressed over loading control showed insulin significantly increased P70S6K pT389 protein level (1.6-fold) in BSA pre-incubated group, PA (0.8 mM) pre-incubated group (2.1-fold) and in the group co-incubated with PA (0.8 mM) and LPA (20 μM)(2.2-fold) compared to their respective non–insulin-stimulated control groups (Figure 3.4 H). Insulin significantly increased P70S6K pT389 protein levels in cells pre-incubated with palmitate (3.8-fold) and cells co-incubated with palmitate and LPA (3.7-fold) compared to cells pre-incubated with BSA (2%) or LPA (20 μM) (Figure 3.4 H). Collectively, these findings suggest that, in the presence of high palmitate concentrations, LPA promotes insulin resistance at the level of AKT, but does not alter P70S6K activation

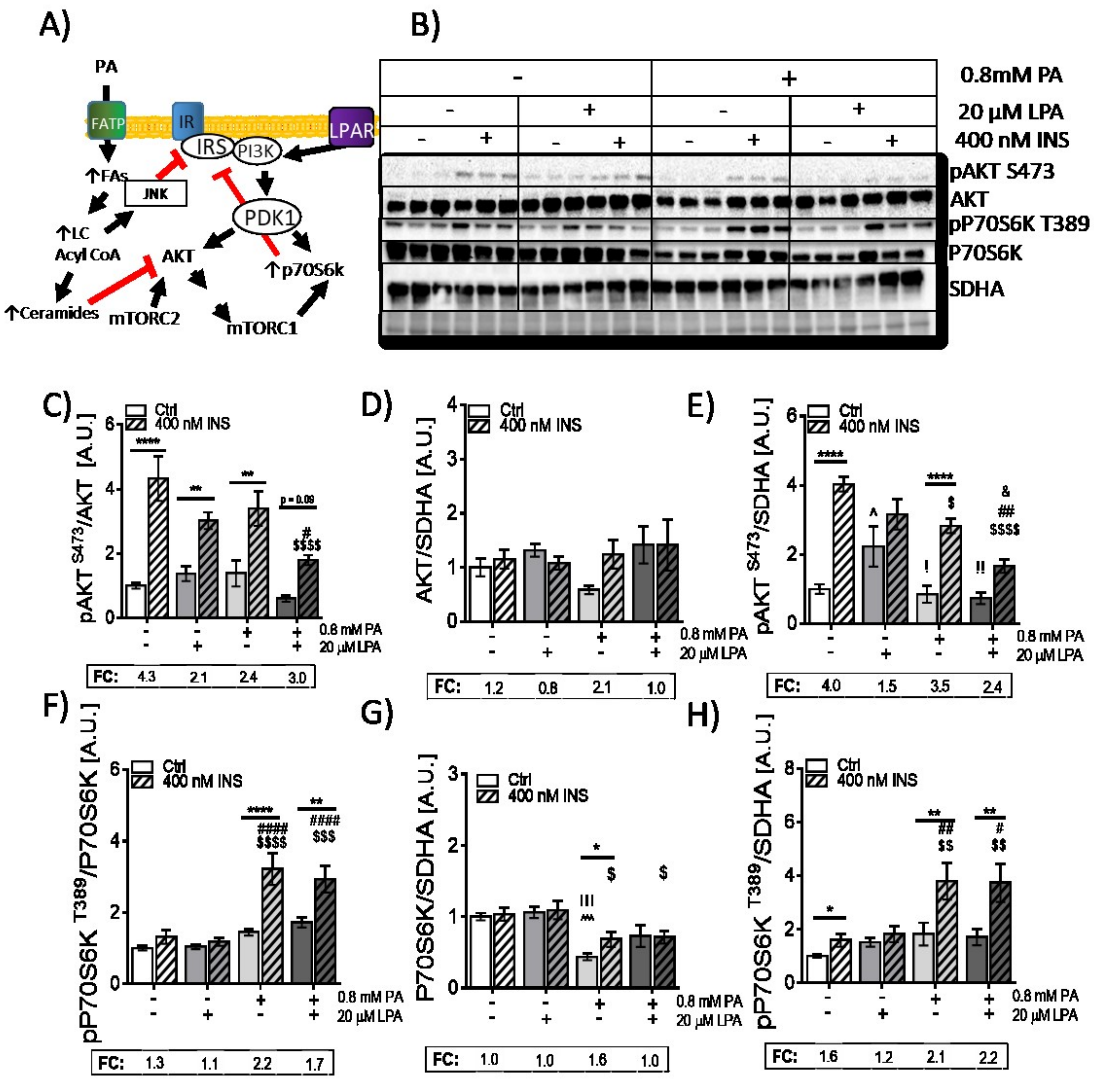

Figure 3. 4. Co-incubation of H9C2 cells with 0.8 mM palmitate and 20 µM LPA decreases levels of AKT pS473.

A) Signalling pathway of LPA, insulin and excessive fatty acids and how they may interact. B) Immunoblot and C) densitometric analysis of AKT phosphorylation at S473 normalized to total AKT, D) densitometric analysis of total AKT normalized to loading control SDHA, E) densitometric analysis of AKT phosphorylation at S473 normalized to total SDHA, F) P70S6K phosphorylation at T389 normalized to total P70S6K, G) densitometric analysis of P70S6K normalized to SDHA, H) densitometric analysis of P70S6K phosphorylation at T389 normalized to SDHA. Graph represents mean ± S.E.M., comparison between control and insulin stimulated groups indicated by *, comparison to vehicle insulin indicated by $, comparison to LPA (20 µM) stimulated with insulin indicated by #; comparison to control LPA (20 µM) indicated by ^; degree of significance is indicated by number of symbols: 1 symbol - $P < 0.05$, 2 symbols - $P<0.01$, 3 symbols - $P<0.001$, 4 symbols - $P<0.0001$; Two-way ANOVA, followed by Sidak's multiple comparison test; n = 9 (three independent experiments with three replicates); Ctrl: no-insulin control, INS: insulin, A.U.: arbitrary units, FC: fold change

3.4 LPA Does not Influence Palmitate-Induced Inflammatory Signalling and Apoptosis in H9C2 Cells.

Once it was established that LPA exacerbated palmitate-induced insulin resistance in H9C2 cells, I next wanted to examine whether LPA's effect on insulin signalling may be due to the stimulation of inflammatory signalling. Increased inflammation is a known mechanism of insulin resistance and plays an important role in palmitate-induced insulin resistance [24, 31, 98]. To examine the effect of LPA on palmitate-induced inflammatory signalling, H9C2 cells were co-incubated with PA (0.8 mM) and LPA (20 μM) for 16 h (Figure 3.5 A). Protein levels of JNK phosphorylated at T183/Y185, a marker of inflammation [153, 154], were determined through immunoblot analysis. As expected, incubation with palmitate led to an upregulation of phosphorylated JNK levels in both non-insulin (3.1-fold increase) and insulin-stimulated (4.6-fold increase) groups compared to cells incubated with BSA (2%) or LPA (20 μM) (Figure 3.5 B, C). Co-incubation of cells with palmitate and LPA led to an upregulation of phosphorylated JNK levels in both non-insulin (3.5-fold increase) and insulin stimulated (4.9-fold increase) groups that was similar to cells incubated with only palmitate (Figure 3.5 B, C). These results suggest that LPA does not ameliorate or exacerbate palmitate-induced inflammatory signalling. In addition to inducing inflammatory signalling, palmitate or, more specifically, palmitate-derived ceramides are known to induce apoptosis leading to ventricular dysfunction [155-157]. Therefore, I next determined if co-incubation of cells with palmitate and LPA exacerbates palmitate-induced apoptosis. Apoptosis was determined by examining protein levels of cleaved caspase 3, a marker of apoptosis and cell viability through PrestoBlue™ cell viability assay (Figure 3.5 D-E). Incubation with

doxorubicin (10 μM, DOX), a potent cytotoxic agent [158, 159], served as positive control in the cell viability assay.

As expected, incubation with palmitate led to an upregulation of cleaved caspase 3 protein levels in both non-insulin (8.1-fold increase) and insulin stimulated (4.6-fold increase) groups compared to cells incubated with 2% BSA or 20 μM LPA (Figure 3.5 B,D). Co-incubation of palmitate and LPA similarly led to an upregulation of cleaved caspase 3 protein levels in both non-insulin (10.0-fold increase) and insulin stimulated (3.1-fold increase) groups compared to cells incubated with BSA (2%) or LPA (20 μM)(Figure 3.5 B,D). Interestingly, 15 min insulin stimulation significantly decreased cleaved caspase 3 levels in cells incubated with palmitate by 1.8-fold and cells incubated with both palmitate and LPA by 3.2-fold compared to their respective controls incubated in the absence of insulin (Figure 3.5 B, D). Cell viability assay showed that a 16 h incubation with PA (0.8 mM) reduced cell viability to 39% compared to DMEM 1X medium supplemented with glucose (5 mM) which was set to 100% cell viability. Additionally, PA (0.8 mM) incubation significantly reduced cell viability compared to cells incubated with DOX (51% cell viability). Cell viability was 88% in the group incubated with BSA (2%) and 84% in cells incubated with LPA (20 μM) (Figure 3.5 E). Co-incubation with PA (0.8 mM) and LPA (20 μM) reduced cell viability to 46%, which was not significantly different to the viability of cells incubated with palmitate alone (Figure 3.5 E). Since PA (0.8 mM) showed a dramatic effect on cell viability, incubation with a lower concentration of palmitate (0.2 mM) was used to determine if LPA exacerbated cell apoptosis at lower and less toxic palmitate concentrations. Cells were incubated with palmitate (0.2 mM) for 24 h, a concentration and time point that induced

insulin resistance, but not significantly increased cleaved caspase 3 levels (Figure 3.3 B). 24 h incubation with PA (0.2 mM) reduced cell viability to 68%, which was significant compared to DMEM 1X medium supplemented with glucose (5 mM) (set to 100% cell viability) and BSA (2%), which showed 98% cell viability. Similarly, co-incubation with PA (0.2 mM) and LPA (20 μM) reduced cell viability to 68%, (Figure 3.5 F). These results suggest that at lower levels of palmitate, LPA does not ameliorate or exacerbate the palmitate-induced reduction in cell viability. In the absence of palmitate, 16-h incubation with LPA did not alter cell viability (84%), while a 24-h incubation with LPA significantly reduced cell viability (75%) compared to control incubated with BSA (2%) (Fig. 3.5 E, F), suggesting that LPA reduces cell survival/proliferation in a time-dependent manner.

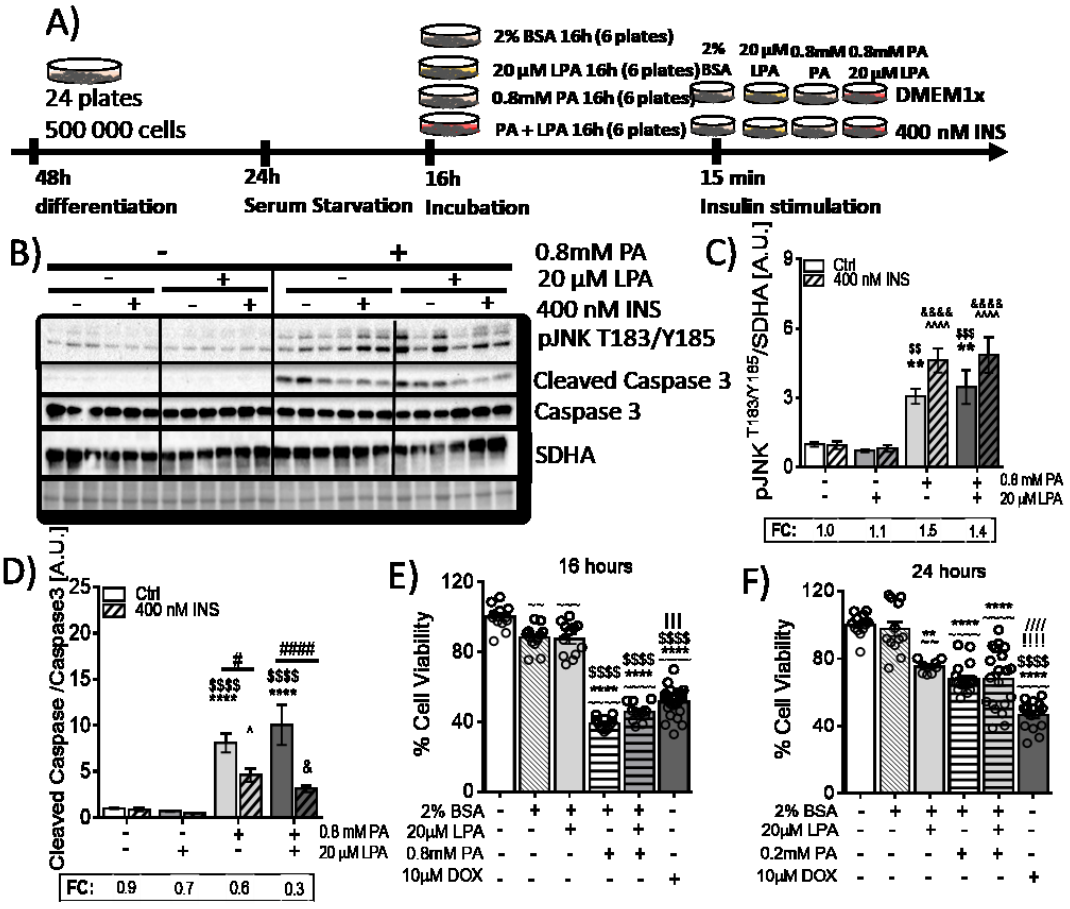

Figure 3. 5. Co-incubation of H9C2 cells with palmitate and LPA does not attenuate palmitate-induced inflammation and apoptosis.

A) Experimental design and timeline of co-incubation of H9C2 cells with PA (0.8mM) and LPA (20 µM) and subsequent insulin stimulation; control cells were incubated with BSA (2%). B) Immunoblot and C) densitometric analysis of JNK phosphorylation at T183/Y185 normalized to loading control SDHA, D) densitometric analysis of cleaved caspase 3 normalized to caspase 3. E) Viability of H9C2 cells 16 h after incubation with 0.8 mM palmitate and/or LPA (20µM). F) Viability of H9C2 cells 24 h after incubation with 0.2 mM palmitate and/or LPA (20µM). Graph represents mean ± S.E.M., comparison to vehicle control indicated by *, comparison to LPA (20 µM) control indicated by $, comparison to vehicle insulin indicated by ^, comparison to LPA (20 µM) insulin indicated by &, comparison between control and insulin groups indicated by #, comparison to DMEM 1X indicated by ~, comparison to palmitate induction indicated by ! , comparison to palmitate and LPA co-incubation indicated by /, degree of significance is indicated by number of symbols: 1 symbol - $P < 0.05$, 2 symbols - $P<0.01$, 3 symbols - $P<0.001$, 4 symbols - $P<0.0001$; Two-way ANOVA, followed by Sidak's multiple comparison test; n = 9 (three independent experiments with three replicates) was used for densitometric statistics; One-way ANOVA, followed by Tukey's multiple comparison test was used for cell viability statistics; n = 12 (3 independent experiments with 4 replicates); Ctrl: no-insulin control, INS: insulin, A.U.: arbitrary units.

3.5 LPA Increases Oxidative Stress in the Presence of Palmitate in H9C2 Cells.

Obesity is associated with increased oxidative stress in the heart and oxidative stress has also been implicated in the pathophysiology of insulin resistance. Thus, I next evaluated if LPA increases oxidative stress in H9C2 cells incubated with palmitate. Cells incubated for 24 h with BSA (2%), LPA (20 μM), PA (0.2 mM) and co-incubated with PA (0.2 mM) and LPA (20 μM) were exposed to MitoSOX (3 μM), a fluorescent indicator of oxidative stress, which is specifically oxidized by superoxides producing an oxidized product that is highly fluorescent upon binding to nucleic acids. Incubation with MitoSOX showed that incubation with BSA (2%) and LPA (20 μM) did not induce oxidative stress through mitochondrial superoxide production (Figure 3.6 B-E). The group incubated with PA (0.2 mM) showed a slight increase in superoxide production, but was not significantly different to cells incubated with BSA (2%) or LPA (20 μM) (Figure 3.6 B-C). Interestingly, co-incubation of cells with PA (0.2 mM) and LPA (20 μM) significantly increased superoxide levels in these cells in comparison to all other groups (Figure 3.6 B-C). Incubation with PA (0.8 mM) and co-incubation of PA (0.8 mM) and LPA (20 μM) significantly increased superoxide levels compared to cells incubated with BSA (2%) or LPA (20 μM) (Figure 3.6 D-E). These results suggest that, depending on the dose of palmitate, LPA can induce oxidative stress through increased mitochondrial superoxide production.

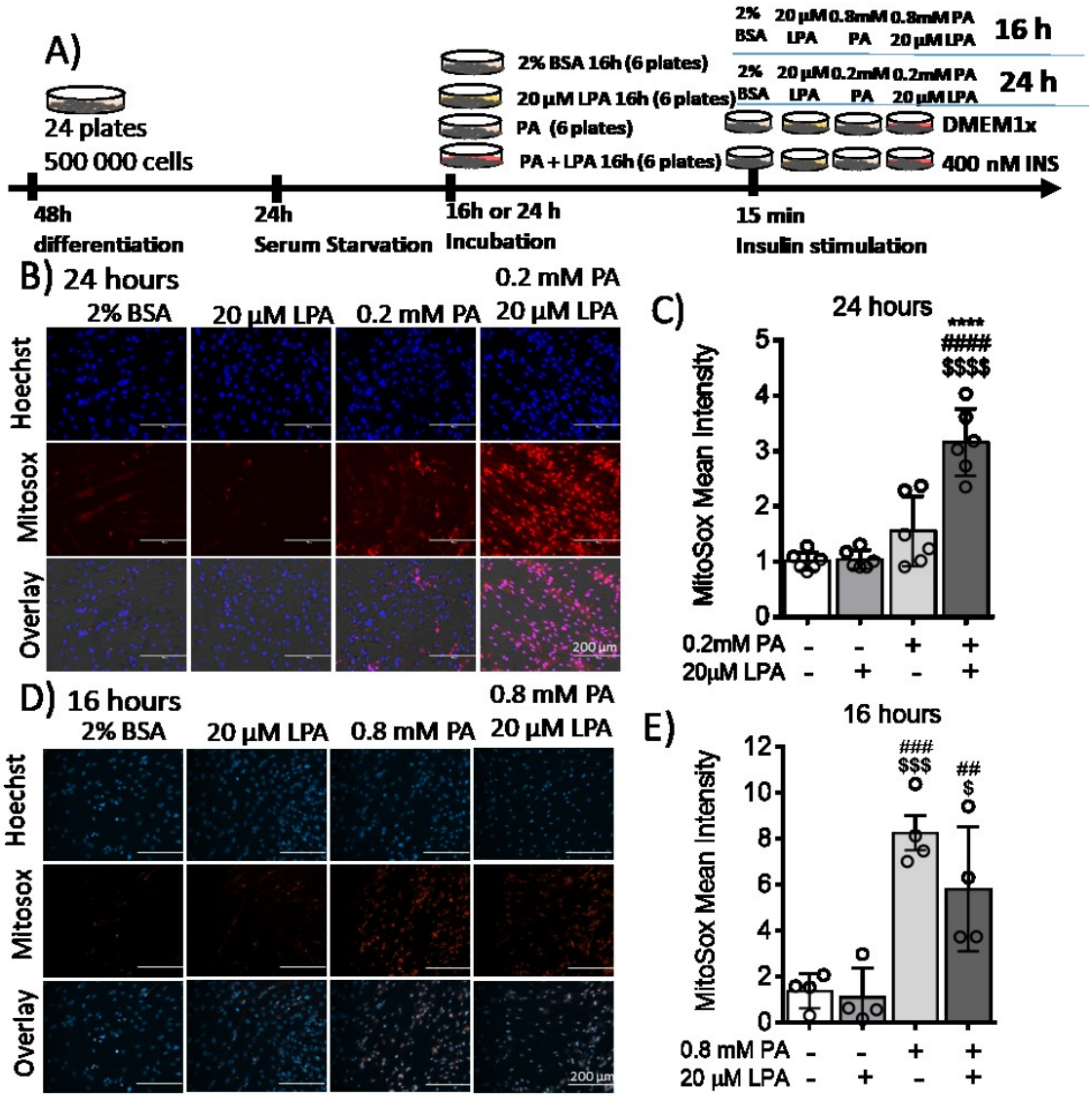

Figure 3. 6. Co-incubation of H9C2 cells with low palmitate and LPA increases oxidative stress.

A) Experimental design and timeline of co-incubation of H9C2 cells with PA (0.8 mM) and LPA (20 µM) and subsequent insulin stimulation; control cells were incubated with 2% BSA. B) Representative fluorescence microscopy images of Hoechst 33342 and MitoSOX (3µM) stained cells after 24 h incubation with indicated substrates, images taken with EVOS Microscope (20X magnification), and C) graphical representation of the fluorescent images. D) Fluorescence microscopy images (20x magnification) of Hoechst 33342 and MitoSOX (3µM) stained cells after 16 h incubation with indicated substrates, images taken with Zeiss Microscope, and E) graphical representation of the fluorescent images. Graph represents mean ± S.E.M., comparison to vehicle control indicated by *, comparison to vehicle insulin indicated by $, degree of significance indicated by number of symbols; 1 symbol - $P < 0.05$, 2 symbols - $P<0.01$, 3 symbols - $P<0.001$, 4 symbols - $P<0.0001$; one-way ANOVA, followed by Tukey's multiple comparison test; n = 4-6 independent experiments with 50-200 florescent measures per image.

3.6 LPA Exacerbates Insulin Resistance in The Presence of Palmitate in Neonatal Rat Cardiomyocytes.

I then examined whether LPA also exacerbates insulin resistance in primary neonatal rat cardiomyocytes (NRCMs), which more closely reflect cardiomyocytes in the intact heart. Incubation with PA (0.8 mM) and/or LPA (20 μM) for 16 h caused extensive cell death in NRCMs (data not shown). Due to this increased sensitivity to palmitate and LPA, cells were incubated with PA (0.6 mM) and/or LPA (10 μM) for 16 h. Co-incubation of cardiomyocytes with PA (0.6 mM) and LPA (10 μM) significantly decreased insulin-stimulated phosphorylation of IR at Y1162/1163, GSK3α/β at S21/9 and S6 at S240/244 in comparison to cells incubated with palmitate alone (Figure 3.7 B, C D, and E). These results are consistent with results obtained with H9C2 cells. Taken together, these data suggest that LPA exacerbates palmitate-induced toxicity and insulin resistance in primary cardiomyocytes.

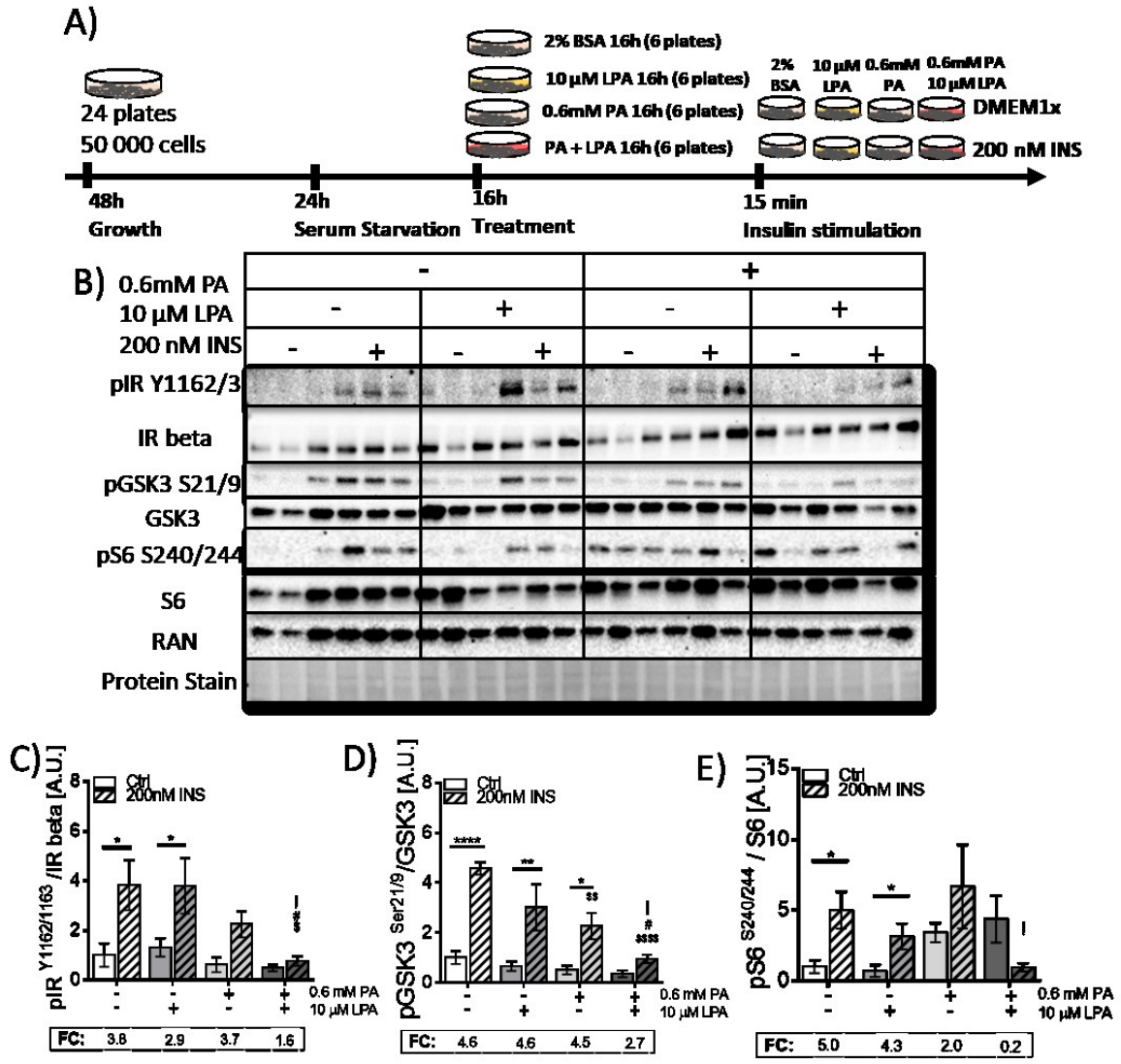

Figure 3. 7. Palmitate and LPA co-incubation decreases protein level of downstream insulin signalling targets in neonatal rat cardiomyocytes.

A) Experimental design and timeline, of NRCMs incubated with BSA (2%), LPA (10 µM), palmitate (0.6 mM) and co-incubated with palmitate (0.6 mM) and LPA (10 µM). B) Immunoblot and C) densitometric analysis of IR phosphorylation at Y1162/1163 normalized to IR beta. D) densitometric analysis of GSK3α/β phosphorylation at S21/9 normalized to GSK3 E) densitometric analysis of S6 phosphorylation at S240/244 normalized to S6. Graph represents mean ± S.E.M., comparison between plus or minus insulin groups indicated by *, comparison to vehicle insulin indicated by $, comparison to LPA (10 µM) insulin indicated by #, comparison to palmitate (0.6 mM) insulin indicated by !, degree of significance is indicated by number of symbols: 1 symbol - $P < 0.05$, 2 symbols - $P<0.01$, 3 symbols - $P<0.001$, 4 symbols - $P<0.0001$; Two-way ANOVA, followed by Sidak's multiple comparison test; and unpaired t test; n = 3 (3 groups of pooled 10-20 hearts).

3.7 Heterozygous Autotaxin Knockout Mice Fed High Fat-High Sucrose Diet, Show Reduced Weight Gain and are Protected From Myocardial Insulin Resistance.

Since our data suggested that LPA exacerbates insulin resistance in lipotoxic conditions *in vitro* using H9C2 cells and NRCMs, I next investigated if a reduction of circulating LPA *in vivo* could improve cardiac insulin sensitivity in mice fed an obesogenic diet containing high fat and high sucrose (HFHS). We utilized mice that were haploid deficient of autotaxin (Het ATX-KO) [160] and littermate wildtype mice as controls. Mice were donated by Dr. Vassilis Aidinis and our mouse cohorts were bred and maintained by Kenneth D'Souza and myself. Het ATX-KO mice have ~50% reduced circulating ATX and LPA levels and display a normal phenotype while total ATX-KO is embryonically lethal [160]. To induce obesity, male wildtype and Het ATX-KO mice were fed chow or HFHS diet for 20 weeks and weight gain was recorded weekly (Figure 3.8 A, B). While both wildtype and Het ATX-KO mice developed obesity following HFHS feeding, Het ATX-KO mice fed HFHS gained less weight than wildtype mice, which was evident after 12 weeks of feeding (Figure 3.8 B). To examine myocardial insulin signalling, chow and HFHS-fed mice were injected with saline or insulin (10 units/kg). Following insulin injection, blood glucose dropped markedly and to a comparable level in all groups examined (Figure 3.8 C). I subsequently performed immunoblot analysis to determine insulin-stimulated AKT phosphorylation in lysates of heart ventricles. Insulin stimulation led to a significant upregulation of AKT phosphorylation at T308 and S473 in all groups (Figure 3.9 B-D). As expected, insulin-stimulated AKT phosphorylation was markedly reduced in hearts from HFHS-fed compared to chow-fed wildtype mice, demonstrating that HFHS feeding led to

myocardial insulin resistance (Figure 3.9 B, -D). Interestingly, levels of phosphorylated AKT at S473 was higher in HFHS-fed Het ATX-KO mice compared to wildtype after insulin injection. Levels of phosphorylated AKT at T308 also increased after insulin injection in HFHS-fed Het ATX-KO mice, but were not significantly different from wildtype mice (Figure 3.9 B, -D). These data suggest that heterozygous ATX deficiency and chronically reduced LPA levels may protect against obesity-induced cardiac insulin resistance *in vivo*.

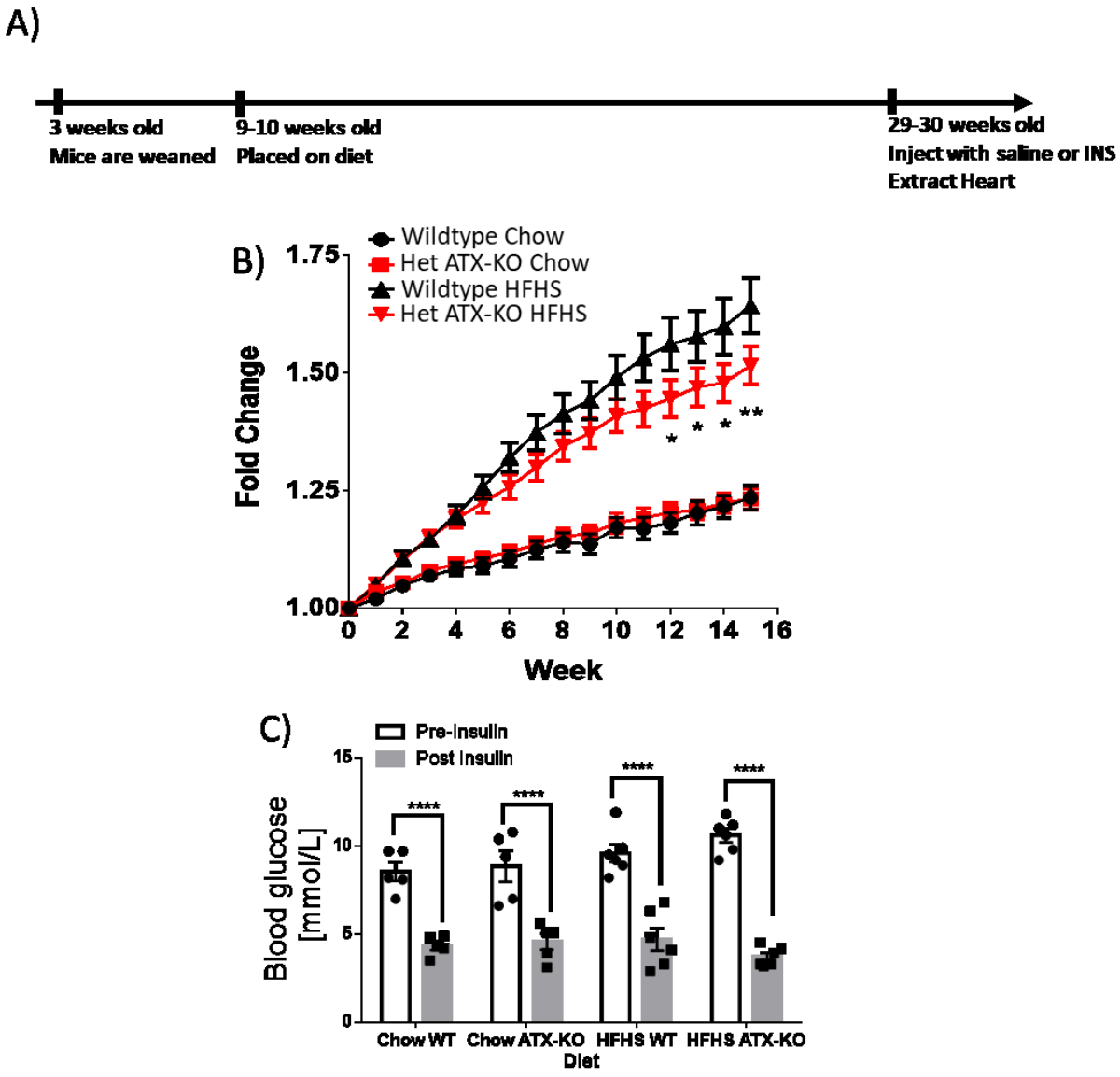

Figure 3. 8. Heterozygous autotaxin knockout mice fed high-fat high-sucrose diet show reduced weight gain and blood glucose drop after 10U/kg insulin injection is evident in all groups.

A) Timeline of HFHS feeding experiments in wildtype and ATX Het KO mice. B) Weight gain expressed as fold change from initial weight of wildtype and Het ATX-KO mice fed chow or HFHS diet. C) Measured blood glucose of wildtype and autotaxin heterozygous knockout mice fed chow or HFHS diet after insulin injection (10U/kg). Graph represents mean ± S.E.M., comparison between wildtype and Het ATX-KO mice indicated by *, comparison between pre and post insulin injection indicated by $, degree of significant indicated by number of symbols: 1 symbol - $P < 0.05$, 2 symbols - $P<0.01$, 3 symbols - $P<0.001$, 4 symbols - $P<0.0001$; Two-way ANOVA, followed by Sidak's multiple comparison test; n = 5-6 mice per group.

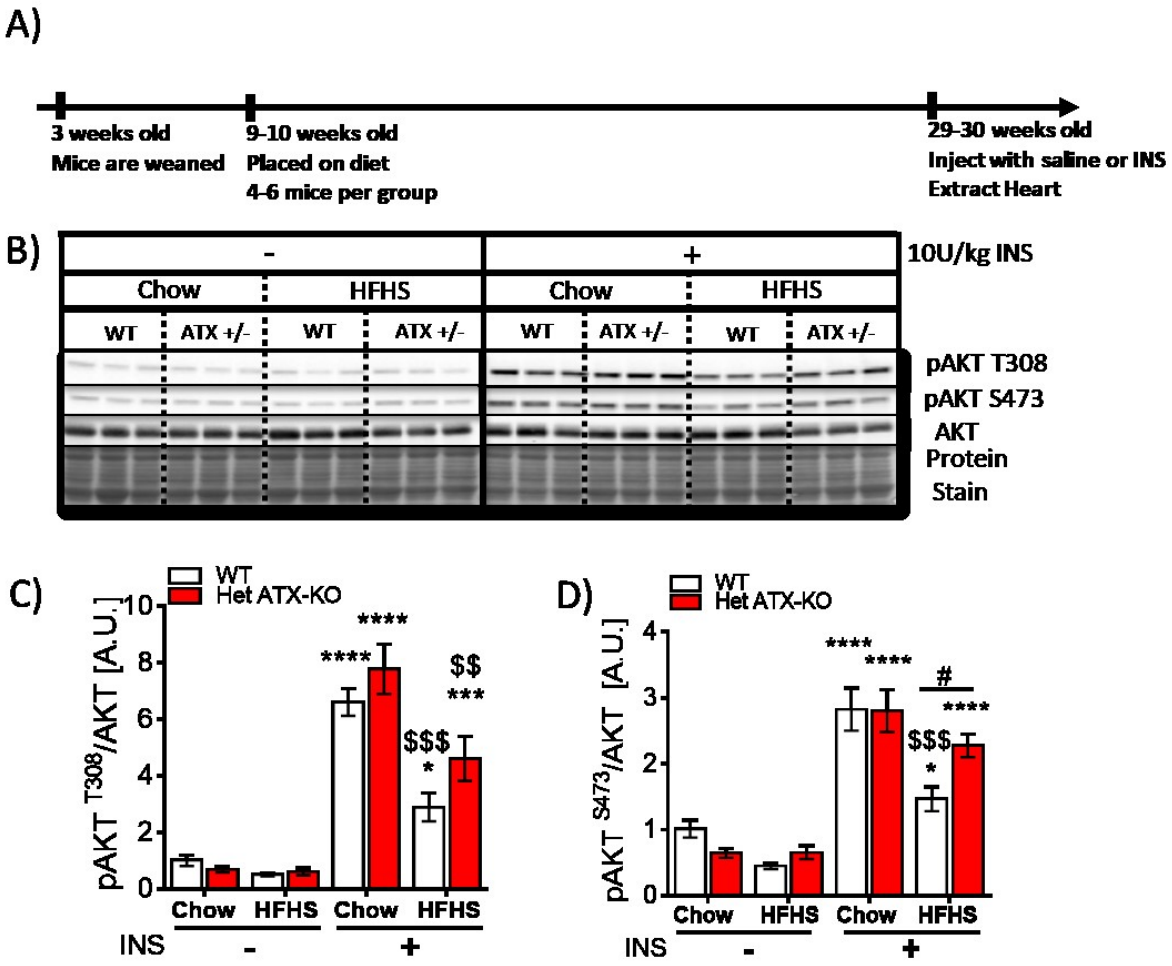

Figure 3. 9. Heterozygous autotaxin knockout mice fed high-fat high-sucrose diet show improved insulin sensitivity compared to wildtype mice.
A) Timeline and experimental design of HFHS diet study and heart extraction. B) immunoblot analysis of whole heart lysates of wildtype and Het ATX-KO mice fed chow or HFHS diet. C) densitometric analysis of AKT phosphorylation at T308 normalized to total AKT, D) densitometric analysis of AKT phosphorylation at S473 normalized to total AKT. Graph represents mean ± S.E.M., comparison to respective insulin minus group indicated by *, comparison to respective chow plus insulin group indicated by $, comparison between wildtype and Het ATX-KO indicated by #, degree of significant indicated by number of symbols: 1 symbol - $P < 0.05$, 2 symbols - $P<0.01$, 3 symbols - $P<0.001$, 4 symbols - $P<0.0001$; Two-way ANOVA, followed by Sidak's multiple comparison test; n = 4-6 mice per group.

3.8 Cardiomyocytes Isolated From Heterozygous Autotaxin Knockout Mice Fed High-Fat High-Sucrose Diet Show Improved Insulin Sensitivity.

Since the heart consists of many cell types besides cardiomyocytes, I next determined insulin signalling specifically in cardiomyocytes isolated from hearts of wildtype and HET ATX-KO mice fed chow or HFHS diet following incubation of cells with insulin (200 nM, 15 mins). Insulin-stimulated AKT phosphorylation at S473 was reduced in cardiomyocytes from HFHS-fed compared to chow-fed wildtype mice (Figure 3.10 B), while cardiomyocytes from HET ATX-KO mice were protected from HFHS diet-induced impairment of AKT phosphorylation (Figure 3.10 B). Similar results were observed for phosphorylation of GSK3α/β at S21/9, a downstream target of AKT (Figure 3.10 C). Cardiomyocytes isolated from Het ATX-KO mice were protected from HFHS-induced downregulation of GSK3 phosphorylation when compared to wildtype mice (Figure 3.10 C). Taken together, these data suggest that a chronic reduction in autotaxin and LPA *in vivo* protects cardiomyocytes from obesity-induced insulin resistance.

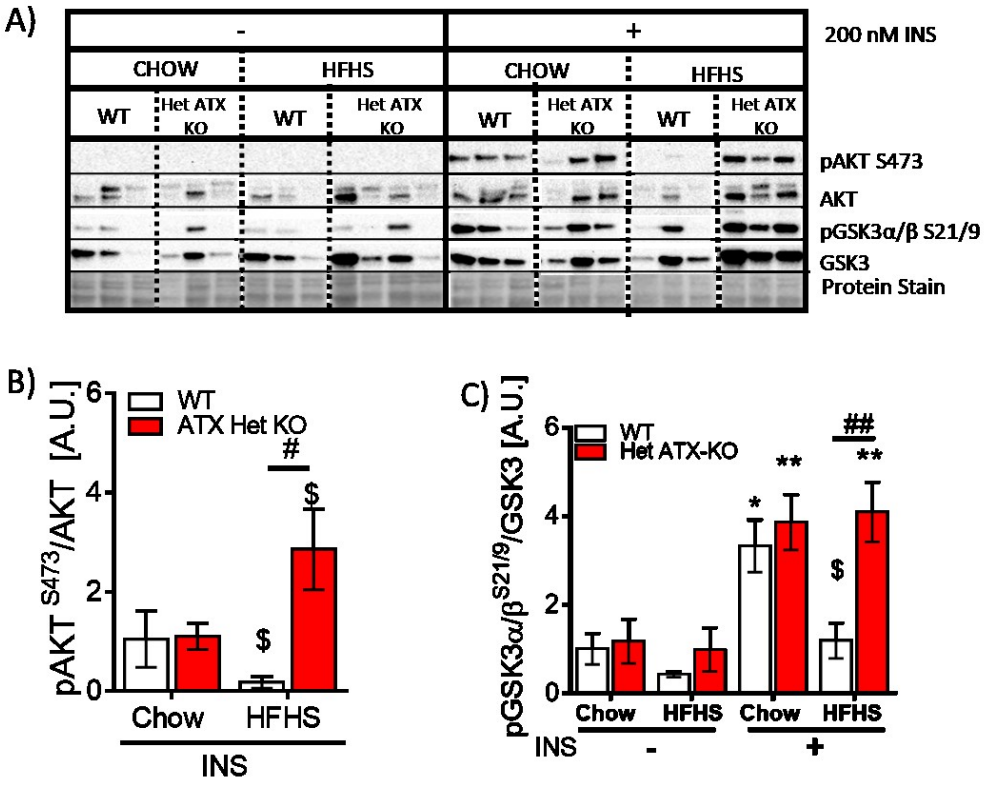

Figure 3. 10. Cardiomyocytes isolated from heterozygous autotaxin knockout mice fed high-fat high-sucrose diet show improved insulin sensitivity compared to wildtype mice.

A) Immunoblot of isolated cardiomyocytes, treated with or without insulin (200 nM) after 2 h serum starvation, from wildtype and Het ATX-KO mice fed chow or HFHS diet. B) densitometric analysis of AKT phosphorylation at S473 normalized to total AKT. C) densitometric analysis of GSK3α/β phosphorylation at S21/9 normalized to total GSK3. Graph represents mean ± S.E.M., comparison to respective no insulin group indicated by *, comparison to respective chow plus insulin group indicated by $, comparison between wildtype and Het ATX-KO indicated by #, degree of significance indicated by number of symbols: 1 symbol - $P < 0.05$, 2 symbols - $P<0.01$, 3 symbols - $P<0.001$, 4 symbols - $P<0.0001$; Two-way ANOVA, followed by Sidak's post hoc test; n = 4 mice per group.

3.9 Cardiomyocytes Isolated From Heterozygous Autotaxin Knockout Mice are Protected From High-Fat High-Sucrose Diet-Induced Contractile Dysfunction

Cardiac insulin resistance impairs the nutritional flexibility of the heart. Rather than rapidly adjusting nutrient metabolism to utilize substrates based on their availability

in circulation, the insulin resistant myocardium must rely mostly on fatty acids for energy and has a reduced ability to utilize glucose as a fuel source [161]. As a result, the insulin-resistant myocardium shows elevated reactive oxygen species production, mitochondrial dysfunction and apoptosis [73, 162-164]. These alterations have the potential to cause myocardial dysfunction leading to cardiomyopathy and the eventual development of heart failure. Since Het ATX-KO mice fed HFHS diet showed better cardiomyocyte insulin sensitivity in comparison to HFHS-fed wildtype mice, I next investigated if Het ATX-KO mice fed HFHS have improved cardiac function using sarcomere shortening analysis in electrically stimulated cardiomyocytes. At baseline, cardiomyocytes isolated from Het ATX-KO mice fed HFHS had moderately longer sarcomeres (Figure 3.11 D) than those from chow-fed Het ATX-KO mice, although sarcomere length for all groups were within normal range. Fractional shortening and rate of contraction and relaxation were significantly reduced in cardiomyocytes from HFHS-fed wildtype mice compared to chow, suggesting that HFHS feeding led to cardiomyocyte dysfunction in wildtype mice (Figure 3.12 A-D). Interestingly, fractional shortening and rate of contraction and relaxation remained unchanged in cardiomyocytes from Het ATX-KO mice compared to chow (Figure 3.12 A-D). Taken together, these data suggest that partial ATX deficiency and reduced LPA levels protect cardiomyocytes from dysfunction following diet-induced obesity.

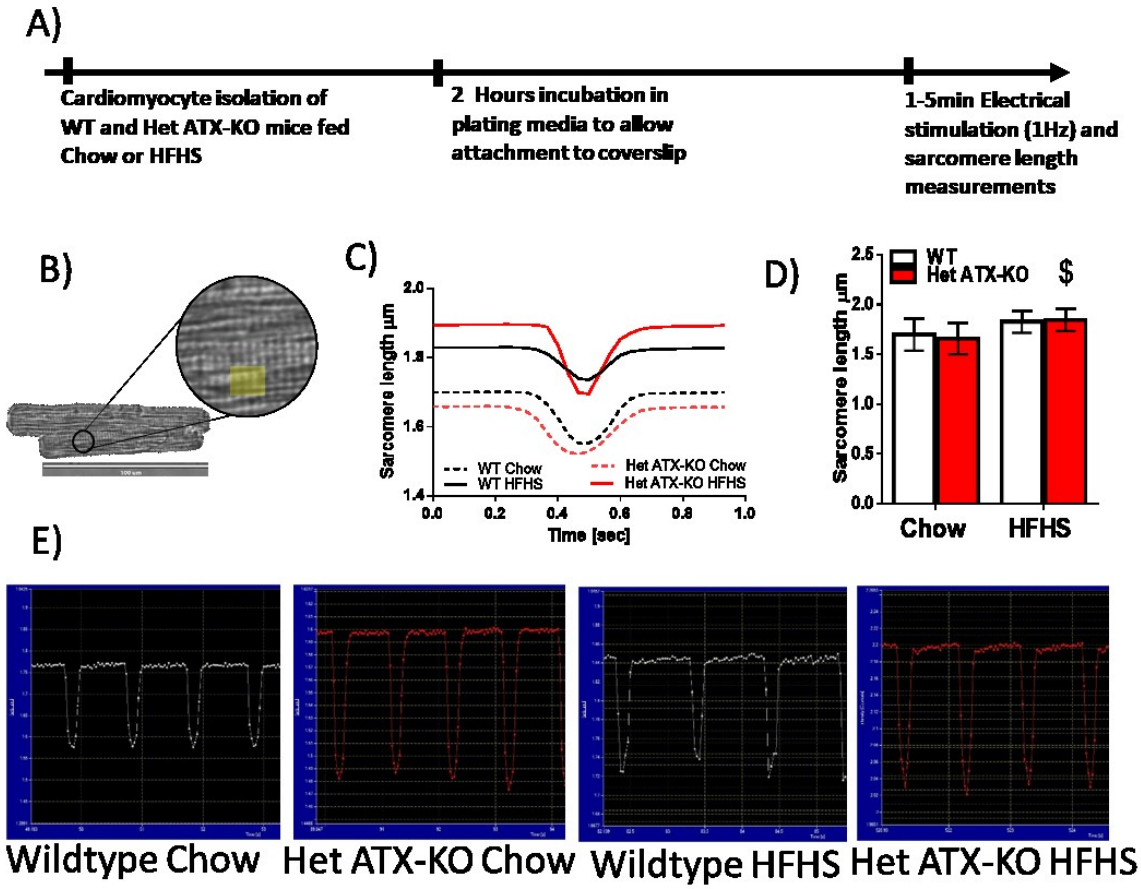

Figure 3. 11. Cardiomyocytes isolated from heterozygous autotaxin knockout mice fed high-fat high-sucrose diet show increased sarcomere length although within normal range.

A) Timeline of cardiomyocyte isolation and sarcomere length measurement. B) Representation of areas selected for sarcomere analysis. C) Resulting contractions after averaging 10 contractions per cardiomyocytes (n = 7-12 cardiomyocytes from 2-3 mice per group). D) Sarcomere length averaged from 10 contractions per cardiomyocyte (n = 7-12 cardiomyocytes from 2-3 mice per group). E) Representative traces collected from cardiomyocytes isolated from wildtype and Het ATX-KO mice fed chow or HFHS diet. Graph represents mean ± S.E.M., comparison to Het ATX-KO fed chow indicated by $, degree of significance indicated by number of symbols: 1 symbol - $P < 0.05$, 2 symbols - $P<0.01$, 3 symbols - $P<0.001$, 4 symbols - $P<0.0001$; Two-way ANOVA, followed by Sidak's multiple comparison test; n = 7-12 cardiomyocytes from 2-3 mice per group.

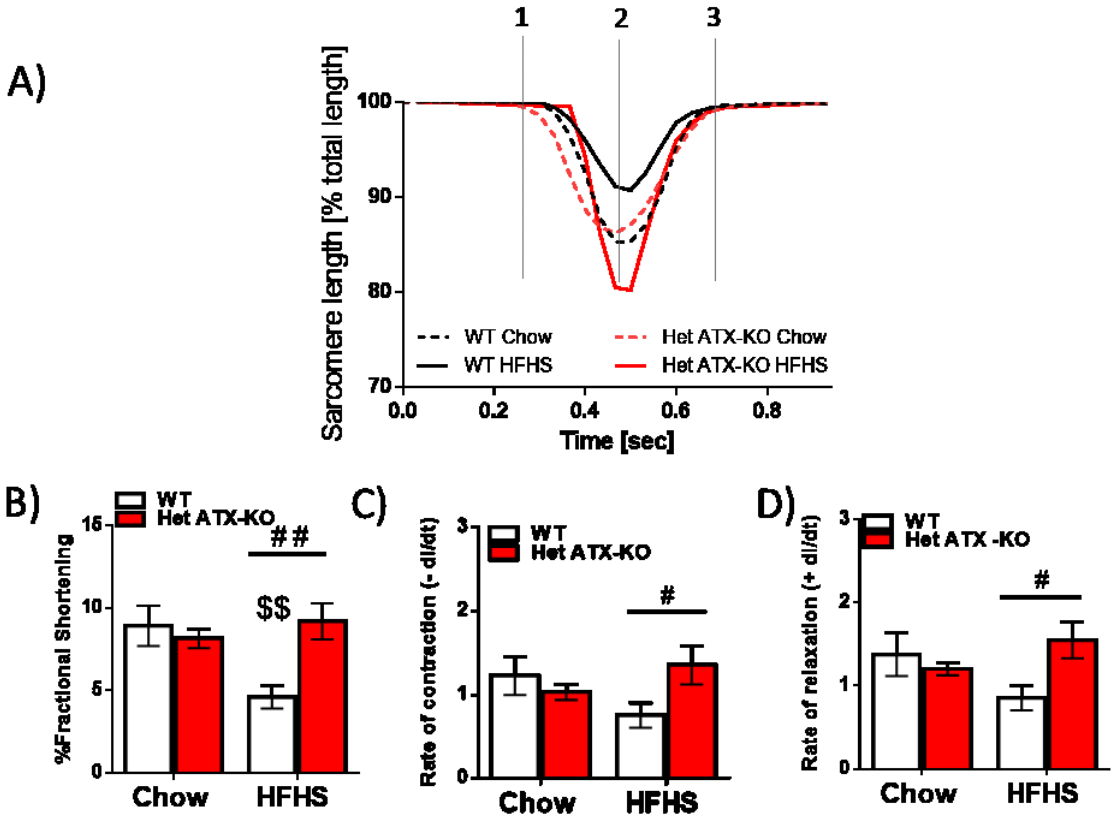

Figure 3. 12. Cardiomyocytes isolated from heterozygous autotaxin knockout mice fed high-fat high-sucrose diet show improved cardiac function compared to wildtype mice.

A) Percent fractional shortening during contraction relative to baseline sarcomere length (100%). B) Percent fractional shortening at the deepest point of contraction/shortest sarcomere length. C) Rate of contraction/rate of transition from fully expanded to fully contracted sarcomeres measured between 1-2 on figure A. D) Rate of relaxation/rate of transition from fully contracted to fully relaxed sarcomeres measured between 2-3 on figure A. Graph represents mean ± S.E.M., comparison between chow and HFHS indicated by $, comparison between wildtype and Het ATX-KO cardiomyocytes indicated by #; degree of significance indicated by number of symbols: : 1 symbol - $P < 0.05$, 2 symbols - $P<0.01$, 3 symbols - $P<0.001$, 4 symbols - $P<0.0001$; Two-way ANOVA, followed by Sidak's multiple comparison test; n = 7-12 cardiomyocytes from 2-3 mice per group.

CHAPTER 4: DISCUSSION

Autotaxin levels increase with obesity-induced insulin resistance in murine models [115] as well as correlate with measures of obesity and insulin resistance in obese humans [116, 117]. As a major generator and regulator of circulating LPA the correlation of ATX to insulin resistance and ultimately glucose homeostasis implicates LPA as a possible mediator. LPA is present in many body fluids, with the highest concentration in serum (10 μM) [140]. The influence of LPA and ATX on insulin signalling in cardiomyocytes has not been heavily investigated. Most of the data collected implicating the ATX-LPA signalling axis in obesity and glucose homeostasis utilized adipose tissue, skeletal muscle and hepatic tissue. Additionally, cardiovascular research involving LPA mostly focused on atherosclerosis, ischemia-reperfusion injury and fibrosis rather than diabetic cardiomyopathy or cardiac insulin resistance. This study was the first to investigate the implication of LPA signalling in cardiomyocytes under lipotoxicity conditions *in vitro* and as well as the first to investigate the role of LPA in cardiac function and cardiac insulin signalling under obesogenic condition *in vivo*.

LPA increased basal AKT and P70S6K phosphorylation in H9C2 cells in the absence of insulin (Figure 3.1), which is consistent with prior studies conducted using other cell types. For example, a colon cancer cell line (Caco-2 cells) incubated with LPA similarly showed upregulation of phosphorylated AKT and p70S6K [165]. LPA signals through six G-coupled receptors which all can activate PI3K p110β through Gαi/oβγ proteins [138]. Additionally, LPA-induced phosphorylation of P70S6K in fibroblast cells depends on phospholipase D activation, which is known to be implicated in mTOR signalling [166]. In addition to activating the PI3K cascade, LPA can also stimulate PDK2 phosphorylation

through PKCδ [167]. The PI3K-AKT pathway regulates an array of cell survival and metabolism pathways and dysregulation of the PI3K-AKT pathway is linked to diseases like cancer, cardiovascular disease and diabetes [168, 169]. AKT activation by LPA contributes to cell survival as well as cell migration and proliferation [140, 170, 171].

As expected, insulin increased levels of AKT pS473 and P70S6K pT389 significantly above non-insulin incubated cardiomyocytes (Figures 3.1). Additionally, insulin stimulated cells pre-exposed to LPA, had higher levels of AKT pS473 and P70S6K pT389 than cells just incubated with LPA. On the other hand, the magnitude of change between insulin-incubated and non-insulin controls decreased with increasing concentration of LPA (Figures 3.1), suggesting that LPA is interfering with insulin sensitivity and that cardiac cells pre-exposed to high levels of LPA are not as responsive to additional stimulation by insulin. As mentioned before, there are conflicting results on the effect of LPA on insulin signalling. In myotubes and adipocytes, LPA was found to upregulate glucose transport and work synergistically with insulin to increase glucose transport [128]. Conversely, isolated islets cells from mouse pancreas showed reduced insulin secretion when exposed to increasing levels of LPA [115], suggesting that in obese conditions, LPA may interfere with insulin secretion, contributing to the reduction in insulin secretion by beta cells seen in late stages of type 2 diabetes [172].

Since the interaction between LPA and insulin showed increased protein levels of phosphorylated insulin signalling targets, but magnitude of increase by insulin was reduced by LPA, the next step was to determine if LPA would improve or exacerbate insulin resistance of insulin resistant cells. Cells were rendered insulin resistant by incubation with palmitate. Palmitate concentrations were selected to be within

physiological range. C57BL6 mice fasted for 12 h have been reported to have ~ 0.87 mEq/l (or mM) serum NEFA [173] and humans have free fatty acid levels between 0.2 - 0.8 mM throughout the day depending on fed and fasted states and levels elevate under conditions of metabolic stress, starvation or diabetes [71]. Women classified as moderately obese were found to have 0.61+/-0.14 mM plasma NEFA and grossly obese women had 0.81+/-0.21 mM plasma NEFA [174]. H9C2 cells were incubated with palmitate (0.2 mM for 24 h, or 0.8 mM for 16 h) to induce insulin resistance. NRCMs were incubated with 0.6 mM palmitate for 16 h, because 0.8 mM palmitate disrupted cell monolayer indicating toxicity, and 0.6 mM palmitate was still in range of the level of NEFA seen in obesity. Palmitate is often used to induce insulin resistance in *in vitro* studies [175]. Recently, palmitate was shown to impair β-oxidation and citric acid cycle flux in neonatal rat cardiomyocytes, suggesting that palmitate hinders lipid clearance and promotes toxic lipid intermediates accumulation in the heart [176]. This accumulation of toxic lipid intermediates is known to induce insulin resistance by inhibiting the activity of insulin receptor substrate and AKT. In this study, palmitate incubation in both H9C2 and neonatal cardiomyocytes significantly blunted insulin-induced phosphorylation of insulin signalling targets, and co-incubation with LPA and palmitate resulted in an additional decrease (Figure 3.4, 3.7). Incubation of palmitate and co-incubation of palmitate and LPA showed increased levels of phosphorylated P70S6K. This may be due to palmitate-induced dysregulation of mTOR. In skeletal muscle cells, palmitate decreases levels of phosphorylated AMPK, Raptor and 4EBP1 while increasing phosphorylated p70S6K levels [177]. Through inhibition of AMPK, palmitate induced hypo-phosphorylation of Raptor, leading to the activation of mTOR and hyper-phosphorylation of p70S6K [177].

This increase in P70S6K activation, by triggering a negative feedback loop that leads to inhibition of insulin receptor substrate activation, may lead to insulin resistance. Additionally, LPA signalling triggers phosphorylation of P70S6K and may contribute to palmitate-induced dysregulation of mTOR signalling also by activating P70S6K. Consequently, cells co-incubated with LPA and palmitate showed exacerbation of palmitate-induced insulin resistance. These data suggest that LPA is detrimental to insulin sensitivity in conditions of high levels of palmitate. In the pathology of obesity-induced insulin resistance levels of circulating NEFA increase and heart tissue preferentially utilizes fatty acids due to their high availability [161]. In this environment, circulating ATX and LPA levels also increase [130, 178-180] and serum ATX levels have also been correlated with insulin resistance in humans with obesity [116, 117]. This suggests increasing levels of circulating ATX and LPA may aid in the progression of insulin resistance in obesity.

However, there are conflicting results in the literature showing LPA injection can both decrease or increase blood glucose level. Aside from differing injection sites and mouse strain, a potential confounding factor is the nutritional state of the mice prior to LPA injections. Fatty acids seem to interact with LPA signalling and reduce insulin sensitivity. Since prolonged starvation/fasting can transiently increase circulating NEFA to levels seen in obesity and levels of NEFA are significantly decreased after feeding, fasted mice injected with LPA may show increased blood glucose levels, while fed mice injected with LPA would show reduced blood glucose levels. A 1996 review by Frayn et al tabulated measured levels of circulating NEFA of individuals under varying metabolic stressors, nutritional states, and health conditions [181]. They showed that circulating

fatty acid levels increased with increasing length of fasting, degree of obesity, severity of diabetes, and emotional stressors like public speaking. Conversely, levels decreased after glucose intake and during insulin infusion [181].

Although LPA induced insulin resistance in the presence of palmitate, LPA was found not to exacerbate palmitate-induced inflammatory signalling and apoptosis (Figure 3.5). Palmitate induces inflammation and apoptosis which contribute to the development of insulin resistance. Palmitate has been shown to directly bind to TLR4 accessory protein MD2. Palmitate stimulates the formation of MD2/TLR4–MyD88 complex, resulting in activation of MAPKs/NF-κB signalling that regulates pro-inflammatory molecules [182]. In addition to stimulating pro-inflammatory molecules, palmitate induces apoptosis by increasing reactive oxygen species generation and activation of the ERK1/2 signalling pathway in H9C2 cells [157]. A study employing embryonic chick cardiomyocytes showed that palmitate-induced apoptosis is mediated through alterations in mitochondria and can be inhibited by cyclosporin A, which inhibits the development of mitochondrial transition pores [155, 183]. LPA has been heavily studied in the development of atherosclerosis and has been shown to promote inflammation. In vascular smooth muscles cells LPA induced IL-6 and monocyte chemoattractant protein secretion through PKC activation of p38 MAPK [184]. ATX is transported in the aortic valve by lipoprotein (a) and is also secreted by valve interstitial cells. This ATX synthesizes LPA which promotes inflammation and mineralization of the aortic valve [185]. LPA accumulates in the atherosclerotic plaque and activates mast cells, which promotes intraplaque hemorrhage leading to atherosclerotic plaque destabilization and increases macrophage recruitment leading to increased vascular inflammation [186]. The role of LPA signalling in apoptosis

in cardiomyocytes has not been investigated, but LPA has been shown to inhibit or protect against apoptosis in cervical cancer cells, mesenchymal stromal cells, and H19-7 cells [187-189]. In C2C12 skeletal muscle cells, prolonged treatment with LPA led to caspase 3 and PARP cleavage and activation of stress-associated MAP kinases JNK and p38, but did not induce cell death [190]. LPA-mediated apoptosis was triggered by blocking LPA-induced ERK1/2 and AKT activation [190]. Similar to these findings, H9C2 cells incubated with LPA (20 μM for 24 h) showed reduced cell viability compared to control cells (Figure 3.5 F). However, in the presence of palmitate, LPA did not decrease cell viability further or increase cleaved caspase 3 or JNK phosphorylation. Although the high palmitate concentration (0.8 mM) used in our study did not show increased inflammation and cleaved caspase levels in the presence of LPA, repeated experiments with low palmitate concentration (0.2 mM) are required to determine if LPA can increase inflammation and apoptosis in the reduction of palmitate-induced inflammation.

Aside from increased apoptosis and inflammation in the diabetic myocardium, diabetic cardiomyopathy is also associated with increased oxidative stress. This is due in part to increased fatty acid oxidation, which must occur to utilize the increased level of circulating fatty acids under conditions where glucose uptake is reduced. In this study, incubation with a relatively lower concentration of palmitate (0.2 mM) or LPA did not induce oxidative stress after 24 h, but co-incubation with LPA and low palmitate significantly increased levels of superoxides (Figure 3.6). Higher levels of palmitate (0.8 mM) were sufficient to increase superoxide levels without additional effects of LPA. LPA increases superoxide anion levels, mRNA levels of NOX4 and p40(phox) (reactive

oxygen species generating enzymes) and decrease superoxide dismutase 1 in porcine coronary arteries and human coronary artery endothelial cells (HCAECs) [191]. Oxidative stress is deleterious to mitochondrial enzyme function and, likewise, LPA-treated HCAECs also showed reduced mitochondrial membrane potential and ATP content [191]. The increased oxidative stress observed after co-incubation with palmitate and LPA may suggest that LPA exacerbates palmitate-induced insulin resistance by increasing oxidative stress which leads to reduced mitochondrial enzyme function. Mitochondrial dysfunction would further reduce fatty acid clearance and exacerbate lipotoxicity in cells co-incubated with LPA and palmitate.

In vitro results showed that in the presence of palmitate at concentrations that are observed during obesity, incubation of cardiomyocytes with LPA, leads to increased insulin resistance. To verify these results *in vivo*, mice haploid deficient in ATX (Het ATX-KO mice) were employed to determine if a~ 50% reduction in circulating levels of ATX/LPA would protect against obesity-induced cardiac insulin resistance. Het ATX-KO mice gained less weight on HFHS diet compared to their wildtype littermates (Figure 3.8). This is consistent with results obtained from transgenic mice overexpressing ATX, which have increased susceptibility to diet-induced obesity compared to wildtype mice [192]. Additionally, Het ATX-KO mice and adipocyte specific ATX- KO mice compared to control mice on HFD, also show reduced weight gain [193], suggesting ATX/LPA contributes to diet induced obesity. In addition to reduced weight gain on an obesogenic diet, Het ATX-KO mice showed improved cardiac insulin sensitivity compared to their wildtype littermates fed HFHS (Figure 3.9). Cardiomyocytes isolated from Het ATX-KO mice fed HFHS were also more sensitive to insulin stimulation than cardiomyocytes

isolated from wildtype mice fed HFHS (Figure 3.10). This result is consistent with results from previous studies obtained from adipocyte specific ATX-KO mice fed HFD, which showed improved whole body glucose tolerance compared to wildtype mice fed HFD [115]. Additionally, mice fed HFD and injected with LPA receptor 1 and 3 inhibitor Ki16425 also showed improved glucose tolerance compared to untreated mice fed HFD [115]. Moreover, injected LPA acutely impaired glucose tolerance and insulin secretion [115, 180], suggesting that the reduction in circulating ATX-LPA levels may improve whole body insulin sensitivity. Similarly, our study shows reduction in circulating ATX-LPA improves cardiac insulin sensitivity.

Since isolated cardiomyocytes from Het ATX-KO mice fed HFHS showed improved insulin sensitivity compared to wildtype mice, I determined if a reduction in ATX/LPA signalling translated to preserved function following HFHS feeding by measuring sarcomere shortening of isolated cardiomyocytes. Cardiomyocytes isolated from HFHS fed wildtype mice showed a significant reduction in % fractional shortening, rate of contraction and rate of relaxation (Figure 3.12). HFD in previous studies, compromises myocardial function and reduces fractional shortening [194-196]. Although baseline sarcomere length was within the range of normal (1.7-2.0 μm) [197-199], HFHS diet significantly increased baseline sarcomere length in Het ATX-KO mice and showed a trend to increase in wildtype mice. This increase in sarcomere length could indicate an increase in cardiomyocyte size, which has been shown to be the case after HFD feeding [194]. Cardiomyocytes isolated from HFHS fed Het ATX-KO mice showed improved fractional shortening, rate of contraction and rate of relaxation compared to wildtype HFHS cardiomyocytes and similar levels compared to cardiomyocytes from chow fed

control mice. Normal fractional shortening in mice was ~10%, while HFHS diet caused a 50% reduction in fractional shortening in wildtype mice, indicating a significant reduction in contractility of these cardiomyocytes (Figure 3.12). This was not seen in cardiomyocytes isolated from Het ATX-KO mice. Together with improved insulin sensitivity, these results suggest that ATX/LPA contributes to cardiomyopathy and cardiac insulin resistance in diet-induced obesity.

CHAPTER 5: CONCLUSION AND FUTURE DIRECTIONS

This study was the first to investigate the role of ATX/LPA in obesity-induced cardiac insulin resistance and cardiac dysfunction and the role of LPA in palmitate induced lipotoxicity. This study yielded three major findings: 1) LPA upregulated downstream targets of insulin signalling at baseline and although LPA increased levels of phosphorylated insulin targets further post insulin stimulation in H9C2 cells, the magnitude of insulin stimulation compared to baseline was reduced. 2) In the presence of palmitate, LPA exacerbated cardiac insulin resistance in H9C2 cells and neonatal rat cardiomyocytes, which may be due in part to the activation of P70S6K. Additionally, in the presence of non-toxic levels of palmitate, LPA significantly increased superoxide production, suggesting that LPA may exacerbate mitochondrial dysfunction during lipotoxicity. 3) Cardiomyocytes from Het ATX-KO mice fed HFHS had improved insulin sensitivity and maintained proper contractility in comparison to cardiomyocytes from wildtype mice fed HFHS, showing that ATX/LPA contributes to cardiac insulin resistance and cardiac dysfunction as seen in obesity-induced cardiomyopathy.

The mechanism by which LPA exacerbates lipotoxicity induced insulin resistance in cardiomyocytes still needs to be investigated. Data collected here suggest that this may involve the dysregulation of mTOR/P70S6K activation, alterations in mitochondrial function, and increased reactive oxygen species production. It is important to note the harmful effects of LPA were primarily seen following prolonged exposure (24h), in the presence of palmitate (in vitro) and high levels of circulating fatty acids in the diet-induced obese mice. Therefore, investigating how LPA affects insulin signalling during

hyperglycemia, hyperinsulinemia and conditions of high levels of glucose and fatty acids, which are seen in obesity and diabetes, beg to be investigated. Additionally, conflicting reports show that mice injected with LPA have both increased and decreased glucose uptake. This discrepancy may be due to differing circulating fatty acids levels; investigating how injected LPA effects glucose levels in fed and fasted states may better elucidate its role in glucose homeostasis. Cardiomyocytes from mice with reduced ATX and LPA levels fed HFHS showed improved function compared to wildtype mice of the same condition. Further investigation is needed to address whole heart function of Het ATX-KO mice after diet-induced obesity.

Het ATX-KO mice employed in this study show both a reduction in circulating ATX and LPA levels. Therefore, to elucidate if the cardioprotection seen when these mice are fed HFHS is due to decreased levels of ATX, decreased levels of LPA or a combination of both, cardiac insulin signalling and function should be investigated in Het ATX-KO mice injected with LPA and wildtype mice injected with LPA receptor inhibitors (Suramin, inhibits LPA receptor binding, Kil6425 LPA receptors 1/3 antagonist, HL 5765834 LPA receptor 1/3/5, HL5186303 LPA receptor 2 antagonist) fed HFHS diet. These mice would represent models of low ATX with normal LPA levels, and normal levels of ATX with low levels of LPA signalling, respectively.

Taken together, this study has opened new avenues to investigate the interplay among ATX/LPA and cardiac insulin signalling, ATX/LPA and substrate utilization and availability, and ATX/LPA and obesity-induced cardiac insulin resistance and dysfunction.

REFERENCES

1. Ng, M., et al., *Global, regional, and national prevalence of overweight and obesity in children and adults during 1980–2013: a systematic analysis for the Global Burden of Disease Study 2013.* The Lancet, 2014. **384**(9945): p. 766-781.

2. Kahn, B.B. and J.S. Flier, *Obesity and insulin resistance.* The Journal of clinical investigation, 2000. **106**(4): p. 473-481.

3. Kabon, B., et al., *Obesity decreases perioperative tissue oxygenation.* The Journal of the American Society of Anesthesiologists, 2004. **100**(2): p. 274-280.

4. Apovian, C.M., et al., *Adipose macrophage infiltration is associated with insulin resistance and vascular endothelial dysfunction in obese subjects.* Arteriosclerosis, thrombosis, and vascular biology, 2008. **28**(9): p. 1654-1659.

5. Di Raimo, T., et al., *Adipokines and their Involvement as a Target of New Drugs.* Journal of Pharmacovigilance, 2015.

6. Wisneski, J.A., et al., *Effects of acute hyperglycemia on myocardial glycolytic activity in humans.* Journal of Clinical Investigation, 1990. **85**(5): p. 1648.

7. Gertz, E., et al., *Myocardial substrate utilization during exercise in humans. Dual carbon-labeled carbohydrate isotope experiments.* Journal of Clinical Investigation, 1988. **82**(6): p. 2017.

8. Carley, A.N. and D.L. Severson, *Fatty acid metabolism is enhanced in type 2 diabetic hearts.* Biochimica et Biophysica Acta (BBA)-Molecular and Cell Biology of Lipids, 2005. **1734**(2): p. 112-126.

9. Dirkx, E., et al., *High fat diet induced diabetic cardiomyopathy.* Prostaglandins, Leukotrienes and Essential Fatty Acids (PLEFA), 2011. **85**(5): p. 219-225.

10. Sun, K., C.M. Kusminski, and P.E. Scherer, *Adipose tissue remodeling and obesity.* The Journal of clinical investigation, 2011. **121**(6): p. 2094-2101.

11. Nguyen, M.A., et al., *A subpopulation of macrophages infiltrates hypertrophic adipose tissue and is activated by free fatty acids via Toll-like receptors 2 and 4 and JNK-dependent pathways.* Journal of Biological Chemistry, 2007. **282**(48): p. 35279-35292.

12. Lumeng, C.N., J.L. Bodzin, and A.R. Saltiel, *Obesity induces a phenotypic switch in adipose tissue macrophage polarization.* The Journal of clinical investigation, 2007. **117**(1): p. 175-184.

13. Choe, S.S., et al., *Adipose tissue remodeling: its role in energy metabolism and metabolic disorders.* Frontiers in endocrinology, 2016. **7**.

14. Lumeng, C.N., et al., *Increased inflammatory properties of adipose tissue macrophages recruited during diet-induced obesity.* Diabetes, 2007. **56**(1): p. 16-23.

15. Patsouris, D., et al., *Ablation of CD11c-positive cells normalizes insulin sensitivity in obese insulin resistant animals.* Cell metabolism, 2008. **8**(4): p. 301-309.

16. Cinti, S., et al., *Adipocyte death defines macrophage localization and function in adipose tissue of obese mice and humans.* Journal of lipid research, 2005. **46**(11): p. 2347-2355.

17. Strissel, K.J., et al., *Adipocyte death, adipose tissue remodeling, and obesity complications.* Diabetes, 2007. **56**(12): p. 2910-2918.

18. Nishimura, S., et al., *Adipogenesis in obesity requires close interplay between differentiating adipocytes, stromal cells, and blood vessels.* Diabetes, 2007. **56**(6): p. 1517-1526.

19. Pajvani, U.B., et al., *Fat apoptosis through targeted activation of caspase 8: a new mouse model of inducible and reversible lipoatrophy.* Nature medicine, 2005. **11**(7): p. 797-803.

20. Virtanen, K.A., et al., *Glucose uptake and perfusion in subcutaneous and visceral adipose tissue during insulin stimulation in nonobese and obese humans.* The Journal of Clinical Endocrinology & Metabolism, 2002. **87**(8): p. 3902-3910.

21. Hosogai, N., et al., *Adipose tissue hypoxia in obesity and its impact on adipocytokine dysregulation.* Diabetes, 2007. **56**(4): p. 901-911.

22. Chen, M.-P., et al., *Elevated plasma level of visfatin/pre-B cell colony-enhancing factor in patients with type 2 diabetes mellitus.* The Journal of Clinical Endocrinology & Metabolism, 2006. **91**(1): p. 295-299.

23. Jung, U.J. and M.-S. Choi, *Obesity and its metabolic complications: the role of adipokines and the relationship between obesity, inflammation, insulin resistance, dyslipidemia and nonalcoholic fatty liver disease.* International journal of molecular sciences, 2014. **15**(4): p. 6184-6223.

24. Xu, H., et al., *Chronic inflammation in fat plays a crucial role in the development of obesity-related insulin resistance.* The Journal of clinical investigation, 2003. **112**(12): p. 1821-1830.

25. Kanda, H., et al., *MCP-1 contributes to macrophage infiltration into adipose tissue, insulin resistance, and hepatic steatosis in obesity.* The Journal of clinical investigation, 2006. **116**(6): p. 1494-1505.

26. Nara, N., et al., *Disruption of CXC motif chemokine ligand-14 in mice ameliorates obesity-induced insulin resistance.* Journal of Biological Chemistry, 2007. **282**(42): p. 30794-30803.

27. Shi, H., et al., *TLR4 links innate immunity and fatty acid–induced insulin resistance.* The Journal of clinical investigation, 2006. **116**(11): p. 3015-3025.

28. Suganami, T., J. Nishida, and Y. Ogawa, *A paracrine loop between adipocytes and macrophages aggravates inflammatory changes.* Arteriosclerosis, thrombosis, and vascular biology, 2005. **25**(10): p. 2062-2068.

29. Carey, G.B., *Mechanisms regulating adipocyte lipolysis*, in *Skeletal Muscle Metabolism in Exercise and Diabetes*. 1998, Springer. p. 157-170.

30. Reynisdottir, S., et al., *Effects of weight reduction on the regulation of lipolysis in adipocytes of women with upper-body obesity.* Clinical Science, 1995. **89**(4): p. 421-429.

31. Schenk, S., M. Saberi, and J.M. Olefsky, *Insulin sensitivity: modulation by nutrients and inflammation.* J Clin Invest, 2008. **118**(9): p. 2992-3002.

32. Lopaschuk, G.D., et al., *Regulation of fatty acid oxidation in the mammalian heart in health and disease.* Biochimica et Biophysica Acta (BBA)-Lipids and Lipid Metabolism, 1994. **1213**(3): p. 263-276.

33. Samuel, V.T. and G.I. Shulman, *Mechanisms for insulin resistance: common threads and missing links.* Cell, 2012. **148**(5): p. 852-871.

34. Zhang, L., et al., *Cardiac diacylglycerol accumulation in high fat-fed mice is associated with impaired insulin-stimulated glucose oxidation.* Cardiovascular research, 2011. **89**(1): p. 148-156.

35. Duncan, R.E., et al., *Regulation of lipolysis in adipocytes.* Annu. Rev. Nutr., 2007. **27**: p. 79-101.

36. Kim, C., N.-H. Xuong, and S.S. Taylor, *Crystal structure of a complex between the catalytic and regulatory (RIα) subunits of PKA.* Science, 2005. **307**(5710): p. 690-696.

37. Anthonsen, M.W., et al., *Identification of novel phosphorylation sites in hormone-sensitive lipase that are phosphorylated in response to isoproterenol and govern activation properties in vitro.* Journal of Biological Chemistry, 1998. **273**(1): p. 215-221.

38. Sztalryd, C., et al., *Perilipin A is essential for the translocation of hormone-sensitive lipase during lipolytic activation.* The Journal of cell biology, 2003. **161**(6): p. 1093-1103.

39. Clifford, G.M., et al., *Translocation of hormone-sensitive lipase and perilipin upon lipolytic stimulation of rat adipocytes.* Journal of Biological Chemistry, 2000. **275**(7): p. 5011-5015.

40. Maeda, N., et al., *Adaptation to fasting by glycerol transport through aquaporin 7 in adipose tissue.* Proceedings of the National Academy of Sciences of the United States of America, 2004. **101**(51): p. 17801-17806.

41. Shen, W.-J., et al., *Functional interaction of hormone-sensitive lipase and perilipin in lipolysis.* Journal of lipid research, 2009. **50**(11): p. 2306-2313.

42. Ragolia, L. and N. Begum, *Protein phosphatase-1 and insulin action.* Molecular and cellular biochemistry, 1998. **182**(1): p. 49-58.

43. Siegrist-Kaiser, C.A., et al., *Direct effects of leptin on brown and white adipose tissue.* Journal of Clinical Investigation, 1997. **100**(11): p. 2858.

44. Frühbeck, G., et al., *Lipolytic Effect ofin VivoLeptin Administration on Adipocytes of Lean and ob/ob Mice, but Not db/db Mice.* Biochemical and biophysical research communications, 1998. **250**(1): p. 99-102.

45. Müller, G., et al., *Leptin impairs metabolic actions of insulin in isolated rat adipocytes.* Journal of Biological Chemistry, 1997. **272**(16): p. 10585-10593.

46. Ottensmeyer, F., et al., *Mechanism of transmembrane signaling: insulin binding and the insulin receptor.* Biochemistry, 2000. **39**(40): p. 12103-12112.

47. Pessin, J.E. and H. Kwon, *Adipokines mediate inflammation and insulin resistance.* Frontiers in endocrinology, 2013. **4**: p. 71.

48. Zhang, W. and H.T. Liu, *MAPK signal pathways in the regulation of cell proliferation in mammalian cells.* Cell research, 2002. **12**(1): p. 9-18.

49. Alessi, D.R., et al., *Characterization of a 3-phosphoinositide-dependent protein kinase which phosphorylates and activates protein kinase Bα.* Current biology, 1997. **7**(4): p. 261-269.

50. Alessi, D.R., et al., *Mechanism of activation of protein kinase B by insulin and IGF-1.* The EMBO journal, 1996. **15**(23): p. 6541.
51. Sarbassov, D.D., et al., *Phosphorylation and regulation of Akt/PKB by the rictor-mTOR complex.* Science, 2005. **307**(5712): p. 1098-1101.

52. DeBosch, B., et al., *Akt2 regulates cardiac metabolism and cardiomyocyte survival.* Journal of Biological Chemistry, 2006. **281**(43): p. 32841-32851.

53. Sun, D., et al., *Ischemia induces translocation of the insulin-responsive glucose transporter GLUT4 to the plasma membrane of cardiac myocytes.* Circulation, 1994. **89**(2): p. 793-798.

54. Wheeler, T.J., R.D. Fell, and M.A. Hauck, *Translocation of two glucose transporters in heart: effects of rotenone, uncouplers, workload, palmitate, insulin and anoxia.* Biochimica et Biophysica Acta (BBA)-Biomembranes, 1994. **1196**(2): p. 191-200.

55. Egert, S., N. Nguyen, and M. Schwaiger, *Contribution of α-adrenergic and β-adrenergic stimulation to ischemia-induced glucose transporter (GLUT) 4 and GLUT1 translocation in the isolated perfused rat heart.* Circulation research, 1999. **84**(12): p. 1407-1415.

56. Palfreyman, R., et al., *Kinetic resolution of the separate GLUT1 and GLUT4 glucose transport activities in 3T3-L1 cells.* Biochemical Journal, 1992. **284**(1): p. 275-282.

57. Tardy-Cantalupi, I., et al., *Effect of transient ischemia on the expression of glucose transporters GLUT-1 and GLUT-4 in rat myocardium.* Journal of molecular and cellular cardiology, 1999. **31**(5): p. 1143-1155.

58. Rosenblatt-Velin, N., et al., *Postinfarction heart failure in rats is associated with upregulation of GLUT-1 and downregulation of genes of fatty acid metabolism.* Cardiovascular research, 2001. **52**(3): p. 407-416.

59. Tian, R. and E.D. Abel, *Responses of GLUT4-deficient hearts to ischemia underscore the importance of glycolysis.* Circulation, 2001. **103**(24): p. 2961-2966.

60. Abel, E.D., et al., *Cardiac hypertrophy with preserved contractile function after selective deletion of GLUT4 from the heart.* The Journal of clinical investigation, 1999. **104**(12): p. 1703-1714.

61. Cross, D.A., et al., *Insulin activates protein kinase B, inhibits glycogen synthase kinase-3 and activates glycogen synthase by rapamycin-insensitive pathways in skeletal muscle and adipose tissue.* FEBS letters, 1997. **406**(1-2): p. 211-215.

62. Luiken, J.J., et al., *Insulin stimulates long-chain fatty acid utilization by rat cardiac myocytes through cellular redistribution of FAT/CD36.* Diabetes, 2002. **51**(10): p. 3113-3119.

63. Brunet, A., et al., *Akt Promotes Cell Survival by Phosphorylating and Inhibiting a Forkhead Transcription Factor.* Cell, 1999. **96**(6): p. 857-868.

64. Ronnebaum, S.M. and C. Patterson, *The FoxO Family in Cardiac Function and Dysfunction.* Annual review of physiology, 2010. **72**: p. 81-94.

65. Boura-Halfon, S. and Y. Zick, *Serine kinases of insulin receptor substrate proteins.* Vitamins & Hormones, 2009. **80**: p. 313-349.

66. Gao, Z., et al., *Aspirin inhibits serine phosphorylation of insulin receptor substrate 1 in tumor necrosis factor-treated cells through targeting multiple serine kinases.* Journal of Biological Chemistry, 2003. **278**(27): p. 24944-24950.

67. Tremblay, F. and A. Marette, *Amino acid and insulin signaling via the mTOR/p70 S6 kinase pathway A negative feedback mechanism leading to insulin resistance in skeletal muscle cells.* Journal of Biological Chemistry, 2001. **276**(41): p. 38052-38060.

68. Hirosumi, J., et al., *A central role for JNK in obesity and insulin resistance.* Nature, 2002. **420**(6913): p. 333-336.

69. Turban, S. and E. Hajduch, *Protein kinase C isoforms: mediators of reactive lipid metabolites in the development of insulin resistance.* FEBS letters, 2011. **585**(2): p. 269-274.

70. Bertrand, L., et al., *Insulin signalling in the heart.* Cardiovascular research, 2008. **79**(2): p. 238-248.

71. Stanley, W.C., F.A. Recchia, and G.D. Lopaschuk, *Myocardial substrate metabolism in the normal and failing heart.* Physiological reviews, 2005. **85**(3): p. 1093-1129.

72. Kodde, I.F., et al., *Metabolic and genetic regulation of cardiac energy substrate preference.* Comparative Biochemistry and Physiology Part A: Molecular & Integrative Physiology, 2007. **146**(1): p. 26-39.

73. Mazumder, P.K., et al., *Impaired cardiac efficiency and increased fatty acid oxidation in insulin-resistant ob/ob mouse hearts.* Diabetes, 2004. **53**(9): p. 2366-2374.

74. Battiprolu, P.K., et al., *Metabolic stress–induced activation of FoxO1 triggers diabetic cardiomyopathy in mice.* The Journal of clinical investigation, 2012. **122**(3): p. 1109-1118.

75. Lee, Y.-S., et al., *Nobiletin improves hyperglycemia and insulin resistance in obese diabetic ob/ob mice.* Biochemical pharmacology, 2010. **79**(11): p. 1674-1683.

76. Belke, D.D., et al., *Insulin signaling coordinately regulates cardiac size, metabolism, and contractile protein isoform expression.* The Journal of clinical investigation, 2002. **109**(5): p. 629-639.

77. Boudina, S., et al., *Contribution of impaired myocardial insulin signaling to mitochondrial dysfunction and oxidative stress in the heart.* Circulation, 2009. **119**(9): p. 1272-1283.

78. Sena, S., et al., *Impaired insulin signaling accelerates cardiac mitochondrial dysfunction after myocardial infarction.* Journal of molecular and cellular cardiology, 2009. **46**(6): p. 910-918.

79. McQueen, A.P., et al., *Contractile dysfunction in hypertrophied hearts with deficient insulin receptor signaling: possible role of reduced capillary density.* Journal of molecular and cellular cardiology, 2005. **39**(6): p. 882-892.

80. Shimizu, I., et al., *Excessive cardiac insulin signaling exacerbates systolic dysfunction induced by pressure overload in rodents.* The Journal of clinical investigation, 2010. **120**(5): p. 1506-1514.

81. Balistreri, C.R., C. Caruso, and G. Candore, *The role of adipose tissue and adipokines in obesity-related inflammatory diseases.* Mediators of inflammation, 2010. **2010**.

82. Ahima, R.S. and J.S. Flier, *Adipose tissue as an endocrine organ.* Trends in Endocrinology & Metabolism, 2000. **11**(8): p. 327-332.

83. Loffreda, S., et al., *Leptin regulates proinflammatory immune responses.* The FASEB Journal, 1998. **12**(1): p. 57-65.

84. Considine, R.V., et al., *Serum immunoreactive-leptin concentrations in normal-weight and obese humans.* New England Journal of Medicine, 1996. **334**(5): p. 292-295.

85. Vidal, H., et al., *The expression of ob gene is not acutely regulated by insulin and fasting in human abdominal subcutaneous adipose tissue.* Journal of Clinical Investigation, 1996. **98**(2): p. 251.

86. Minokoshi, Y., et al., *Leptin stimulates fatty-acid oxidation by activating AMP-activated protein kinase.* Nature, 2002. **415**(6869): p. 339-343.

87. Steppan, C.M., et al., *The hormone resistin links obesity to diabetes.* Nature, 2001. **409**(6818): p. 307-312.

88. Banerjee, R.R., et al., *Regulation of fasted blood glucose by resistin.* Science, 2004. **303**(5661): p. 1195-1198.

89. Weyer, C., et al., *Hypoadiponectinemia in obesity and type 2 diabetes: close association with insulin resistance and hyperinsulinemia.* The Journal of Clinical Endocrinology & Metabolism, 2001. **86**(5): p. 1930-1935.

90. Tao, C., A. Sifuentes, and W.L. Holland, *Regulation of glucose and lipid homeostasis by adiponectin: effects on hepatocytes, pancreatic β cells and adipocytes.* Best Practice & Research Clinical Endocrinology & Metabolism, 2014. **28**(1): p. 43-58.

91. Schindler, M., et al., *Adiponectin stimulates lipid metabolism via AMPK in rabbit blastocysts.* Human Reproduction, 2017: p. 1-11.

92. Ruan, H. and L.Q. Dong, *Adiponectin signaling and function in insulin target tissues.* Journal of molecular cell biology, 2016. **8**(2): p. 101-109.

93. Jernås, M., et al., *Separation of human adipocytes by size: hypertrophic fat cells display distinct gene expression.* The FASEB Journal, 2006. **20**(9): p. 1540-1542.

94. Skurk, T., et al., *Relationship between adipocyte size and adipokine expression and secretion.* The Journal of Clinical Endocrinology & Metabolism, 2007. **92**(3): p. 1023-1033.

95. Hotamisligil, G.S., N.S. Shargill, and B.M. Spiegelman, *Adipose Expression of Tumor Necrosis Factor- : Direct Role in Obesity-Linked Insulin Resistance.* SCIENCE-NEW YORK THEN WASHINGTON-, 1993. **259**: p. 87-87.

96. Sartipy, P. and D.J. Loskutoff, *Monocyte chemoattractant protein 1 in obesity and insulin resistance.* Proceedings of the National Academy of Sciences, 2003. **100**(12): p. 7265-7270.

97. Rotter, V., I. Nagaev, and U. Smith, *Interleukin-6 (IL-6) induces insulin resistance in 3T3-L1 adipocytes and is, like IL-8 and tumor necrosis factor-α, overexpressed in human fat cells from insulin-resistant subjects.* Journal of Biological Chemistry, 2003. **278**(46): p. 45777-45784.

98. Rehman, K. and M.S.H. Akash, *Mechanisms of inflammatory responses and development of insulin resistance: how are they interlinked?* Journal of biomedical science, 2016. **23**(1): p. 87.

99. Fujimaki, S., et al., *The significance of measuring plasma leptin in acute myocardial infarction.* Journal of international medical research, 2001. **29**(2): p. 108-113.

100. Schulze, P.C., et al., *Elevated serum levels of leptin and soluble leptin receptor in patients with advanced chronic heart failure.* European journal of heart failure, 2003. **5**(1): p. 33-40.

101. Dong, F., X. Zhang, and J. Ren, *Leptin regulates cardiomyocyte contractile function through endothelin-1 receptor–NADPH oxidase pathway.* Hypertension, 2006. **47**(2): p. 222-229.

102. Hall, M.E., R. Harmancey, and D.E. Stec, *Lean heart: role of leptin in cardiac hypertrophy and metabolism.* World journal of cardiology, 2015. **7**(9): p. 511.

103. Kanda, T., et al., *Leptin deficiency enhances myocardial necrosis and lethality in a murine model of viral myocarditis.* Life sciences, 2004. **75**(12): p. 1435-1447.

104. Barouch, L.A., et al., *Disruption of leptin signaling contributes to cardiac hypertrophy independently of body weight in mice.* Circulation, 2003. **108**(6): p. 754-759.

105. McGaffin, K.R., C.S. Moravec, and C.F. McTiernan, *Leptin signaling in the failing and mechanically unloaded human heart.* Circulation: Heart Failure, 2009: p. CIRCHEARTFAILURE. 109.869909.

106. McGaffin, K.R., et al., *Cardiac-specific leptin receptor deletion exacerbates ischaemic heart failure in mice.* Cardiovascular research, 2010. **89**(1): p. 60-71.

107. Nakamura, K., J.J. Fuster, and K. Walsh, *Adipokines: a link between obesity and cardiovascular disease.* Journal of cardiology, 2014. **63**(4): p. 250-259.

108. Wong, A.K., et al., *AMP-activated protein kinase pathway: a potential therapeutic target in cardiometabolic disease.* Clinical Science, 2009. **116**(8): p. 607-620.

109. Russell, R.R., et al., *Translocation of myocardial GLUT-4 and increased glucose uptake through activation of AMPK by AICAR.* American Journal of Physiology-Heart and Circulatory Physiology, 1999. **277**(2): p. H643-H649.

110. Marsin, A., et al., *Phosphorylation and activation of heart PFK-2 by AMPK has a role in the stimulation of glycolysis during ischaemia.* Current biology, 2000. **10**(20): p. 1247-1255.

111. Luiken, J.J., et al., *Contraction-induced fatty acid translocase/CD36 translocation in rat cardiac myocytes is mediated through AMP-activated protein kinase signaling.* Diabetes, 2003. **52**(7): p. 1627-1634.

112. Nishimura, M., et al., *Adiponectin prevents cerebral ischemic injury through endothelial nitric oxide synthase–dependent mechanisms.* Circulation, 2008. **117**(2): p. 216-223.

113. Kondo, M., et al., *Caloric restriction stimulates revascularization in response to ischemia via adiponectin-mediated activation of endothelial nitric-oxide synthase.* Journal of Biological Chemistry, 2009. **284**(3): p. 1718-1724.

114. Ohashi, K., et al., *Adiponectin replenishment ameliorates obesity-related hypertension.* Hypertension, 2006. **47**(6): p. 1108-1116.

115. Rancoule, C., et al., *Lysophosphatidic acid impairs glucose homeostasis and inhibits insulin secretion in high-fat diet obese mice.* Diabetologia, 2013. **56**(6): p. 1394-1402.

116. Reeves, V.L., et al., *Serum Autotaxin/ENPP2 correlates with insulin resistance in older humans with obesity.* Obesity, 2015. **23**(12): p. 2371-2376.

117. Rachakonda, V.P., et al., *Serum autotaxin is independently associated with hepatic steatosis in women with severe obesity.* Obesity, 2015. **23**(5): p. 965-972.

118. Tigyi, G. and A.L. Parrill, *Molecular mechanisms of lysophosphatidic acid action.* Progress in lipid research, 2003. **42**(6): p. 498-526.

119. Castagna, D., et al., *Development of Autotaxin Inhibitors: An Overview of the Patent and Primary Literature: Miniperspective.* Journal of medicinal chemistry, 2016. **59**(12): p. 5604-5621.

120. Tokumura, A., et al., *Identification of human plasma lysophospholipase D, a lysophosphatidic acid-producing enzyme, as autotaxin, a multifunctional phosphodiesterase.* Journal of Biological Chemistry, 2002. **277**(42): p. 39436-39442.

121. Moolenaar, W.H. and A. Perrakis, *Insights into autotaxin: how to produce and present a lipid mediator.* Nature reviews. Molecular cell biology, 2011. **12**(10): p. 674.

122. Sonoda, H., et al., *A Novel Phosphatidic Acid-selective Phospholipase A1That Produces Lysophosphatidic Acid.* Journal of Biological Chemistry, 2002. **277**(37): p. 34254-34263.

123. Pyne, S., K.-C. Kong, and P.I. Darroch. *Lysophosphatidic acid and sphingosine 1-phosphate biology: the role of lipid phosphate phosphatases*. in *Seminars in cell & developmental biology*. 2004. Elsevier.

124. Tomsig, J.L., et al., *Lipid phosphate phosphohydrolase type 1 (LPP1) degrades extracellular lysophosphatidic acid in vivo.* Biochemical Journal, 2009. **419**(3): p. 611-618.

125. Escalante-Alcalde, D., et al., *The lipid phosphatase LPP3 regulates extra-embryonic vasculogenesis and axis patterning.* Development, 2003. **130**(19): p. 4623-4637.

126. Tanaka, M., et al., *Autotaxin stabilizes blood vessels and is required for embryonic vasculature by producing lysophosphatidic acid.* Journal of Biological Chemistry, 2006. **281**(35): p. 25822-25830.

127. Lin, M.-E., D.R. Herr, and J. Chun, *Lysophosphatidic acid (LPA) receptors: signaling properties and disease relevance.* Prostaglandins & other lipid mediators, 2010. **91**(3): p. 130-138.

128. Yea, K., et al., *Lysophosphatidic acid regulates blood glucose by stimulating myotube and adipocyte glucose uptake.* Journal of molecular medicine, 2008. **86**(2): p. 211-220.

129. Coy, P.E., et al., *LPA is a novel lipid regulator of mesangial cell hexokinase activity and HKII isoform expression.* American Journal of Physiology-Renal Physiology, 2002. **283**(2): p. F271-F279.

130. Dusaulcy, R., et al., *Adipose-specific disruption of autotaxin enhances nutritional fattening and reduces plasma lysophosphatidic acid.* Journal of lipid research, 2011. **52**(6): p. 1247-1255.

131. Chen, J., et al., *Specific LPA receptor subtype mediation of LPA-induced hypertrophy of cardiac myocytes and involvement of Akt and NFκB signal pathways.* Journal of cellular biochemistry, 2008. **103**(6): p. 1718-1731.

132. Cremers, B., et al., *Modulation of myocardial contractility by lysophosphatidic acid (LPA).* Journal of molecular and cellular cardiology, 2003. **35**(1): p. 71-80.

133. Xu, Y.-J., et al., *Mechanism of the positive inotropic effect of lysophosphatidic acid in rat heart.* Journal of cardiovascular pharmacology and therapeutics, 2002. **7**(2): p. 109-115.

134. Pulinilkunnil, T., et al., *Lysophosphatidic acid-mediated augmentation of cardiomyocyte lipoprotein lipase involves actin cytoskeleton reorganization.* American Journal of Physiology-Heart and Circulatory Physiology, 2005. **288**(6): p. H2802-H2810.

135. Lin, G., et al., *Acute inhibition of Rho-kinase improves cardiac contractile function in streptozotocin-diabetic rats.* Cardiovascular research, 2007. **75**(1): p. 51-58.

136. Chen, H., et al., *Lysophosphatidic acid pretreatment attenuates myocardial ischemia/reperfusion injury in the immature hearts of rats.* Frontiers in Physiology, 2017. **8**.

137. Boucher, J., A. Kleinridders, and C.R. Kahn, *Insulin receptor signaling in normal and insulin-resistant states.* Cold Spring Harbor perspectives in biology, 2014. **6**(1): p. a009191.

138. Guillermet-Guibert, J., et al., *The p110β isoform of phosphoinositide 3-kinase signals downstream of G protein-coupled receptors and is functionally redundant with p110γ.* Proceedings of the National Academy of Sciences, 2008. **105**(24): p. 8292-8297.

139. Baudhuin, L.M., et al., *Akt activation induced by lysophosphatidic acid and sphingosine-1-phosphate requires both mitogen-activated protein kinase kinase and p38 mitogen-activated protein kinase and is cell-line specific.* Molecular pharmacology, 2002. **62**(3): p. 660-671.

140. Riaz, A., Y. Huang, and S. Johansson, *G-protein-coupled lysophosphatidic acid receptors and their regulation of AKT signaling.* International journal of molecular sciences, 2016. **17**(2): p. 215.

141. Plas, D.R. and C.B. Thompson, *Akt-dependent transformation: there is more to growth than just surviving.* Oncogene, 2005. **24**(50): p. 7435-7442.

142. Klionsky, D.J., et al., *Autophagy and p70S6 kinase.* Autophagy, 2005. **1**(1): p. 59-61.

143. Kuznetsov, A.V., et al., *H9c2 and HL-1 cells demonstrate distinct features of energy metabolism, mitochondrial function and sensitivity to hypoxia-reoxygenation.* Biochimica et Biophysica Acta (BBA)-Molecular Cell Research, 2015. **1853**(2): p. 276-284.

144. Chen, X., et al., *Serum lysophosphatidic acid concentrations measured by dot immunogold filtration assay in patients with acute myocardial infarction.* Scandinavian journal of clinical and laboratory investigation, 2003. **63**(7-8): p. 497-504.

145. Cooney, G., et al., *Muscle long-chain acyl CoA esters and insulin resistance.* Annals of the New York Academy of Sciences, 2002. **967**(1): p. 196-207.

146. Holland, W.L., et al., *Inhibition of ceramide synthesis ameliorates glucocorticoid-, saturated-fat-, and obesity-induced insulin resistance.* Cell metabolism, 2007. **5**(3): p. 167-179.

147. Schubert, K.M., M.P. Scheid, and V. Duronio, *Ceramide inhibits protein kinase B/Akt by promoting dephosphorylation of serine 473.* Journal of Biological Chemistry, 2000. **275**(18): p. 13330-13335.

148. Bourbon, N.A., L. Sandirasegarane, and M. Kester, *Ceramide-induced Inhibition of Akt Is Mediated through Protein Kinase Cζ IMPLICATIONS FOR GROWTH ARREST.* Journal of Biological Chemistry, 2002. **277**(5): p. 3286-3292.

149. Talukder, M.H., et al., *Heterozygous caveolin-3 mice show increased susceptibility to palmitate-induced insulin resistance.* Physiological reports, 2016. **4**(6): p. e12736.

150. Perdomo, L., et al., *Protective role of oleic acid against cardiovascular insulin resistance and in the early and late cellular atherosclerotic process.* Cardiovascular diabetology, 2015. **14**(1): p. 75.

151. Glatz, J.F., et al., *CD36 as a target to prevent cardiac lipotoxicity and insulin resistance.* Prostaglandins, Leukotrienes and Essential Fatty Acids (PLEFA), 2013. **88**(1): p. 71-77.

152. Nobuhara, M., et al., *Mitochondrial dysfunction caused by saturated fatty acid loading induces myocardial insulin-resistance in differentiated H9c2 myocytes: a novel ex vivo myocardial insulin-resistance model.* Experimental cell research, 2013. **319**(7): p. 955-966.

153. Liu, G. and C.M. Rondinone, *JNK: bridging the insulin signaling and inflammatory pathway.* Current opinion in investigational drugs (London, England: 2000), 2005. **6**(10): p. 979-987.

154. Drosatos, K., et al., *Inhibition of c-Jun-N-terminal kinase increases cardiac peroxisome proliferator-activated receptor α expression and fatty acid oxidation and prevents lipopolysaccharide-induced heart dysfunction.* Journal of Biological Chemistry, 2011. **286**(42): p. 36331-36339.

155. Kong, J.Y. and S.W. Rabkin, *Palmitate-induced cardiac apoptosis is mediated through CPT-1 but not influenced by glucose and insulin.* American Journal of Physiology-Heart and Circulatory Physiology, 2002. **282**(2): p. H717-H725.

156. Listenberger, L.L., D.S. Ory, and J.E. Schaffer, *Palmitate-induced apoptosis can occur through a ceramide-independent pathway.* Journal of Biological Chemistry, 2001. **276**(18): p. 14890-14895.

157. Wei, C.D., et al., *Palmitate induces H9c2 cell apoptosis by increasing reactive oxygen species generation and activation of the ERK1/2 signaling pathway.* Molecular medicine reports, 2013. **7**(3): p. 855-861.

158. Bartlett, J.J., et al., *Doxorubicin impairs cardiomyocyte viability by suppressing transcription factor EB expression and disrupting autophagy.* Biochemical Journal, 2016. **473**(21): p. 3769-3789.

159. Arola, O.J., et al., *Acute doxorubicin cardiotoxicity involves cardiomyocyte apoptosis.* Cancer research, 2000. **60**(7): p. 1789-1792.

160. Van Meeteren, L.A., et al., *Autotaxin, a secreted lysophospholipase D, is essential for blood vessel formation during development.* Molecular and cellular biology, 2006. **26**(13): p. 5015-5022.

161. Abel, E.D., K.M. O'Shea, and R. Ramasamy, *Insulin resistance: metabolic mechanisms and consequences in the heart.* Arteriosclerosis, thrombosis, and vascular biology, 2012. **32**(9): p. 2068-2076.

162. Kim, J.-a., Y. Wei, and J.R. Sowers, *Role of mitochondrial dysfunction in insulin resistance.* Circulation research, 2008. **102**(4): p. 401-414.

163. Houstis, N., E.D. Rosen, and E.S. Lander, *Reactive oxygen species have a causal role in multiple forms of insulin resistance.* Nature, 2006. **440**(7086): p. 944-948.

164. Buchanan, J., et al., *Reduced cardiac efficiency and altered substrate metabolism precedes the onset of hyperglycemia and contractile dysfunction in two mouse models of insulin resistance and obesity.* Endocrinology, 2005. **146**(12): p. 5341-5349.

165. Bell, A.K., Z. Zhang, and K. Meier, *Receptor mediated signaling by lysophosphatidic acid and epidermal growth factor in a colon cancer cell line.* The FASEB Journal, 2013. **27**(1 Supplement): p. 1096.7-1096.7.

166. KAM, Y. and J.H. EXTON, *Role of phospholipase D1 in the regulation of mTOR activity by lysophosphatidic acid.* The FASEB journal, 2004. **18**(2): p. 311-319.

167. Lynch, C.M., L.A. Leandry, and R.W. Matheny Jr, *Lysophosphatidic acid-stimulated phosphorylation of PKD2 is mediated by PI3K p110β and PKCδ in myoblasts.* Journal of Receptors and Signal Transduction, 2013. **33**(1): p. 41-48.

168. Schultze, S.M., et al., *Promiscuous affairs of PKB/AKT isoforms in metabolism.* Archives of physiology and biochemistry, 2011. **117**(2): p. 70-77.

169. Yu, H., T. Littlewood, and M. Bennett, *Akt isoforms in vascular disease.* Vascular pharmacology, 2015. **71**: p. 57-64.

170. Ye, X., et al., *Lysophosphatidic acid as a novel cell survival/apoptotic factor.* Biochimica et Biophysica Acta (BBA)-Molecular and Cell Biology of Lipids, 2002. **1585**(2): p. 108-113.

171. Kim, E.K., et al., *Lysophosphatidic acid induces cell migration through the selective activation of Akt1.* Experimental & molecular medicine, 2008. **40**(4): p. 445-452.

172. Butler, A.E., et al., *β-Cell deficit and increased β-cell apoptosis in humans with type 2 diabetes.* Diabetes, 2003. **52**(1): p. 102-110.

173. Johnston, T.P. and D.J. Waxman, *Circulating free fatty acids are increased independently of PPAR γ activity after administration of poloxamer 407 to mice.* Canadian journal of physiology and pharmacology, 2008. **86**(9): p. 643-649.

174. Opie, L.H. and P.G. Walfish, *Plasma free fatty acid concentrations in obesity.* New England Journal of Medicine, 1963. **268**(14): p. 757-760.

175. Sears, B. and M. Perry, *The role of fatty acids in insulin resistance.* Lipids in health and disease, 2015. **14**(1): p. 121.

176. Haffar, T., A. Akoumi, and N. Bousette, *Lipotoxic Palmitate Impairs the Rate of β-Oxidation and Citric Acid Cycle Flux in Rat Neonatal Cardiomyocytes.* Cellular Physiology and Biochemistry, 2016. **40**(5): p. 969-981.

177. Kwon, B. and H.W. Querfurth, *Palmitate activates mTOR/p70S6K through AMPK inhibition and hypophosphorylation of raptor in skeletal muscle cells: Reversal by oleate is similar to metformin.* Biochimie, 2015. **118**: p. 141-150.

178. Boucher, J., et al., *Potential involvement of adipocyte insulin resistance in obesity-associated up-regulation of adipocyte lysophospholipase D/autotaxin expression.* Diabetologia, 2005. **48**(3): p. 569-577.

179. Ferry, G., et al., *Autotaxin is released from adipocytes, catalyzes lysophosphatidic acid synthesis, and activates preadipocyte proliferation up-regulated expression*

with adipocyte differentiation and obesity. Journal of Biological Chemistry, 2003. **278**(20): p. 18162-18169.

180. Rancoule, C., et al., *Involvement of autotaxin/lysophosphatidic acid signaling in obesity and impaired glucose homeostasis.* Biochimie, 2014. **96**: p. 140-143.

181. Frayn, K.N., C.M. Williams, and P. Arner, *Are increased plasma non-esterified fatty acid concentrations a risk marker for coronary heart disease and other chronic diseases?* Clinical Science, 1996. **90**(4): p. 243-253.

182. Wang, Y., et al., *Saturated palmitic acid induces myocardial inflammatory injuries through direct binding to TLR4 accessory protein MD2.* Nature communications, 2017. **8**: p. 13997.

183. Kong, J.Y. and S.W. Rabkin, *Palmitate-induced apoptosis in cardiomyocytes is mediated through alterations in mitochondria: prevention by cyclosporin A.* Biochimica et Biophysica Acta (BBA)-Molecular and Cell Biology of Lipids, 2000. **1485**(1): p. 45-55.

184. Hao, F., et al., *LPA induces IL-6 secretion from aortic smooth muscle cells via an LPA 1-regulated, PKC-dependent, and p38α-mediated pathway.* American Journal of Physiology-Heart and Circulatory Physiology, 2010. **298**(3): p. H974-H983.

185. Bouchareb, R., et al., *Autotaxin derived from lipoprotein (a) and valve interstitial cells promotes inflammation and mineralization of the aortic valve.* Circulation, 2015: p. CIRCULATIONAHA. 115.016757.

186. Bot, M., et al., *Lysophosphatidic acid triggers mast cell-driven atherosclerotic plaque destabilization by increasing vascular inflammation.* Journal of lipid research, 2013. **54**(5): p. 1265-1274.

187. Sui, Y., et al., *Lysophosphatidic acid inhibits apoptosis induced by cisplatin in cervical cancer cells.* BioMed research international, 2015. **2015**.

188. Chen, J., et al., *Lysophosphatidic Acid Protects Mesenchymal Stem Cells Against Hypoxia and Serum Deprivation-Induced Apoptosis.* Stem Cells, 2008. **26**(1): p. 135-145.

189. Sun, Y., et al., *Lysophosphatidic acid activates β-catenin/T cell factor signaling, which contributes to the suppression of apoptosis in H19-7 cells.* Molecular medicine reports, 2013. **8**(6): p. 1729-1733.

190. Jean-Baptiste, G., et al., *Lysophosphatidic acid mediates pleiotropic responses in skeletal muscle cells.* Biochemical and biophysical research communications, 2005. **335**(4): p. 1155-1162.

191. Chen, C., et al., *Lysophosphatidic acid causes endothelial dysfunction in porcine coronary arteries and human coronary artery endothelial cells.* Atherosclerosis, 2012. **222**(1): p. 74-83.

192. Federico, L., et al., *Autotaxin and its product lysophosphatidic acid suppress brown adipose differentiation and promote diet-induced obesity in mice.* Molecular endocrinology, 2012. **26**(5): p. 786-797.

193. Nishimura, S., et al., *ENPP2 contributes to adipose tissue expansion and insulin resistance in diet-induced obesity.* Diabetes, 2014. **63**(12): p. 4154-4164.

194. Ternacle, J., et al., *Short-term high-fat diet compromises myocardial function: a radial strain rate imaging study.* European Heart Journal-Cardiovascular Imaging, 2017: p. jew316.

195. Apaijai, N., et al., *Combined vildagliptin and metformin exert better cardioprotection than monotherapy against ischemia-reperfusion injury in obese-insulin resistant rats.* PloS one, 2014. **9**(7): p. e102374.

196. Hua, Y., et al., *Cathepsin K Knockout Mitigates High-Fat Diet–Induced Cardiac Hypertrophy and Contractile Dysfunction.* Diabetes, 2013. **62**(2): p. 498-509.

197. Yu, Z.-B., H. Wei, and J.-P. Jin, *Chronic coexistence of two troponin T isoforms in adult transgenic mouse cardiomyocytes decreased contractile kinetics and caused dilatative remodeling.* American Journal of Physiology-Cell Physiology, 2012. **303**(1): p. C24-C32.

198. Nance, M.E., et al., *Sarcomere Length-Ventricular Filling Pressure Relationship in the Perfused Murine Heart Visualized with 2-Photon Fluorescence Microscopy.* Biophysical Journal, 2014. **106**(2): p. 645a.

199. Kobirumaki-Shimozawa, F., et al., *Real-Time Imaging of Sarcomere Dynamics in the Mouse Heart In Vivo.* Biophysical Journal, 2014. **106**(2): p. 645a-646a.